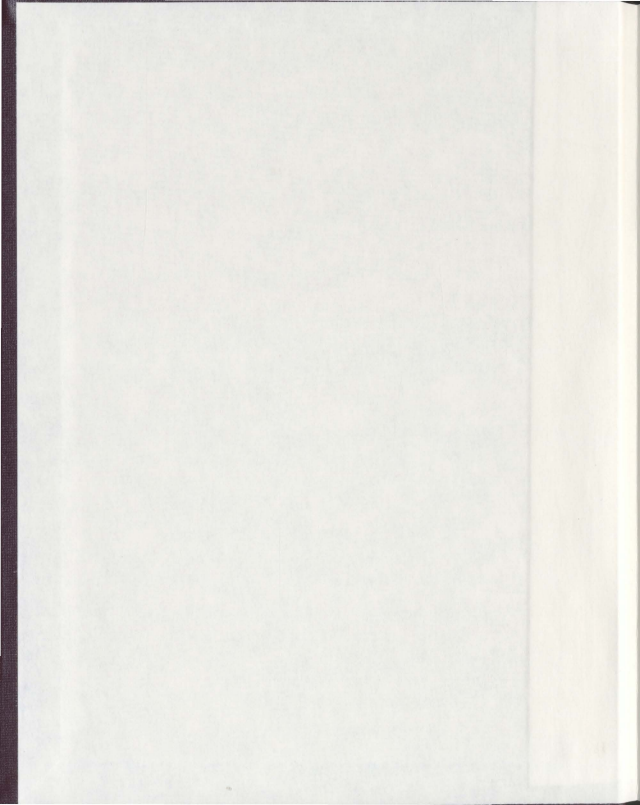


ASSESSMENT OF ICE KEEL/SOIL AND PIPELINE/SOIL  
INTERACTIONS:  
CONTINUUM MODELLING IN CLAY

CHRISTOPHER ROSSITER







Assessment of Ice Keel/Soil and Pipeline/Soil Interactions: Continuum Modelling in Clay

by

© Christopher Rossiter

A thesis submitted to the  
School of Graduate Studies  
in partial fulfillment of the  
requirements for the degree of  
Master of Engineering

Memorial University of Newfoundland  
Faculty of Engineering and Applied Science

May 2012

St. John's

Newfoundland

Canada

## **ABSTRACT**

Pressure ridges are created from the build up of ice sheets, driven by winds and ocean currents and are a potential hazard to buried pipelines in cold ocean environments. These ice masses can ground in shallow waters, gouging the ocean floor and cause soil displacements well beneath the maximum gouge depth. If the pressure ridge passes over a pipeline, the soil displacements can be large enough to cause pipeline failure even if the pipeline is buried beneath the gouge depth. In regions that are prone to iceberg incursion, gouging of the seabed is also of utmost importance; however, this study focuses mainly on regions that encounter pressure ridges.

These ice keel/seabed/pipeline events can be simulated numerically using a fully coupled continuum model, or decoupled structural model approach. Due to the complexity of the fully coupled analysis, it is important to gain insight into and validation of numerical models through a systematic approach that conducts analysis of subsystems to the problem. The problem is then broken into ice keel/soil and soil/pipeline interactions where the numerical simulation procedures can be validated against available analytical solutions and physical modelling data. If an acceptable level of certainty can be achieved in each constituent problem, then a higher level of certainty can be obtained for the more complex coupled problem.

Advancements in Finite Element software allow for such complex problems to be solved more efficiently and effectively. A numerical assessment of both subsystems was conducted and validated against available physical test data. Numerical modelling

procedures were developed in ABAQUS/Explicit using an ALE framework. The initial objective of the research program was to compare the results from simulated ice gouge events, using ALE and CEL formulations, with available physical data, comparatively assess these two formulations for ice keel/soil and pipeline/soil interaction problems, and provide guidance on improved engineering models. However, the CEL formulation within ABAQUS/Explicit did not properly account for the equivalent shear stress limit specified at the ice keel/soil interface. This has implications when modeling scenarios when the defined interface shear strength is exceeded. When using the CEL formulation, the interface shear strength would cap at a value much lower than that defined by the user. This can lead to incorrect predictions of soil clearing mechanisms, seabed reaction forces, and subgouge deformations. This was an important observation and conclusion from this study that has not been recognized in the public domain. This outcome shifted the focus of the research program to parametric studies conducted exclusively within the ALE framework and to determine various factors that were imperative to the analyses.

Ice keel/soil interaction models assessed the effects of soil shear strength profile, remoulded soil strength at the ice keel/soil interface, and assumed shape of the ice keel. Ice keel strength and consolidation were not considered in this study and these features were assumed to be rigid indenters. Measurements of subgouge soil deformations, berm heights, and seabed reaction forces were taken and potential trends examined. It was determined that proper modeling of soil strength and remoulding at the interface was important when calibrating the numerical model to physical data. Examination of the data revealed important trends between extent of plastic strain zone and berm geometry.

Pipeline/soil interactions models studied the effects of soil shear strength, shear strength profiles, pipeline diameter, embedment ratio, and pipeline direction of travel in the lateral-vertical plane. The pipelines in this study were assumed to be rigid. Measurements of interaction forces were taken and assessed to determine ultimate load and displacement to ultimate load. Comparison of the current numerical data with current engineering guidelines revealed that current guidelines have the potential to incorrectly estimate ultimate load and displacement to ultimate load. Analyses demonstrated that normalized interaction forces varied depending on soil shear strength and pipeline diameter.

## ACKNOWLEDGEMENTS

I would like to extend my gratitude to Dr. Shawn Kenny for his assistance and expertise throughout this entire project. Also, I would like to thank Dr. Michael Paulin for presenting the opportunity for me to pursue this endeavour after completing a work term at IMV Projects Atlantic. Through IMV Projects Atlantic I was provided with a MITACS Accelerate Internship Program Fellowship. A thank you to Kenton Pike and Ali Fatemi, both PhD candidates under the supervision of Dr. Shawn Kenny, for the insightful discussions on the subject matter of this thesis and their expertise in numerical modelling in the fields of computational mechanics and soil mechanics.

I would like to thank the School of Graduate Studies for providing me with the School of Graduate Studies Baseline Fellowship for the duration of my program. I also extend my thanks to the Research and Development Council of Newfoundland for selecting me for an RDC Scholarship in my last year of studies. I would like to also thank the Wood Group for their financial support during this program through the Wood Group Chair in Arctic and Harsh Environments Engineering.

Last but not least, I would like to thank my Mom, Dad, Andrew, and my Grandparents for their endless support in all endeavours I undertake.

## TABLE OF CONTENTS

ABSTRACT.....	II
ACKNOWLEDGEMENTS.....	V
LIST OF TABLES.....	VIII
LIST OF FIGURES.....	IX
LIST OF SYMBOLS.....	XIV
1 INTRODUCTION.....	18
2 ICE GOUGING: A REVIEW.....	24
2.1 General.....	24
2.2 Relict Land Gouges.....	26
2.3 Small Scale Observations.....	28
2.4 Ice Ridge Formation and Geometries.....	28
2.5 Ice Gouge Data for the Beaufort Sea.....	35
2.6 Interface Friction Coefficients.....	38
2.7 Theoretical and Analytical Models.....	42
2.8 Experimental Research.....	44
2.8.1 1g Models.....	44
2.8.2 Centrifuge Models.....	56
2.9 Numerical Simulations.....	67
2.9.1 Winkler Model.....	69
2.9.2 Two-Dimensional Continuum Models.....	75
2.9.3 Three-Dimensional Continuum Models.....	83
3 PIPELINE SOIL INTERACTION: A REVIEW.....	109
3.1 General.....	109
3.2 Analytical Models.....	110
3.3 Experimental Research.....	113
3.4 Numerical Models.....	139
3.5 Current Engineering Guidelines.....	163
3.5.1 Guidelines for the Seismic Design and Assessment of Natural Gas and Liquid Hydrocarbon Pipelines.....	163
3.5.2 Guidelines for the Design of Buried Steel Pipe.....	170
4 PROJECT DESCRIPTION.....	171
4.1 Scope of Work.....	171

5	ASSESSMENT OF ICE/SOIL INTERACTIONS: CONTINUUM MODELING IN CLAYS .....	174
5.1	Introduction.....	174
5.2	Previous Numerical Models.....	177
5.3	Physical Experiments.....	181
5.4	NUMERICAL MODELLING PROCEDURES .....	183
5.4.1	Overview.....	183
5.4.2	Numerical Model Definition.....	184
5.5	NUMERICAL ANALYSIS .....	185
5.5.1	Calibration/Sensitivity Exercise.....	185
5.6	Model Calibration .....	187
5.7	Parametric Study.....	195
5.8	Conclusions.....	201
5.9	References.....	203
6	EVALUATION OF LATERAL-VERTICAL PIPE/SOIL INTERACTION IN CLAY.....	205
6.1	Introduction.....	206
6.2	Previous Investigations .....	209
6.3	Numerical Model .....	213
6.4	Effect of Burial Depth on Yield Envelopes .....	216
6.5	Effect of Soil Strength Profile on Yield Envelopes for Oblique Loading Events .....	222
6.6	Effect of Overburden Pressure on Lateral Pipeline Response .....	224
6.7	Bi-linear Representation of Force-Displacement Curve.....	230
6.8	Conclusion .....	235
6.9	References.....	239
7	SUMMARY AND CONCLUSIONS .....	241
8	REFERENCES .....	247

## LIST OF TABLES

Table 1-1- Iceberg sightings from Grand Banks Drill Sites (Venkatesh and El-Tahan, 1988) .....	19
Table 2-1 – Summary of Canadian Beaufort Sea Ice Gouge Surveys (Caines, 2009) .....	36
Table 2-2 - Summary of American Beaufort Sea Ice Gouge Surveys (Caines, 2009) .....	37
Table 2-3- Static friction coefficients (Utt and Clark, 1980).....	39
Table 2-4 – Friction coefficients (Shapiro and Metzner, 1987).....	40
Table 2-5- Kinetic friction coefficients for various construction materials (Frederking and Barker, 2001) .....	40
Table 2-6- Static and mean kinetic friction coefficients (Barker and Timco, 2003) .....	41
Table 2-7- Range of Test Parameters (Abdelnour and Graham, 1984) .....	47
Table 2-8- Test Parameters (Porooshab and Clark, 1990) .....	49
Table 2-9- Force Results Summary (Porooshab and Clark, 1990).....	50
Table 2-10- Centrifuge Modeling Scaling Relationships (Rizkalla et al., 1992).....	56
Table 2-11- Proposed Test Matrix (Lach, 1996) .....	59
Table 2-12- Material Parameters (Yang et al., 1994) .....	76
Table 2-13 – Keel-Seabed Cases (Phillips et al., 2010).....	98
Table 2-14- Mesh density parameters (Phillips and Barrett, 2011) .....	106
Table 5-1 - Calibration Study Cases .....	188
Table 5-2 - Seabed Reaction Forces for Calibration Study .....	190
Table 5-3 - Frontal Mound and Side Berm Geometries .....	194
Table 5-4 - Gouge Parameter Test Matrix .....	195
Table 5-5 - Seabed Reaction Forces for Case 5 to Case 9 .....	197
Table 6-1 - Parameters for burial depth study .....	217
Table 6-2 - Normalized values for lateral pipeline/soil interaction using various measurement methods.....	233
Table 6-3 - Normalized values for 70° oblique pipeline/soil interaction using various measurement methods.....	233

## LIST OF FIGURES

Figure 1-1- Drift Pattern for Canadian East Coast Icebergs (Murray, 1969) .....	19
Figure 1-2 – Beaufort Sea Winter Ice Zones (Wadhams, 1975).....	20
Figure 2-1- Section View Showing Zone Separation (Nobahar, 2005).....	26
Figure 2-2- Schematic illustration of a first-year ice ridge (Timco and Burden, 1997) ...	29
Figure 2-3- Schematic of an average first-year ice ridge (Timco and Burden, 1997).....	31
Figure 2-4- Schematic of an average multi-year ice ridge (Timco and Burden, 1997)....	32
Figure 2-5 – Relationships for $H_k$ as a function of $H_s$ .....	34
Figure 2-6 - Relationships for $W_k$ as a function of $W_s$ .....	35
Figure 2-7 – Canadian Beaufort Sea Ice Gouge Depth Data (Caines, 2009) .....	37
Figure 2-8 - American Beaufort Sea Ice Gouge Depth Data (Caines, 2009) .....	38
Figure 2-9 - Model Shapes used in Prasad Test Program (Prasad, 1985).....	46
Figure 2-10- Beam Load Cell 2, Test 2 (Paulin, 1992) .....	52
Figure 2-11- Horizontal Load Cell 2, Test 1 (Paulin, 1992).....	53
Figure 2-12 - Test 04 pore pressure responses during event (Lach, 1996).....	60
Figure 2-13 - Test 04 horizontal and vertical components of the resultant force (Lach, 1996) .....	61
Figure 2-14 - Vertical and horizontal components of soil displacement (Test 04) (Lach, 1996) .....	62
Figure 2-15 - Test 05 horizontal and vertical components of the resultant force (Lach, 1996) .....	63
Figure 2-16 - Vertical and horizontal components of soil displacement (Test 05) (Lach, 1996) .....	64
Figure 2-17- Schematic Illustration of a Winkler Analysis (Kenny et al., 2000).....	68
Figure 2-18- Effect of Scour Width (Konuk and Fredj, 2004) .....	70
Figure 2-19- Pipeline axial strain response, 10 m gouge width (Kenny et al., 2000).....	72
Figure 2-20- Pipeline axial strain response, 25 m gouge width (Kenny et al., 2000).....	72
Figure 2-21- Max pipeline displacement for different gouge widths (Fredj et al., 2008) .	73
Figure 2-22- Max pipeline plastic strain for different gouge widths (Fredj et al., 2008) ..	74
Figure 2-23- Pipeline deformed shape, decoupled model (Liferov et al., 2007) .....	75
Figure 2-24- Pipeline axial plastic strains, decoupled model (Liferov et al., 2007).....	75
Figure 2-25 - Contour plot of pressure for reference case after 5 s (Sayed and Timco, 2008) .....	78

Figure 2-26- Test 04 comparison of measured and computed values of horizontal and vertical components of resultant force plotted against horizontal position (Lach and Clark, 1996) .....	82
Figure 2-27- Particle trajectories for soft soil (Konuk and Gracie, 2004) .....	84
Figure 2-28- Particle Trajectories for stiffer soil (Konuk and Gracie, 2004) .....	85
Figure 2-29- Maximum pipe displacements and stress for different scour widths, Continuum Model (Konuk and Yu, 2007a) .....	87
Figure 2-30- Maximum pipe displacements and strains for different scour widths, Winkler Model (Konuk and Fredj, 2004) .....	88
Figure 2-31- Comparison of maximum and steady state stress conditions (Nobahar, 2005) .....	90
Figure 2-32- Pipeline displacements, Pressurized vs. Unpressurized (Fredj et al., 2008) 94	
Figure 2-33- Pipeline plastic strain, Pressurized vs. Unpressurized (Fredj et al., 2008)..	94
Figure 2-34 - Effect of gouge depth on ice keel reaction forces (Fredj et al., 2008).....	96
Figure 2-35 - Effect of gouge width on ice keel reaction forces (Fredj et al., 2008).....	96
Figure 2-36 - Effect of pipeline on horizontal ice keel reaction force (Fredj et al., 2008)97	
Figure 2-37 - Effect of pipeline on vertical ice keel reaction force (Fredj et al., 2008) ...	97
Figure 2-38 - Normalised horizontal keel reaction force development (Phillips et al., 2010) .....	99
Figure 2-39 – Development of keel horizontal to vertical reaction force ratios (Phillips et al., 2010) .....	100
Figure 2-40 –Berm height versus keel attack angle (Phillips et al., 2010) .....	100
Figure 2-41 - Horizontal deformation comparison, Cases 1 to 3 (Phillips et al., 2010). 101	
Figure 2-42 - Vertical Profile of Horizontal and Vertical Subgouge Soil Deformations, Free Field (Pike et al., 2011).....	103
Figure 2-43 - Vertical profile of vertical subgouge soil deformations, pipe in soil (Pike et al., 2011) .....	104
Figure 2-44- Plan view of lateral subgouge deformations at the ice gouge depth, free field (Pike et al., 2011).....	105
Figure 2-45- Horizontal keel reaction force (Phillips and Barrett, 2011).....	107
Figure 2-46- Vertical to Horizontal reaction force (Phillips and Barrett, 2011) .....	107
Figure 2-47 - Subgouge displacement profiles (Phillips and Barrett, 2011) .....	108
Figure 3-1 – Coefficient $N_y$ for laterally loaded piles (Prakash and Sharma., 1990) .....	111
Figure 3-2 – Coefficient $N_c$ for laterally loaded piles (Prakash and Sharma., 1990) .....	111
Figure 3-3 – Assumed flow pattern for pipe buried in an open trench (Wantland et al., 1979) .....	113

Figure 3-4 – $N_c$ versus H/D for strip anchors in clay after Mackenzie (1955) (Das, 1990)	116
Figure 3-5 – Relationship between $N_c$ and H/D (Wantland et al., 1979)	120
Figure 3-6 – Normalized relationship between displacement at failure and embedment ratio	121
Figure 3-7 – $N_h$ as a function of $H_e/D$ for loose, medium, and dense sands (Trautmann and O'Rourke., 1985)	122
Figure 3-8 – $N_h$ versus H/D for pipeline design (Trautmann and O'Rourke, 1985)	124
Figure 3-9 – Burial Depth Tests Data Comparison to Rowe and Davis and Hansen (Paulin et al., 1995)	128
Figure 3-10 – Evaluated trends through undrained interaction factor data (Paulin, 1998)	131
Figure 3-11 – Interaction Factor Comparison (Phillips et al., 2004b)	133
Figure 3-12 - Trench Effects (Phillips et al., 2004b)	134
Figure 3-13 – p-y curve for laterally loaded trenched pipeline (Phillips et al., 2004b)	135
Figure 3-14 - Normalised horizontal force for centrifuge tests (Oliveira et al., 2010)	138
Figure 3-15 – Rowe and Davis (1982) anchor capacity for a vertical plate anchor in clay (Poulos, 1988)	140
Figure 3-16 – Numerical results for lateral rigid pipeline displacement in clay: failure mechanisms (Popescu et al., 2002a)	145
Figure 3-17 – Predicted and recommended interaction forces for lateral loading of a rigid pipeline in clay (Popescu et al., 2002a)	145
Figure 3-18 – Lateral bearing capacity factors (Phillips et al., 2004b)	147
Figure 3-19 – Lateral interaction factor contributions, for 10 kPa and 20 kPa soils (Phillips et al., 2004b)	148
Figure 3-20 – Effect of burial depth on lateral interaction factor (Phillips et al., 2004b)	149
Figure 3-21 - Effect of burial depth on axial interaction factor (Phillips et al., 2004b)	150
Figure 3-22 – Axial-lateral force interaction diagram (Phillips et al., 2004b)	150
Figure 3-23 – Variations in the weight term of the lateral interaction factor with H/D and $\gamma H/s_u$ (Daiyan et al., 2009)	153
Figure 3-24 - Variations in the weight term of the vertical interaction factor with H/D and $\gamma H/s_u$ (Daiyan et al., 2009)	154
Figure 3-25 – Effect of overburden ratio on lateral interaction factor (Daiyan et al., 2009)	155
Figure 3-26 - Effect of overburden ratio on vertical interaction factor (Daiyan et al., 2009)	155

Figure 3-27 - Lateral interaction factors as a function of H/D .....	157
Figure 3-28 – Methods used to obtain peak loads for lateral interaction factors (Pike and Kenny, 2011).....	158
Figure 3-29 - Soil failure mechanisms for lateral pipe/soil interaction (a) H/D = 1.8, (b) H/D = 3 (Seo et al., 2011).....	159
Figure 3-30 – Soil failure mechanisms for axial pipe/soil interaction, H/D = 1.8 (Seo at al., 2011) .....	160
Figure 3-31 – Normalized failure envelopes (Borges and Oliveira, 2011).....	161
Figure 3-32 - Failure envelopes normalized by their maximum values (Borges and Oliveira, 2011) .....	162
Figure 3-33 - Idealized representation of soil with discrete springs (Honegger and Nyman, 2004) .....	163
Figure 3-34 - Plotted Values for the Adhesion Factor, $\alpha$ (Honegger and Nyman, 2004).....	166
Figure 3-35 - Values of $N_{qh}$ and $N_{ch}$ (Hansen, 1961).....	167
Figure 3-36 - Ranges for values of $N_{qv}$ (Trautmann and O'Rourke, 1983).....	168
Figure 3-37 - Ranges for values of $N_{cv}$ (Trautmann and O'Rourke, 1983).....	168
Figure 3-38 - Plotted values of bearing capacity factors ( $N_q$ , $N_c$ , and $N_r$ ) (Honegger and Nyman, 2004) .....	169
Figure 5-1 - OCR profile used in study .....	186
Figure 5-2 - Case 4 with Lach (1996) Keel .....	189
Figure 5-3 - V/H comparison of Lach (1996) to FE study .....	190
Figure 5-4 - Horizontal subgouge deformations for Calibration Tests.....	191
Figure 5-5 - Vertical Subgouge Deformations for Calibration Tests .....	192
Figure 5-6 - Method of berm measurements.....	194
Figure 5-7 - Horizontal subgouge deformations for varying gouge widths.....	197
Figure 5-8 - Plot of $\epsilon_{eq}$ contours for a) Case 5 and b) Case 8 .....	199
Figure 5-9 - Vertical extent of $\epsilon_{eq}$ versus width of frontal mound.....	199
Figure 5-10 - Frontal mound width versus horizontal seabed reaction force .....	200
Figure 5-11 - Frontal Mound Height/ Side Berm Height versus W/D .....	201
Figure 6-1 - Schematic illustration for lateral-vertical pipeline/soil interaction.....	208
Figure 6-2 - Numerical comparison of FEA and Phillips et al. (2004b) data for H/D of 1.5 .....	214
Figure 6-3 - Numerical comparison of FEA and Phillips et al. (2004b) data for H/D of 3.0 .....	215
Figure 6-4 - Lateral-vertical interaction factors for pipeline with D = 24 in. ....	218
Figure 6-5 - Lateral-vertical limit load interaction forces as a function of embedment ratio (H/D) and attack angle.....	219

Figure 6-6 - Lateral-vertical interaction factors for 25 kPa soil .....	220
Figure 6-7 - Plot of plastic strain contours for $H/D = 4$ and $s_u = 25$ kPa: a) $D = 24$ in. b) $D = 36$ in. ....	221
Figure 6-8 - Failure envelope comparison for constant and varying soil shear strengths with depth.....	224
Figure 6-9 - $N_{ch}$ as a function of $H/D$ for various undrained shear strengths .....	225
Figure 6-10 - Effect of undrained shear strength on plastic strain contours for $H/D$ of 10 and 25 kPa.....	226
Figure 6-11 - Effect of undrained shear strength on plastic strain contours for $H/D$ of 10: 100 kPa.....	227
Figure 6-12 - $N_{ch}^*$ as a function of $H/D$ for various undrained shear strengths .....	228
Figure 6-13 - Comparison of numerical results for soil weight study for 25 kPa soil....	229
Figure 6-14 - $\beta_h$ as a function of undrained shear strength.....	230
Figure 6-15 - Methods of determining peak load .....	232
Figure 6-16 - Normalized pipeline displacement to peak load for lateral pipeline/soil interaction .....	235

## LIST OF SYMBOLS

A	soil activity
ALE	Arbitrary Lagrangian Eulerian
B	trench width
$b_f$	footing width
c	soil cohesion
CEL	Coupled Eulerian Lagrangian
CF	clay fraction
cm	centimetre
CPT	cone penetrometer test
D	gouge depth or pipeline diameter
$D^*$	modified pipeline diameter
$D/t$	pipeline diameter to thickness ratio
E	elastic modulus
$F_h$	horizontal seabed reaction force
$F_v$	vertical seabed reaction force
ft	foot
g	gravity constant
G	shear modulus
GB	gigabyte
H	pipeline burial depth or horizontal keel reaction force
HDD	horizontal directional drilling
$H_k$	keel height
$H_s$	sail height
H/D	embedment ratio
$(H/D)_{CR}$	critical embedment ratio
hr	hour
in	inch
$I_r$	rigidity index

kg	kilogram
km	kilometre
kN	kilonewton
$K_o$	coefficient of pressure
kPa	kilopascal
L	length
m	metre
M	critical state stress ratio
$m^2$	squared metre
$m^3$	cubic metre
mm	millimetre
min	minute
MPa	megapascal
N	Newton
$N_b$	T-bar factor
$N_{ch}$	lateral interaction factor for clay
$N_{qh}$	lateral interaction factor for sand
$N_{cv}$	vertical interaction factor for clay
$N_{qv}$	vertical interaction factor for sand
$N_{ch}^*$	lateral interaction factor associated with soil strength
OCR	over consolidation ratio
$p_{nom}$	normalized lateral force
$P_u$	lateral soil spring force
$P_{ult}$	ultimate lateral load on pipeline
PI	plasticity index
PL	plastic limit
PRISE	Pressure Ridge Ice Scour Experiment
q	vertical effective overburden pressure
$Q_d$	vertical bearing soil spring force

$Q_u$	vertical uplift soil spring force
RSM	Response Surface Methodology
s	second
$s_u$	undrained shear strength
SOP	state of practice
t	pipeline wall thickness
$T_u$	axial soil spring force
UL	Updated Lagrangian
USGS	United States Geological Survey
u	subgouge displacement in x direction
v	subgouge displacement in y direction
V	vertical keel reaction force
W	gouge width
$W_k$	keel width
$W_s$	sail width
$y_{norm}$	normalized displacement
$Y_{ult}$	ultimate pipeline displacement
YS	yield stress
z	subgouge displacement in z direction
$\alpha$	resultant force angle or adhesion factor
$\beta_n$	factor to determine effect of soil overburden pressure
$\gamma$	soil unit weight
$\gamma'$	submerged soil unit weight
$\Gamma$	specific volume
$\delta$	interface friction angle
$\varepsilon$	epsilon
$\theta$	keel attack angle or pipeline attack angle
$\kappa$	gradient of swelling lines
$\lambda$	gradient of normal consolidation lines

$\mu$	coefficient of friction
$\nu$	Poisson's ratio
$\rho$	density
$\sigma$	stress
$\tau$	shear stress
$\tau_{\text{eq}}$	equivalent shear stress limit
$\tau_{\text{max}}$	maximum shear stress
$\phi$	internal angle of soil friction
$^{\circ}$	degree

## 1 INTRODUCTION

The United States Geological Survey (USGS) have indicated that arctic and ice covered regions hold significant reserves of oil and gas. The development of these regions is important as the world's current oil and gas reserves become depleted, however, there are many issues that must be considered when producing from these areas. Various hazards that need to be acknowledged when developing oil and gas facilities offshore in cold regions are: waves, icebergs, freezing spray, sea ice, pressure ridges and characteristics of the seabed. Icebergs and sea ice are of great concern when producing in these regions, as these ice formations can be damaging to surface, subsea and subsurface equipment.

The two types of ice that are common to cold ocean regions off the coast of Canada are: glacial ice in the form of icebergs, which originate mainly off the coast of Greenland, and sea ice which is the result of freezing seawater occurring mainly in the northern seas.

The drift pattern of an iceberg depends on multiple factors including wind, ocean currents, wind generated currents and the Coriolis Effect. The Greenland ice cap can produce as many as 40,000 icebergs per year but normally 10,000 to 30,000 are produced annually (Nadreau, 1986). These icebergs are carried to the north end of Baffin Bay by the West Greenland Current and then southward with the Baffin Island Current. They are then finally carried to the Grand Banks by the Labrador Current (See Figure 1-1). Of all the icebergs produced by the Greenland ice cap, only an average of 400 drift into the Grand Banks region each year (Dinsmore, 1972). Due to ongoing climate change the statistics quoted in these studies may not be valid at the present. Sightings of icebergs off

the Grand Banks have reported these masses of being in the order of the tens of millions of tons. Given in

Table 1-1 is the size distribution of a number of icebergs tracked off the Grand Banks drilling sites in 1984 to 1987.

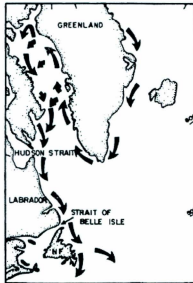


Figure 1-1- Drift Pattern for Canadian East Coast Icebergs (Murray, 1969)

Table 1-1- Iceberg sightings from Grand Banks Drill Sites (Venkatesh and El-Tahan, 1988)

Mass Range (tonnes)	Number of Sightings
25-275	9
275-2750	32
2750-27500	51
27500-275000	64
275000-2750000	59
2275000-27500000	17

In the more northern oceans, such as the Beaufort Sea, sea ice is of great concern. Annual freeze up along the coast of the Beaufort Sea is widely varied but can occur as early as September 1<sup>st</sup> and breakup can occur as late as the end of August (Kovacs and Mellor, 1974). Sea ice in the Beaufort Sea has been divided into three zones (Wadhams, 1975): Fast Ice Zone, Shear Zone, and the Pack Ice Zone. The Shear Zone extends from the edge of the fast ice zone to the edge of the continental shelf. The ridges are created by the build up of sea ice in the Shear Zone (See Figure 1-2) and can have keels, which extend well below the water surface. These ridges are driven primarily by wind and secondarily by ocean currents, wind generated currents, and by direct loading from other ice and can potentially be carried into water where the keel depth is sufficient to ground.

Gouging occurs when the ice mass moves while in contact with the seabed, which can generate incisions metres deep, tens of metres in width and hundreds of meters to several kilometres in length.

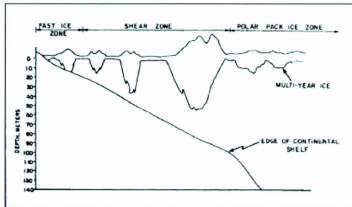


Figure 1-2 – Beaufort Sea Winter Ice Zones (Wadhams, 1975)

In regions where the ice has adequate draft to gouge the seabed, one must consider the effect that this can have on seabed and buried facilities. An implicit assumption during early ice gouge research was that a buried pipeline would only be endangered if it was located just above the base of the scouring keel, where the ice mass could make direct contact with the pipeline. Later research determined that the forces transmitted through the soil during a scouring event were high enough to cause failure of the pipeline. Simplified calculations (Palmer et al., 1990) established the expected loads during a gouging event were one to two times higher than anchor dragging forces, which are known to cause damage. This is of great concern when developing and transporting oil and gas through pipelines in shallow water where ice formations can have sufficient keel depth to gouge the seabed. This could potentially cause bending, buckling, ovalisation, or a loss of pressure containment in the pipeline that results in a leak or rupture.

There are various safe guards that can be used to protect a pipeline from damage during a gouging event: pipe-in-pipe solution, construction of a high strength pipeline, casing pipeline in cement, and determination of a safe burial depth with backfilled trench. The conventional and most widely used solution is trenching to a safe burial depth. Trenching methods include ploughing (Brown and Palmer, 1985), jetting (Andrier, 1981), dredging (deVries, 1981), and mechanical trenching techniques (Gibson, 1981). Choosing an appropriate backfill for the trench can increase protection by impeding the transfer of the force through the soil onto the pipeline. In situations where trenching to a safe burial depth is not an economically viable other solutions will have to be examined.

Due to the complexity of the ice gouge problem and the significant cost of field programs and large scale experiments, the examination of ice ice/soil/pipeline interaction scenarios have been conducted using analytical, numerical and reduced scale physical modeling techniques. Physical modeling techniques have been the most popular option for the investigation into the gouge problem; especially centrifuge modeling, which has the benefit to accurately model the in-situ soil stress state. But recent advancements in computer hardware and software technology have provided a technical framework to develop advanced numerical tools for the simulation of ice gouge events and a cost-effective approach for conducting these investigations. Before these numerical tools can be used to analyse complex problems they must be first calibrated against available physical data sets. Aside from using physical models to study the nature of ice keel/soil/pipeline interactions and calibrating numerical models against these data sets, it is necessary to study these situations using a decoupled approach (i.e. ice keel/soil and

pipeline/soil) to gain confidence in each component of the problem. If an acceptable level of certainty can be achieved in each constituent problem, then a higher level of certainty can be obtained for the more complex coupled problem. Various research groups have published work studying both the ice-soil-pipe interaction and the ice-soil and pipe-soil interactions. Even with these laborious efforts, there is still some uncertainty inherent in these numerical approaches.

This thesis investigates the validity of the finite element method pertaining to the ice keel/soil interaction and the pipeline/soil interaction problems. Initially, the test program was to incorporate a comparison of ALE and CEL modeling procedures in ABAQUS/Explicit; however, problems were encountered with CEL's ability to properly model the contact at the ice keel/soil interface. CEL procedures do not correctly account for the defined equivalent shear stress limit ( $\tau_{eq}$ ) at the contact interface. Although ABAQUS CEL numerical models have been partially calibrated with reduced-scale centrifuge data, the numerical modelling procedures may not be valid, outside this domain, with respect to clearing mechanisms, interface conditions and contact mechanics. An Arbitrary Lagrangian Eulerian (ALE) formulation was then adopted to assess the problem, utilizing the finite element package ABAQUS/Explicit. A parametric study on free field ice gouging was conducted and calibrated against available physical model data in literature.

Oblique pipeline/soil interactions were assessed within an ALE framework using ABAQUS/Explicit and calibrated against applicable physical data. In addition to a tool

capable of aiding in the understanding of ice keel/soil/pipeline interaction, pipeline/soil interaction models are also used to assess the accuracy of current guidelines and to make suggestions for their improvement.

## **2 ICE GOUGING: A REVIEW**

### **2.1 General**

With the demand for hydrocarbon development increasing, focus has shifted toward less explored regions such as the North Atlantic and Arctic. Sea ice and icebergs pose potential hazards to buried facilities in these regions and have become a primary focal point when looking into the possible development of these areas. Focus has only recently been devoted to the understanding of the ice gouge mechanism, with the majority of the research occurring over the last thirty years. An extensive collection of literature exists on the ice gouge phenomenon from full scale observations of relict land gouges, such as those conducted in Lake Agassiz (Dredge, 1982; Mollard, 1983; Woodworth-Lynas and Guigne, 1990), to recent numerical approaches (Konuk and Gracie, 2004; Kenny et al., 2005; Jukes et al., 2008) created to simulate a gouge event.

Up until the mid 1980's it was generally believed that the influence of a scouring ice keel on the seabed was essentially restricted to horizontal bulldozing. This mechanism would clear material to side berms, as the keel moved forward, creating a trough or gouge mark. This would result in little to no subgouge deformation of the soil, and pipelines, if buried slightly below the gouge depth, would be unharmed.

However, in 1985, a paradigm shift began as a result of the Dynamics of Iceberg Grounding and Scouring (DIGS) experiment (Hodgson et al., 1989). Grounding icebergs on the Labrador continental shelf of eastern Canada were equipped with accelerometer packages and monitored. Data retrieved from these accelerometers were the first ever

direct measurement of iceberg grounding forces and valuable insight was gained into the mechanics of the ice gouge phenomenon. Physical model studies, subsequent to these experiments, helped expand the knowledge base of subgouge soil behaviour during a gouge event (Porooshab and Clark, 1989; Paulin, 1992; Lach and Clark, 1996).

There are three failure zones of importance to the ice gouge problem (Palmer et al., 1990), shown in Figure 2-1. Zone 1 extends from the surface to the basal plane of the ice keel. There are very large strains and soil deformations in this zone. Soil is generally moved upward and then pushed laterally to side berms while some soil is subducted into Zone 2. Current analysis generally predicts failure for a pipeline buried in this zone. Zone 2 experiences large soil deformations while Zone 3 is a small strain zone that acts in a somewhat elastic manner. Zone 3 would provide sufficient protection for the pipeline but this zone may be neither technically or economically feasible to trench in. Zone 2 is the most likely zone to contain the pipeline. The pipeline should be engineered to withstand the soil displacements experienced in this zone.

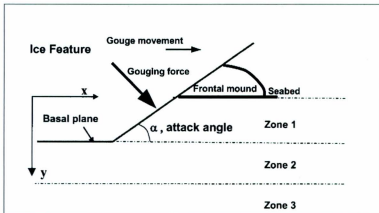


Figure 2-1- Section View Showing Zone Separation (Nobahar, 2005)

## 2.2 Relict Land Gouges

Direct observation of contemporary ice gouges is only possible by diving or submersibles, and studying subgouge deformations of offshore gouge marks is near impossible and methods such as echo sounder and side scan sonar are necessary to obtain gouge statistics. An alternate method of studying these formations is to observe relict land based gouges that were created during a time of higher sea level. The subgouge deformation data obtained in these investigations are thought to be representative of full scale events involving large ice masses. However, because the mass of the ice feature that produced the relict gouge is unknown it is not possible to know the energy it had during the gouging event. Also, the state of the soil before the gouging event is not known. Without this information, relict gouges only provide evidence that subgouge deformations occur and may provide information on gouge mechanisms but are of limited value for the calibration of numerical modelling procedures.

In northern Manitoba, glacial land based gouges can be seen in the old Lake Agassiz. The geometry of these gouge marks are known to be both linear segments and arcs, with the most common being linear segments. The linear tracks range in length from 300 m to 1800 m with widths measuring from 6 m to 40 m (Dredge, 1982). These tracks form a U-shaped cross section in clays with a maximum observed depth of 2 m. In sands, gouges have been seen to have a more rounded track. The rounded track is likely due to different infill behaviour.

Excavation studies (Woodworth-Lynas and Guigne, 1990) have been conducted on the ice gouge formations in Lake Agassiz to determine the extent of subgouge deformations caused by ice gouging in these regions. Two gouges were excavated at a depth of approximately 8 m. These gouges were 50 m in width and approximately 6 km to 8.5 km in length. From analysis three types of faults were observed; low angle faults, sub-horizontal thrust faults, and high angle faults. Low angle faults, which occur between the gouge centreline and the inner berm flanks, were seen to extend to at least three metres below the bottom of the gouge trough. Extrapolation of these faults suggests that they can extend to a depth of about 6 m below the bottom of the gouge trough. An understanding of these low angle faults has considerable implications when considering the protection of buried pipelines. Sub-horizontal thrust faults occur within the berms and are related to the stacking of clay slabs and are responsible for the structural berm building process. High-angle faults occur on the outer berm flanks and are related to the collapse of stacked clay slabs.

### **2.3 Small Scale Observations**

Small scale field programs have been conducted on the tidal flats of the St. Lawrence River (Poo-roo-shasb and Clark, 1990). When the St. Lawrence thaws during spring the ice cover breaks up causing small ice masses, approximately 25 tonnes in size, to gouge the seabed. These ice masses are carried by the rivers current and the outgoing tide causing small gouge marks.

A site study was conducted on five scour marks. Indications of subgouge soil deformations were obtained through the variation in shear strength measured at various depths. The shear strength profile correlated with surface contours suggested that the subgouge soil deformations were associated with surface displacements during the scour event.

### **2.4 Ice Ridge Formation and Geometries**

Ice ridge formation differs from the formation of an iceberg. Icebergs are formed from freshwater glacial ice that breaks off into the sea from the parent glacier. This mechanism is known as calving. Ice ridges are formed from frozen saline water and have a porous and very complex internal structure. Due to the structural nature of ice ridges, they are significantly weaker than icebergs. Ice ridges are formed from compression loading that occurs in the plane of the ice cover caused by winds, currents, and Coriolis forces. Ice ridges are categorized into two groups: first year and multi-year ridges. Multi-year ridges are thicker ridges that survive one or more summer thaws and as a result of brine drainage and keel consolidation have higher strengths than first year ridges.

An analysis was conducted by Timco and Burden (1997), on 176 ice ridges comprising of 112 first-year and 64 multi-year ridges. The first-year ice ridges were further subdivided into Beaufort and temperate locations such as Labrador Sea, Baltic Sea, south Bering Sea, and Northumberland Strait with each group containing 46 and 66 ice ridges respectively. The multi-year ice ridges were also subdivided into Beaufort and Queen Elizabeth Island locations. With each group containing 53 and 11 ice ridges respectively. The ridge information was taken from 22 different data sources. The information included in the various data sets were sail geometry, keel geometry, thickness of the consolidated layer, thickness and distribution of the snow layer, and the strength and porosity of the ridge.

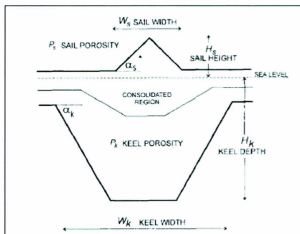


Figure 2-2- Schematic illustration of a first-year ice ridge (Timco and Burden, 1997)

The different data were plotted to investigate any trends using two different curve fits: a simple linear relationship (forced through the origin) and the best fit power relationship.

For most cases there was very little difference between both approaches. The authors noted that there were large asymmetries in the ridge, with non-symmetrical sails and keel, and a non-alignment of their centres. Although some keels had the characteristics of a classical first-year ridge.

There was seen to be a trend of increasing keel depth with increasing sail height. The best fit linear relationship and best fit power relationship are shown in Equation 2-1.

$$H_k = 3.95H_s \text{ or } H_k = 4.60H_s^{0.88} \quad (2-1)$$

The data was also fitted to a log-normal distribution in which the mean was 4.46 with a standard deviation of 1.85.

There was also a general trend of increasing keel width to increasing keel depth. The best fit linear relationship and best fit power relationship are shown in Equation 2-2:

$$W_k = 3.91H_k \text{ or } W_k = 5.67H_k^{0.87} \quad (2-2)$$

Because the keel depth is related to the sail height and keel width, a plot of keel width versus sail height was constructed and revealed an increasing trend. The best fit linear relationship and best fit power relationship are shown in Equation 2-3:

$$W_k = 14.85H_s \text{ or } W_k = 20.75H_s^{0.78} \quad (2-3)$$

The sail and keel angles were also studied in the Timco and Burden (1997) analysis. There was seen to be a high variability between sail and keel angles for both regions and therefore the data and individual log-normal plots were constructed (Timco and Burden, 1997). For the temperate ridges, the mean sail angle was 20.7°, with a standard deviation

of  $11.5^\circ$ , while the Beaufort ridges had a mean sail angle of  $32.9^\circ$ , with a standard deviation of  $13.4^\circ$ . Figure 2-3 below shows a sketch of a typical first-year ice ridge.

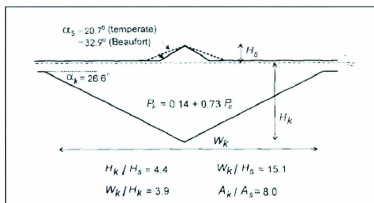


Figure 2-3- Schematic of an average first-year ice ridge (Timco and Burden, 1997)

A similar analysis of multi-year ice ridge data was conducted by Timco and Burden (1997). A plot of keel depth versus sail angle was generated from both Beaufort and QE Islands. However, there was considerable scatter seen in the QE Islands data and therefore it was omitted. There was seen to be a trend of increasing keel depth with increasing sail height with the Beaufort data. The best fit linear relationship and best fit power relationship are shown in Equation 2-4:

$$H_{k,m} = 3.17H_{s,m} \text{ or } H_{k,m} = 3.66H_{s,m}^{0.91} \quad (2-4)$$

The data was also fitted to a log-normal distribution in which the mean was 3.34 with a standard deviation of 0.85. The keel to sail ratio of the QE Islands region were higher, with a mean of 4.7 and a standard deviation of 1.5.

The sail and keel angles for the multi-year ridges were also studied in the Timco and Burden (1997) analysis. Unlike the first-year ridges the data for the multi-year ridges appear to follow a normal distribution. The mean sail angle was seen to be  $19.5^\circ$ , with a standard deviation of  $8.5^\circ$ . Figure 2-4 below shows a sketch of a typical multi-year ice ridge.

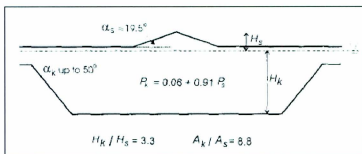


Figure 2-4- Schematic of an average multi-year ice ridge (Timco and Burden, 1997)

The keels of multi-year ridges were found to be much broader than that of first year ridges. Also, the shape of multi-year ridges is rectangular while first-year ridges are generally triangular in shape.

A study by Frederking et al. (1999) analysed data presented in studies by Beketsky et al. (1997) and Surkov and Truskov (1995) on first-year ice ridges in the Okhotsk Sea of the Sakhalin region. The data from both studies were compiled by Frederking et al. (1999). It was determined that the data collected by Surkov and Truskov (1995) give an average keel to sail ratio ( $H_k/H_s$ ) of 5.4. Surkov and Truskov (1995) proposed an average ratio

of 4.0. Beketsky et al. (1997) plotted the distribution of the relationship of  $H_s/H_k$  and determined that 50% of the ridges studied had a ratio in the range of 5.0 to 7.0.

The data presented by Beketsky et al. (1997) and Surkov and Truskov (1995) were compiled with the data by Timco and Burden (1997) to compare the Sakhalin area with the Arctic area. The same keel proportions were seen across both regions. When the entire ridge data is compiled an average  $H_k/H_s$  of 5.0 is seen, but with values ranging from 2.0 to 7.0.

Beketsky et al. (1997) proposed the following relationships for a first-year ice ridge:

$$H_k = 5.0H_s \quad (2-5)$$

$$W_s = 4.60H_s \quad (2-6)$$

$$W_k = 19H_s \quad (2-7)$$

with the keel and sail angles equal to  $24^\circ$  and  $14^\circ$  respectively.

Figure 2-5 and Figure 2-6 plot the keel height and width as a function of sail height, respectively. There is good agreement seen between Timco and Burden (1997) and Surkov and Truskov (1995) relationships for  $H_k$  and Frederking et al. (1999) and Beketsky et al. (1997) relationships for  $H_k$ . The power relationship defined by Timco and Burden (1997) is in agreement with Frederking et al. (1999) and Beketsky et al. (1997) for small values of  $H_s$  and tends toward the linear relationship proposed by Timco and Burden (1997) and Surkov and Truskov (1995) for larger values of  $H_s$ .

There is some discrepancy between Timco and Burden (1997) and Beketsky et al. (1997) relationships for keel width as a function of sail height. The power relationship derived by Timco and Burden (1997) over predict the other relationships but tend towards Beketsky et al. (1997) at larger sail heights.

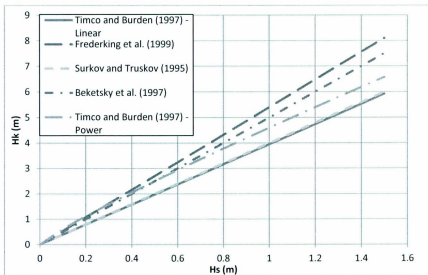


Figure 2-5 – Relationships for  $H_k$  as a function of  $H_s$

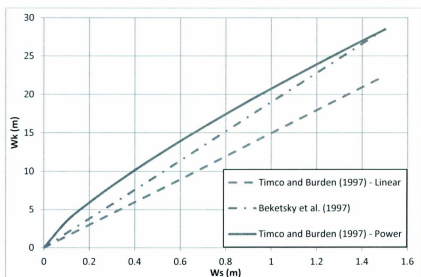


Figure 2-6 - Relationships for  $W_k$  as a function of  $W_s$

## 2.5 Ice Gouge Data for the Beaufort Sea

An understanding of ice gouge characteristics is essential when studying the effects of ice on the seabed and in turn the effects on buried facilities. Through repetitive mapping surveys, gouge features such as, depth, width, side berm height, and length have been obtained. This data has been collected through extensive programs, which utilize side scan sonar and echo sounders to capture this data. The first major gouge survey in the Beaufort Sea was undertaken by Environmental Studies Research Funds (ESRF). This information was known to be critical to engineering design and it was stored in the Beaufort Sea Ice Scour Base SCOURBASE system (Gilbert and Pedersen, 1986). The SCOURBASE project combined over 5000 km of acoustic survey data into a computerized format (SCOURBASE and ECHOBASE). Both SCOURBASE and

ECHOBASE are no longer updated (Myers et al., 1996). All new gouge data is added to the new gouge data base NEWBASE which contains gouge records from 1978 to 2005 of new ice gouges. The United States Geological Survey (USGS) has collected a significant amount of gouge data through seabed survey programs conducted in the 1970's and 1980's with little information added since then.

A thesis prepared by Caines (2009) studying gouge statistics from the Canadian and American Arctic Oceans gives an excellent compilation of gouge data collected for these areas. See Table 2-1 and Table 2-2 below for a summary of the Canadian and American Beaufort Sea gouge data used in Caines (2009). Figure 2-7 and Figure 2-8 show Histograms divided into 0.1 m bins of Canadian and American Beaufort Sea gouge data, respectively.

Table 2-1 – Summary of Canadian Beaufort Sea Ice Gouge Surveys (Caines, 2009)

Ice Gouge Data Collection	Survey Date	Age of Data	Number of Gouge Depth Records per Water Depth		
			< 5 m	5 - 25 m	> 25 m
Wahlgren (1979)	1974	Old	0	0	177
Shearer et al. (1986)	1974-1984	New	0	472	63
Comfort et al. (1990)	Unknown	Old	0	2580	2660
Myers et al. (1996)	1989 & 1990	Old	0	45	144
Myers et al. (1996)	1978-1990	New	0	4686	171

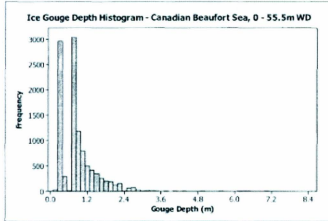


Figure 2-7 – Canadian Beaufort Sea Ice Gouge Depth Data (Caines, 2009)

Table 2-2 - Summary of American Beaufort Sea Ice Gouge Surveys (Caines, 2009)

Ice Gouge Data Collection	Survey Date	Age of Data	Number of Gouge Depth Records per Water Depth		
			< 5 m	5 - 25 m	> 25 m
USGS 78-730 (Barnes et al., 1978)	1973 & 1975-1977	Old	0	130	0
USGS 78-730 (Barnes et al., 1978)	1973 & 1975-1977	New	0	125	0
USGS 83-706 (Rearic & McHendrie, 1983)	1972-1973 & 1975-1981	Old	403	1446	556
USGS 89-151 (Weber et al., 1989)	1977-1985	New	11	2356	11

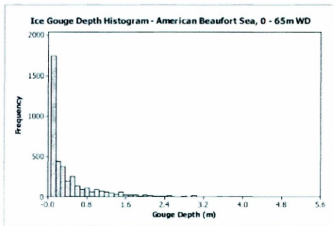


Figure 2-8 - American Beaufort Sea Ice Gouge Depth Data (Caines, 2009)

## 2.6 Interface Friction Coefficients

The coefficient of friction ( $\mu$ ) that is seen at the interface of an ice block moving along a soil surface is not well quantified or verified and thus some uncertainty exists when selecting appropriate values. The friction observed at the interface between an ice keel and soil can be highly variable. The formation of an ice feature from ice rubble will have surface undulations that can have a great effect on the interface friction while smoother ice pieces will experience a lower interface friction due to fewer irregularities in its surface. Also, normal loads will tend to consolidate the ice keel and also provide increased friction force between blocks of ice, however, the keel will ultimately deform and fail through shear.

Various studies focused on predicting ice ride up on beaches and shorelines were conducted (Shapiro and Metzner, 1987; Utt and Clark, 1980; Barker and Timco, 2003).

The main purpose of these investigations was to determine an appropriate friction coefficient, which could be used in ice ride up prediction formulae.

Utt and Clark (1980) performed friction tests on three types of soil: silt, sand, and gravel. In these tests the ice block was submerged in water using lead weights. High friction coefficients were seen in all three cases (see Table 2-3 ). The authors attribute these values to low contact pressures, smoothed surfaces, and the submerged test blocks.

Table 2-3- Static friction coefficients (Utt and Clark, 1980)

<b>Material</b>	<b>Static</b>
Silt	0.9
Sand	1.01
Gravel	1.28

Shapiro and Metzner (1987) conducted a large-scale field study to assess the friction coefficient between gravel and ice. Large blocks of sea ice, which were cut from a leading ice edge, were dragged along a gravel beach by a bull dozer at approximately 0.3 m/s. Two types of ice blocks were considered, one with a vertical plane face (3 m by 3 m by 2m) and one with a sloping plane face (2.7 m by 2.2 m by 1.2 m). The authors determined that the shape of the leading face of the ice mass was not important to the friction coefficient. The static and kinetic friction coefficients for this study are shown below in Table 2-4.

Table 2-4 – Friction coefficients (Shapiro and Metzner, 1987)

Beach	Ice Face	Static	Kinetic (0.3 m/s)
Sloped	Sloped	0.49	0.38
Sloped	Vertical	0.51	0.39
Flat	Vertical	0.64	0.54

A laboratory study by Frederking and Barker (2001) investigated the coefficient of friction between sea ice and various construction materials such as smooth and rough concrete, corroded and smoothed steel, wood, and ice. The authors found that the friction was higher at lower speeds and on rough materials. The average coefficient of friction of sea ice on smooth materials was about 0.05 for speeds greater than 0.05m/s and increased to 0.1 when the speed was 0.01m/s. The average coefficient of friction on rough concrete and corroded steel was approximately 0.1 at speeds greater than 0.01m/s and 0.2 at a speed of 0.01m/s. A weak trend between a lower coefficient of friction at high contact pressures was also seen. The kinetic friction coefficients for this study are shown below in Table 2-5.

Table 2-5- Kinetic friction coefficients for various construction materials (Frederking and Barker, 2001)

Material	( $\geq 0.01$ m/s)	( $\geq 0.05$ m/s)	(0.1 m/s)
Concrete (Rough)	0.2	n/a	0.1
Concrete (Smooth)	0.12	0.06	0.05
Steel (smooth painted)	0.09	0.06	0.05
Steel (corroded)	0.15	0.1	0.13
Wood	0.15	0.12	0.08
Saline Ice	0.09	0.05	0.03

Barker and Timco (2003) conducted experiments to investigate the friction coefficient between freshwater ice and soil. The soil used in this study was a mixture of fine well-graded gravel and coarse well-graded sand. The mixture consisted of 1 part sand to 2/3 part gravel. Both smooth and rough soil surfaces were considered in the study. Four different friction coefficients were measured: static, bulldozing, transition, and sliding. The results of this study are shown in Table 2-6.

Table 2-6- Static and mean kinetic friction coefficients (Barker and Timco, 2003)

<b>Velocity</b>	<b>Static</b>	<b>Bulldozing</b>	<b>Transition</b>	<b>Sliding</b>
0.05	0.52	0.55	0.54	0.43
0.1	0.50	0.46	0.39	0.25
0.2	0.52	0.36	0.27	0.22
0.1	0.51	0.38	0.31	0.23
0.02	0.52	0.42	0.41	0.33
0.05	0.48	0.43	0.38	0.30

Static friction coefficient was calculated from the initial force at the moment of contact between the ice and the seabed. Bulldozing section was the region where the ice would dig into the seabed creating a trench and the transition zone occurs when the ice rides up out of the trench it had created. After the transition zone the ice moves into a steady state sliding friction zone.

A decreasing trend in friction coefficient was seen as the block moved from static to sliding. Also, a decrease in the coefficient of friction with an increase in velocity was seen. Static friction coefficients were consistent over all tests with a mean of 0.5.

## **2.7 Theoretical and Analytical Models**

Chari (1975) developed a work energy balance analytical model in order to analyze the effects of an iceberg gouge event. Environmental driving forces were ignored and the only driving force for the iceberg was its own kinetic energy. The kinetic energy of the moving iceberg was balanced with the work done in clearing the soil along the scour, which was calculated based on soil mechanics theory. This model was able to predict theoretical gouge lengths and depths for various physical parameters but underestimated both the resistance and the load.

Chari and Muthukrishnaiah (1978) extended the model to account for current effects. Theoretical gouge lengths calculated using this model could be up to 160% longer than this calculated by the initial model. Chari and Green (1981) included side friction of the gouging iceberg into the analytical model. They found an overestimation in gouge depths of about 10% occurred when side friction was ignored.

When Prasad (1985) included non-linear velocity effects, of the iceberg during the gouging event, he concluded that the gouge depths were 16% higher than those calculated using linear velocity.

A work-energy model was developed by FENCO (1975) along with a dynamic model, which uses a force-balance approach for the gouge event. The first model incorporated a block shaped iceberg gouging along a sloping seabed constrained only to move in the horizontal direction. The dynamic model also uses a sloping seabed but allows the iceberg to pitch and heave while moving horizontally (three degrees of freedom).

Comfort and Graham (1986) evaluated the model by Chari (1975) and the two models by FENCO (1975). It was concluded that both models over predicted gouge depths by up to a factor of two, where the model by Chari (1975) yielded gouge depths approximately 20% greater than those predicted by FENCO (1975).

These analytical models discussed above may not be representative of an actual ice gouge event. Chari (1975) does not consider heave of the iceberg or vertical forces that occur during a gouging event (only considered horizontal motion). Research has proven that icebergs do ride up as gouge depths remain constant during travel upslope (Woodworth-Lynas et al., 1986). Also, the model shape studied by FENCO (1975) may not be applicable to an actual gouging event. Been et al. (1990) stated that most Beaufort Sea keel have a low angle to the horizontal, usually less than  $30^\circ$ , and that their widths are larger than their depths, and this must be considered in the analysis of the gouge.

Been et al. (1990) developed an energy force model which uses plasticity theory as soil mechanics theories usually only consider small displacements. Analytical models of ice gouge have typically been considered a combination of passive earth pressure failure acting in the horizontal direction and bearing capacity failure acting in the vertical direction. Been et al. (1990) thought that serious error may occur when using this approximation. As a first validation exercise of the model the calculated gouge depths agreed well with an observed Beaufort Sea gouge.

## **2.8 Experimental Research**

### ***2.8.1 Ig Models***

These experiments are conducted in a laboratory under standard gravity. Various methods are used for preparing the test bed; from manual transfer of the soil followed by compaction, to acquire a certain density, to more advanced soil layout procedures such as raining sand down from a hopper to ensure seabed uniformity (Paulin, 1992). Markers are placed in the test bed to document subgouge deformations and gouge geometry. There are problems in modelling ice keel/soil interaction in the laboratory at single gravity because all of the laws of similitude cannot be followed. Some of these problems arrive from trying to scale sediment grain size, density, and shear strength. However, single gravity experiments are important for gaining insight into the various factors and relationships important to an ice gouge event.

As a validation exercise for his analytical model Chari (1975) performed a series of model tests in a sloping test bed to verify the soil resistance on a model iceberg during gouging. The model tests were also used to gain information on the scouring mechanics. Pressure and forces were measured on the model during the test.

It was determined that the main source of resistance on the model iceberg was due to passive soil resistance in front of the model. During the test, soil movement was observed below the gouge and pressure increases were recorded up to 1.5m away by pressure transducers in the soil. A subset of experiments was conducted where bands of coloured soil (sand and clay) were used in the test bed to observe the soil movement during

gouging. Failure surfaces were seen ahead of the model iceberg and also below the maximum gouge depth. However, subgouge soil displacements were not measured.

During these tests failure surfaces were observed to originate at the toe of the iceberg model and run at an angle of 25 to 30° to the horizontal toward the test bed surface. Failure surfaces were also observed up to 0.5 m in front of the model

A series of tests were conducted by Green (1984) in dry cohesionless sand. This set of tests studied the effects of different keel size and shapes, and measured pressure and forces on the model keel. The test bed was 6 m wide, 14 m long and approximately 1 m deep and also incorporated a model pipeline, which was equipped with pressure transducers. The test bed was also raked to attain a slope of 1:35.

Similar to Chari (1975), Green (1984) observed failure planes developing well in front of the model iceberg and the primary resistance on the model iceberg arising from passive soil resistance. The pipeline pressure cells responded to the iceberg 116 mm below the gouge base, which was the deepest burial depth of the model pipeline. No information was gained on pipeline displacement as the model pipeline was rigid compared to the soil.

Prasad (1985) extended the work by Green (1984) to analyze the effects of iceberg keel shape on seabed resistance when gouging into a sloping test bed. Six model shapes were used (See Figure 2-9).

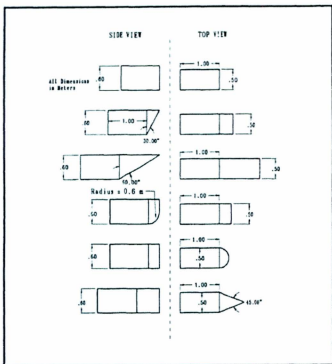


Figure 2-9 - Model Shapes used in Prasad Test Program (Prasad, 1985)

The gouge profile did not vary a lot with various model shapes but the pressures on the model and towing resistance did. It was determined that soils resistance on the model increased with increasing face inclination. However, interface pressures and subgouge soil displacements were not measured.

In 1979, as part of an APOA (Arctic Petroleum Operator's Association) project, model tests of ice gouging were performed to study a range of factors influencing this problem (Abdelnour et al., 1981). The experimental program consisted of 110 tests where soil

types, keel shapes, model scale, gouge depth, and gouge velocities were varied. The purpose of the program was to gain insight into the ice gouge process by studying model resistance, pressures generated in the test bed, pressures on the keel face and the scour morphology and how altering the above parameters influenced the test results. See Table 2-7 below for the range of test parameters used.

Table 2-7- Range of Test Parameters (Abdelnour and Graham, 1984)

<b>Test Parameters</b>	<b>Range</b>
Keel Shape	inverted pyramid (63° to horizontal) and rectangular prism
Keel Width (Rectangular)	26 cm and 52 cm
Gouge Depth	1 cm to 30 cm

The gouge characteristics provided information about the cut depth versus observed gouge depth as well as the gouge width. This data is valuable in predicting the possible shape of an ice keel from available data on gouge track configurations (Abdelnour et al., 1981). Through analysis of this data, potential ice keel shapes can be backed out of the results and matched to specific gouge configurations. This can provide valuable insight into the specific shape of gouges that produced certain seabed gouge marks.

Golder Associates Ltd. carried out 46 small scale gouge tests using both sand and clay test beds (Been et al., 1990). These tests were carried out to study soil deformations during a gouging event. Ball bearings were placed in the test bed in order to measure soil displacements beneath the gouging keel. Forces on the model keel were also measured.

Failure planes were observed in the tests along with a dead wedge of material in front of the inclined face of the keel. The series of tests showed subgouge displacements below

the keel. In medium and dense sand subgouge displacements were seen at approximately 2 cm below the keel while in loose sands, displacements were measured at a depth of approximately 7 cm. These subgouge displacements were attributed to a shear dragging mechanism (Been et al., 1990). It is important to note that these tests were not to steady state conditions.

It was determined that the extent of the shear dragging layer is important when determining a safe burial depth for a pipeline (Been et al., 1990). The pipeline should be situated far enough away from this zone to ensure its integrity. This zone is seen to be deepest in loose sands and soft clays. This study provides evidence that subgouge soil deformations are dependent on soil state.

A series of four model tests sponsored by the Canadian Oil and Gas and Gas Lands Administration were conducted at the Memorial University sand tank (Porooshab et al., 1989; Porooshab and Clark, 1990) to determine the size and nature of the deformation zone after a free field gouge event, surface morphology and how it changed after gouging, and the pore pressure response during gouging. Also, the effect of keel width and attack angle of the iceberg on the subgouge reaction was considered.

Dry silica sand with a residual friction angle of  $33^\circ$  was utilized for testing. This was overlain with a 10-20 mm layer of silty clay with a shear strength of about 10kPa and a plasticity index (PI) of about 8 (Porooshab and Clark, 1990). The sand was rained down from a hopper into the test bed (3 m wide, 8 m long and 0.6 m deep) at various rates to achieve several relative densities. During intervals in the raining procedure, load

cells and displacement markers were positioned within the soil. Displacement markers consisted of steel ball bearings, strands of solder, and chains of paper clips. The model keel was made from an aluminum alloy and was equipped with pressure cells that measured the normal pressures acting on the keel face. The model keel was mounted to a gantry via model struts and equipped with springs to allow for it to pitch and heave during gouging. See Table 2-8 for test parameters for this study. Gouge depth was set to 0.075 m in all tests.

Table 2-8- Test Parameters (Porooshab and Clark, 1990)

<b>Test</b>	<b>Attack Angle</b>	<b>Width (mm)</b>	<b>Relative Density (%)</b>
1	15	430	8/36
2	15	860	8/29
3	30	860	-2/46
4	15	860	60/18

During the experiment, as the keel advanced in the soil, a berm forming in front was observed. At the same time, rupture planes surfaced ahead and to the side of the keel, with rigid blocks of sand being pushed to the sides by the advancing keel. In looser sands there were numerous rupture planes with small blocks of material, while dense sands experienced few rupture planes with larger blocks.

Two factors that significantly affected the extent of subgouge deformation were soil density and the attack angle of the keel. Slight deformations were observed in dense soils with the amount of soil damage extending only 0.005 m below the gouge. However, for loose sands, soil deformations extended to 0.065m below the gouge. In Test 3 the attack angle of the keel was set to 30°. The increased angle of attack decreased the amount of

subgouge deformation along with a decrease in vertical force and an increase in the horizontal force seen by the sand. Table 2-9 is a summary of the vertical and horizontal forces experienced in each test and the orientation of their resultant vector.

Table 2-9- Force Results Summary (Pooorooshasb and Clark, 1990)

Test	$F_v$ pk	$F_h$ pk	$\alpha_{dense}$	$F_v$	$F_h$	$\alpha_{loose}$
1	6.5	5	50	2.5	2	50
1(corrected to gouge width)	13	10	50	5	4	50
2	9	8	49	7.25	6.5	48
3	7.5	8.5	41	2.25	2.75	40
4	12.5	9.5	51	8.5	7.5	49

From the data above, it can be seen that the denser sands contain a higher resultant angle, which denotes a higher vertical force. During gouging, the total stress was seen to dip with the approach of the model keel, then rise sharply, and then drop again to a steady state stress change.

As part of his thesis research, Paulin (1992) conducted several small scale physical model tests in the ice gouge research tank at Memorial University to measure displacements, soil stress response, forces acting on the model keel, and post gouge profiles. Tests were conducted for both dry and submerged conditions. The tank was approximately 14 m long, 6 m wide and 1.1 m deep and is divided into two smaller tanks by a centre wall. The test bed was made up of 6 to 7 m<sup>3</sup> of clean, dry silica sand. The test beds were prepared by raining down sand from about 2 to 10 cm above the sand surface.

The angle of friction between the model iceberg and the sand was determined by shearing samples of the sand against a block cut from the same type of aluminum as that used in the construction of the model iceberg. The angle of friction measured was 23°.

Instrumentation was placed in the test bed in order to measure pore pressures, stresses and displacements. Total stresses in the soil were measured using two waterproof load cells. Displacement markers were placed in the test bed to provide information on soil displacements. The markers consisted of 0.5 in diameter stainless steel ball bearings, 1 mm diameter solder strands and spaghetti strands which became soft when exposed to moisture.

The aluminum model iceberg was 0.43 m wide, 1.2 m long, and had an attack angle of 15°. The model iceberg was parallelepiped geometry with the bottom face 0.412 m in length. The gouge depth for the tests was set to 4cm. The results of this study were not scaled to a prototype event; however, they were used to gain insight in the factors and trends that are imperative to the ice gouge process. The model was connected to a mounting frame via four beam load cells which measured the vertical forces acting on the iceberg during scouring. The model was also equipped with two horizontal load cells and five face pressure load cells.

During both tests a spoil of sand was seen to build in front of the model iceberg and cleared to side berms. It was observed that the frontal mound reached a maximum height of about 15 cm above the test bed surface. Some infilling of the track path behind the model was also seen as it progressed. Blocks of soil were seen to surface between

rupture planes during gouging and failures were noticed up to approximately 50 cm in front of the model. Ball bearings positioned beneath the gouge were seen to be pushed down and laterally in the gouge direction. Balls located above the gouge cut depth were caught in the mound in front of the model and deposited in the berm.

The vertical forces experienced by the model tend to increase to a steady state value, until the model reached the end of the test bed where it is no longer in contact. Horizontal forces experience the same trend, where a steady state value is reached during the gouging event. Figure 2-10 and Figure 2-11 illustrate typical results of vertical and horizontal forces on the model iceberg during testing.

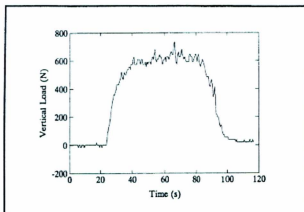


Figure 2-10- Beam Load Cell 2, Test 2 (Paulin, 1992)

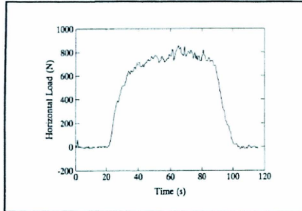


Figure 2-11- Horizontal Load Cell 2, Test 1 (Paulin, 1992)

The stress increases were measured to a depth of 1.5 gouge depths below the model keel. This was to the extent of the measurement devices. Displacement markers were also measured to their extent at 0.12m below the gouge depth.

Ishikawa et al. (2005) conducted a small scale tests program in dry sand to study the effects of keel attack angle, gouge rate, and gouge depth on the soil stress field and the seabed reaction forces. The model keel was restrained to only move in the direction of gouging, with three different attack angles of  $30^\circ$ ,  $45^\circ$ , and  $90^\circ$ . The gouge rate of the keel varied between 1 cm/s to 30 cm/s and the gouge depth was 3 cm to 6 cm, which was set prior to gouging. The specific gravity of the sand was 2.66 and the dynamic frictional coefficient at the interface of the keel and soil was 0.32. The stress state of the soil was measured by pressure sensors buried 30 mm below the gouge depth at three different locations along the gouge centreline. At the middle pressure sensor, two additional

sensors were placed at 30 mm and 60 mm below the initial sensor to measure varying soil stress with depth.

The stress in the seabed was highest when the leading edge of the keel was nearly directly above the pressure sensors. This was observed as a sharp peak in the pressure sensor response. The distance between the ice keel and the pressure sensor, when the peak response was observed, increased with a decrease in the keel attack angle. The distance ranged from 50 to 80 cm with a gouge depth of 3 cm and from 80 to 120 cm with a gouge depth of 6 cm. The effect of gouge rate on the keel was not clearly observed. However, the vertical stress within the seabed was seen to decrease with an increase in gouging rate while the stress in the horizontal direction did not show a clear dependency on the rate of gouging. The authors, however, used the peak values from the pressure sensors as a representation of the stress within the seabed. This may not be truly representative of the actual stress state in the soil. Also, the stress seen in the soil tended to increase with a decrease in attack angle but with only a small difference between the 30° and 45° cases. Measurement of keel reaction forces, for the 30° keel case, demonstrated a higher horizontal force than vertical, with values of approximately 500 N and 400 N respectively. When the attack angle was increased to 90° the vertical force decreased to near zero while the horizontal force was approximately 280 N.

To compliment the test program by Ishikawa et al. (2005) described above, a set of medium scale tests were conducted by Kioka et al. (2006) at the dredge soil disposal site on the western wharf in the Ishikari Bay New Port. These tests also considered the effect

of relative soil density on the stress developed in the seabed. The size of the keel and the gouge depth were four times that of the small scale model tests. The keel attack angle was set to  $45^\circ$  for all tests while the gouge rate was varied between 8.1 cm/s to 24.4 cm/s.

The horizontal force was measured with a load cell connected to the towing wire used to advance the keel. The ice keel was made of two components and the vertical forces on the keel were measured by a three point load cell placed between the two layers. Stress within the soil was measured by pressure sensors positioned along the gouge centreline and perpendicular to the gouge centreline.

In all cases the soil stress peaked just before the leading edge of the keel passed over the pressure sensors, which was the same tendency seen in the small scale tests by Ishikawa et al. (2005). The soil stress also showed a decrease with increase in depth below the gouge with negligible stresses occurring at about three gouge depths. The relativity density of the soil was determined an important factor as the soil stress for the high density case was almost twice that of the normal density soil used for all other cases. Due to short gouge lengths not allowing the keel to reach a steady state, limited information was gained after about four gouge lengths.

### 2.8.2 Centrifuge Models

A geotechnical centrifuge is used to conduct model tests for the purposes of studying geotechnical problems such as the strength, stiffness and capacity of foundations for bridges and buildings, and can also be utilized to predict soil response during an ice gouge event. The centrifuge may be useful for scale modeling of any large-scale nonlinear problem for which gravity is a primary force. The centripetal acceleration of the centrifuge, during rotation, simulates earth's gravitational pull. For example, if a model has a scale of  $N$  ( $N$  times smaller in its linear dimensions than that of full scale) and is placed in an acceleration field of  $N$  gravities, then the model will experience the same stresses as that of a full scale model. See Table 2-10 for scaling relationships for a centrifuge modeling program (Rizkalla et al., 1992).

Table 2-10- Centrifuge Modeling Scaling Relationships (Rizkalla et al., 1992)

Quantity	Full Scale (Prototype)	Centrifuge Model at $N$ g's
Linear Dimension	1	$1/N$
Stress (Force/Area)	1	1
Strain (Displacement/Unit Length)	1	1
Density	1	1
Mass	1	$1/N^3$
Force	1	$1/N^2$
Displacement (Distance)	1	$1/N$

Another advantage of the centrifuge is its small size allows for quicker seabed preparation and instrumentation set up than a full scale test. However this method, as with other small scale tests, has limitations which include: scaling of particle size, linked

to the formations of shear zones (Palmer et al., 2003), and permeability and path length for pore pressure dissipation.

Ice gouge experiments were performed on the beam centrifuge at the University of Cambridge Geotechnical Centrifuge Centre in Cambridge, England on a 1/100 scale model (Lach and Clark, 1994). Lach (1996) analysed this test series as part of his doctoral work. The experimental program considered nine tests, in which the test variables included: the prescribed soil stress history, attack angle and width of the model keel, and the gouge depth attained during steady state. Lach (1996) also tested the validity of the finite element method as a means of predicting soil response under an idealised scouring scenario was also evaluated. The numerical model adopted a two-dimensional plane strain representation of the scour event, where the soil was modeled as a two-phase nonlinear elastic-plastic material.

The soil consisted of Speswhite kaolin clay that was prepared in the laboratory in a steel cylindrical container, 850 mm in diameter and 400 mm deep. This container also served as the in-flight test bed for the experiments. Soil was consolidated by applying a pressure, in increments, through a solid piston, until the desired soil stress level was attained. The soil was equipped with pore pressure transducers to measure soil response during the gouge event and also to monitor the extent of consolidation during specimen preparation. Easily deformable materials were placed in a grid formation, both vertically and horizontally, to measure subsurface deformations. Lead shot markers placed in specified locations were used to evaluate surface soil displacements.

Model pipeline segments were positioned in the soil at various depths, perpendicular to the gouge direction. Stainless steel tubing 800 mm in length, 6.35 mm outside diameter, and a wall thickness of 0.25 mm were used to represent the model pipeline. The model pipelines were set into trenches that were excavated and then backfilled with the native soil.

The model keel was constructed from aluminum plates, for geometry, and balsa wood to provide buoyancy and establish the vertical stiffness of the model in free surface water. The model iceberg was connected to a gantry and was allowed six degrees of freedom. The drive system cable was connected to the model iceberg via a tension load cell which measured the horizontal force developed when the model was advancing. Contact pressures acting on the horizontal bottom face and the inclined face were measured to provide insight into the interface stresses during gouging. Table 2-11 shows the proposed test matrix and the variables studied in each of the tests. A comprehensive parametric study was not possible due to the limited number of tests able to be conducted.

Table 2-11- Proposed Test Matrix (Lach, 1996)

Test Number	$\sigma'_{va}$ (kPa)	Attack Angle (deg.)	Width (mm)	Vertical Stiffness (N/mm)	Test Variable
1	140	15	100	26	soil state
2	110	15	100	26	baseline
3	110	15	100	26	scour depth
4	110	15	100	61	soil state
5	140	15	100	61	baseline
6	200	15	100	61	soil state
7	140	15	50	31	model width
8	140	25	100	61	attack angle
9	140	15	80	49	125 g test

Due to the lack of restriction on the degrees of freedom of the model keel, it was not possible to accurately establish the magnitude of the gouge cut. In Tests 01 to 03 the model vertical stiffness was set to 2.6 MN/m which corresponds to a slab-sided free-floating ice mass of 265 m<sup>2</sup>. This below the range of vertical stiffness usually associated with an iceberg or pressure ridge. Therefore, the uplift seen in these tests were exaggerated. The vertical stiffness was then increased in subsequent tests to provide more realistic conditions.

The average gouging rate for Test 04 was 72.9 mm/s. An average gouge depth of 14.6 mm was attained from a brief period of up rise from the model icebergs nominal initial position of 20 mm. The corresponding berm elevations averaged about 3.1 mm above the original surface level.

In the steady state gouge region the maximum increase in pore pressure was about 88 kPa at a depth of 9.5 m below the initial surface and 0.9 m laterally outward from the scour

axis (at prototype scale). The peak value occurred when the model iceberg was at a horizontal distance of 8.6 m from the transducer. Pore suction of 37 kPa was experienced at the same location when the model iceberg had attained a distance of 5.2 m from the transducer. Figure 2-12 shows a plot of the pore pressure response for the eight transducers during gouge Test 04.

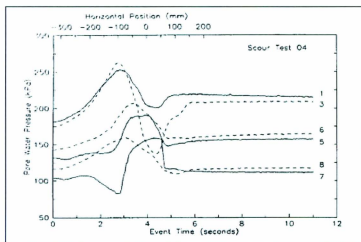


Figure 2-12 - Test 04 pore pressure responses during event (Lach, 1996)

Figure 2-13 displays the vertical and horizontal components of force versus horizontal position of the model iceberg. The vertical component of force was nearly four times as large as that of the horizontal component. The inclination of the resultant force vector was slightly above perpendicular to the scour face of the model iceberg, which indicates a smooth interface. The average magnitudes of the horizontal and vertical force, during steady state, were 4.1 and 16.1 MN (prototype scale) respectively.

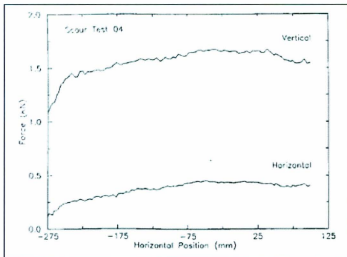


Figure 2-13 - Test 04 horizontal and vertical components of the resultant force (Lach, 1996)

Horizontal and vertical displacements are given in Figure 2-14 below. The maximum vertical and horizontal displacements immediately below the gouge base were 0.94 m and 1.52 m respectively (prototype scale). The maximum depths below the base of the scour at which vertical and horizontal displacements measured were 3.2 m and 3.1 m respectively at prototype scale. Normalized values of vertical and horizontal displacements extended to 2.1 and 2.0 gouge depths below the gouge base.

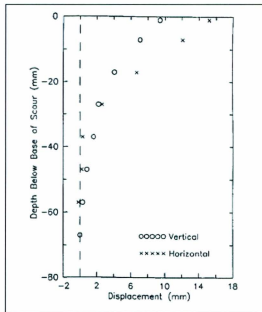


Figure 2-14 - Vertical and horizontal components of soil displacement (Test 04) (Lach, 1996)

Test 05 was the baseline for Tests 04 to 09. This test considered the same test conditions as Test 04 with the exception of the consolidation stress, which was set in the laboratory to 140 kPa. The average gouging rate for Test 05 was 72.1 mm/s. An average gouge depth of 12.1 mm was attained. The corresponding berm elevations averaged about 4.3 mm above the original surface level.

Figure 2-15 displays the vertical and horizontal components of force versus horizontal position of the model iceberg. The vertical component of force was 3.4 times larger than that of the horizontal component. The average magnitudes of the horizontal and vertical force, during steady state, were 5.0 MN and 16.9 MN (prototype scale) respectively.

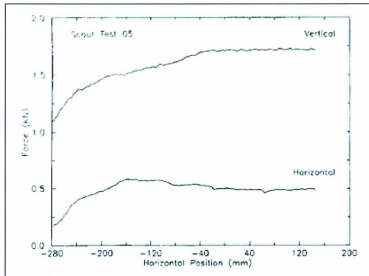


Figure 2-15 - Test 05 horizontal and vertical components of the resultant force (Lach, 1996)

Horizontal and vertical displacements are given in Figure 2-16 below. The maximum vertical and horizontal displacements immediately below the scour base were 0.88 m and 1.29 m respectively (prototype scale). The maximum depths below the base of the scour at which vertical and horizontal displacements measured were 6.2 m and 3.0 m respectively at prototype scale. Normalized values of vertical and horizontal displacements extended to 5.1 and 2.5 scour depths below the scour base.

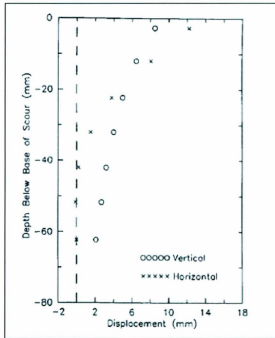


Figure 2-16 - Vertical and horizontal components of soil displacement (Test 05) (Lach, 1996)

Test 08 examined the effect of keel angle on soil response, with the attack angle of the model iceberg set to  $25^\circ$ . The model iceberg experienced water leakage under elevated pressures in the centrifuge which increased the buoyant weight of the model. After 3.1 seconds the model advanced a distance of 171 mm, with an average scouring rate of 61.0 mm/s. The model was stopped for a duration of 160 seconds and restarted with an average rate of 0.52 mm/s. The model advanced an additional 174 mm in 325 seconds. A steady state scour depth of 22.3 mm was attained. The corresponding berm elevations averaged about 7.7 mm above the original surface level.

In the steady state scour region the maximum increase in pore pressure was about 47 kPa at a depth of 7.2 m below the initial surface (at prototype scale). The peak value occurred when the model iceberg was at a horizontal distance of 0.3 m from the transducer.

The horizontal force data was considered unreliable as the magnitudes were much lower than anticipated for this type of keel geometry. The vertical component of force was 3.0 times larger than that of the horizontal component. The average magnitudes of the horizontal and vertical force, during steady state, were 5.9 and 17.6 MN (prototype scale) respectively over the final section of the gouge event.

The maximum vertical and horizontal displacements immediately below the scour base were 0.44 m and 2.84 m respectively (prototype scale). The maximum depths below the base of the gouge at which vertical and horizontal displacements measured were 0.7 m and 2.8 m respectively at prototype scale. Normalized values of vertical and horizontal displacements extended to 0.3 and 1.4 gouge depths below the gouge base.

Woodworth-Lynas et al. (1996) developed empirical relationships to predict subgouge deformations in soft and medium clays for a flat faced indenter with a rectangular gouge cross section. The data used to derive these equations was from PRISE centrifuge tests conducted in C-CORE's geotechnical centrifuge. The experimental program consisted of ten tests with various, soil types, keel attack angles, gouge depths, and gouge widths. Passive markers of spaghetti and layers of coloured sand were used to measure the soil displacements. Horizontal gouge deformations were seen to extend to at least three gouge depths.

The empirical relationships below, developed by Woodworth-Lynas et al. (1996), considered a right handed coordinate system in which the x-direction was parallel with the advancement of the gouge, y-direction was measured transversely, and z was positive downwards. Displacement components are u, v, and w in the x, y, and z directions. The value u (0, 0, 0) is the horizontal displacement just below the gouge given by Equation 2-8

$$u(0,0,0) = 0.6\sqrt{WD} \quad (2-8)$$

where W is the gouge width and D is the gouge depth

The horizontal displacements are a maximum just below the gouge and exhibit an exponential decay as the depth below the gouge (z) increases (see Equation 2-9). A similar relationship can be seen from the vertical subgouge deformations (see Equation 2-10). However, the vertical displacements tend to decrease at a slower rate than the horizontal. But, the vertical deformation model was developed on limited data and is not reliable for predicting downward movement (Woodworth-Lynas et al., 1996).

$$\frac{u(0,0,z)}{u(0,0,0)} = \exp\left(-\frac{2}{3}\frac{z}{D}\right) \quad (2-9)$$

$$\frac{v(0,0,z)}{D} = \exp\left(-\frac{1}{3}\frac{z}{D}\right) \quad (2-10)$$

Horizontal displacements off the gouge centreline are given by the following piecewise model (See Equation 2-11). If u (0, 0, z) is the displacement in the gouging direction on the gouge centreline at a depth z, then the displacement u (0, y, z) at the same depth away from the centreline is given by:

$$\frac{u(0,y,z)}{u(0,0,z)} = \begin{cases} 1 & \text{if } \frac{y}{W} < \frac{1}{4} \\ \frac{1}{2} \left( 1 + \cos \left( \frac{2y}{W} - \frac{1}{2} \right) \pi \right) & \text{if } \frac{1}{4} < \frac{y}{W} < \frac{3}{4} \\ 0 & \text{if } \frac{y}{W} > \frac{3}{4} \end{cases} \quad (2-11)$$

## 2.9 Numerical Simulations

There are three main modeling techniques currently used to model ice keel/pipeline/soil interactions: Winkler (structural) analysis, two-dimensional continuum models and three-dimensional continuum models.

A Winkler Analysis uses a decoupled model evolved from the sub grade reaction proposed by Winkler in 1867. In this method, soil displacements are imposed on nonlinear springs that are placed along the pipeline at each node. The springs are placed in the axial, transverse vertical and transverse horizontal directions, which can be seen in Figure 2-17 below. The pipeline is usually modeled with structural beam elements. Each soil spring is independent and shear stresses between springs are not considered and rotation of the structure is usually ignored. Because of the decoupled model, any effects that the presence of the pipeline would have on soil displacement are ignored and lead to a conservative estimate of pipeline stress and strains. This is believed to lead to larger displacements of the springs, which in turn impose greater loads on the pipeline. This approach could lead to proposed burial depths that are neither technically nor economically feasible.

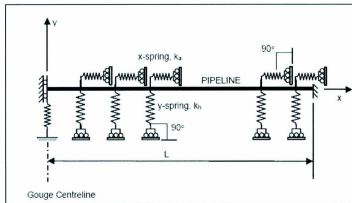


Figure 2-17- Schematic Illustration of a Winkler Analysis (Kennedy et al., 2000)

A two-dimensional continuum model uses a plane strain simplification of a complex three-dimensional problem. The coupled techniques used in these models allow for more accurate modelling of the pipeline/soil interactions than the Winkler Analysis. However, due to the two dimensional simplification, this method generally has a problem reaching steady state. The mound of soil that builds up in front of the keel during this process does not clear to the sides to form berms. This is due to the assumption that the keel has an infinite width (plane strain). Because the model does not reach a steady state, the user must know when the data obtained is no longer useful or use clearing criterion to keep the mound in front of the keel to an acceptable size.

A more accurate model can be built using a coupled three-dimensional model. The model uses the same techniques as the two dimensional continuum models but without the inability to model berm formation and to achieve a steady state during the gouging process. Because the keel has a finite width, berms form around the side as the frontal

ground clears, allowing the keel to reach steady state. The clearing of soil to side berms allow for lower and more accurate stress states in the soil. For continuum simulations of clay a total stress analysis is usually conducted assuming undrained conditions prevail. For modeling frictional seabeds effective stress parameters can be used within models such as Drucker-Prager.

### ***2.9.1 Winkler Model***

A Winkler model (Konuk and Fredj, 2004) was developed using ANSYS Mechanical FEM Software to conduct the analysis of various factors inherent in the ice gouge problem and the effect they have on pipeline stress and strain. A function that predicts subgouge deformations is used to determine the displacements of the springs. The pipeline is modeled using PIPE20 elements and also SHELL181 elements. The effects of temperature and pressure (1000 psi and 40 °C) on the pipeline are also considered in this model.

The analysis looked at various parameters such as pipeline burial depth, pipeline operating temperature and gouge width, and the effect that they have on pipeline strains. The stresses experienced by the pipeline were found to be a maximum at the centre of the gouge, however, this may not always be the case. As the pipeline burial depth increased, the strains in the pipeline decreased. This is due to smaller soil deformations at greater depths. Increasing the operating temperature was found to increase the strain on the pipeline.

As the gouge width increases, pipeline strains reach an asymptotic value while pipeline and soil displacements increased (See Figure 2-18). This would allow a pipeline size to be chosen depending on ice gouge widths experienced in the area being considered.

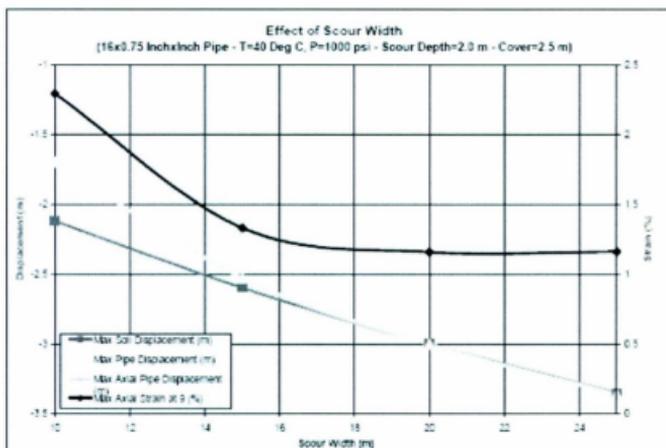


Figure 2-18- Effect of Scour Width (Konuk and Fredj, 2004)

A decoupled model developed at C-CORE using ABAQUS/Standard was used for the simplified analysis of the ice gouge problem (Kenny et al., 2000). The soil was modeled by one dimensional spring elements (SPRINGA) in which the response functions were derived from PRISE. The pipeline was discretized using beam (PIPE22) elements.

The beam elements were based on Timoshenko beam theory assuming linear elastic, transverse shear behaviour. Three degrees of freedom per node and quadratic shape

functions were used to define their behaviour. These elements do not consider local buckling of the pipeline or pipeline ovalisation.

The soil was assumed to be an elasto-plastic material. The subgouge deformation was determined at the soil's neutral axis for a given pipeline burial depth and keel geometry. The soil displacements were then imposed on the springs.

Cohesive and granular soils were the two base case soils that were used in this gouge analysis. The granular type soil was shown to cause less pipeline curvature due to its lower stiffness. The gouge width and depth was 10 m and 1 m respectively.

It was determined that a pressurized pipeline will experience greater strains than an unpressurized pipeline. The distribution of strain in both pressurized and unpressurized cases were similar.

A gouge width of 25 m was also analysed and caused the axial tensile strains to be reduced, as the axial strains near the centre were no longer additive (See Figure 2-19 and Figure 2-20 below).

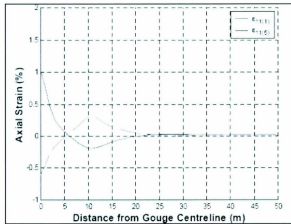


Figure 2-19- Pipeline axial strain response, 10 m gouge width (Kenny et al., 2000)

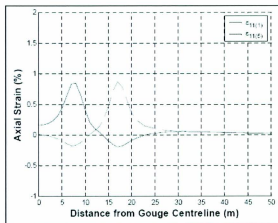


Figure 2-20- Pipeline axial strain response, 25 m gouge width (Kenny et al., 2000)

Increasing the gouge depth to 1.5 m showed a similar longitudinal strain distribution for both base cases with an increase in strain magnitude.

A study developed for BMT Fleet (Fredj et al., 2008) used two models in the analysis: one developed with ANSYS with idealized pipeline elements and one with LS-DYNA using shell elements. Both models used PRISE subgouge functions. The pipeline was restrained in the axial direction at both ends.

Maximum pipeline displacements were found to increase with increasing gouge width (Figure 2-21) and the maximum pipeline plastic strain and bending moment occurred at a critical gouge width of 6 m (Figure 2-22). Gouge widths of 6 m, 8 m, and 10 m were analysed. The Winkler model with shell elements is conservative when compared to the Winkler model with pipeline elements. This is attributed to the PIPE elements formulation. Both Winkler models were shown to be more conservative than the ALE model.

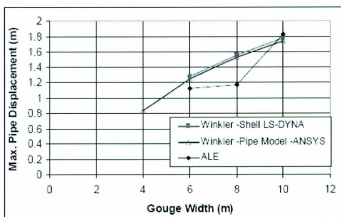


Figure 2-21- Max pipeline displacement for different gouge widths (Fredj et al., 2008)

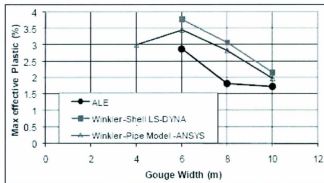


Figure 2-22- Max pipeline plastic strain for different gouge widths (Fredj et al., 2008)

Liferov et al. (2007) conducted a study to determine the pipeline response using both coupled and decoupled models. The pipeline was buried at a depth of 1.5m and was subjected to a 15 m wide by 1 m deep gouge with the keel having an attack angle of 30°. For the decoupled models, the pipeline was discretized using PIPE elements and the soil-pipeline interaction was simulated using non-linear spring elements in the axial, lateral horizontal, and lateral vertical directions. The gouge variables were the same as those given for the coupled simulation and an internal pressure was applied to the pipeline. The internal friction angle ( $\phi$ ) and submerged weight ( $\gamma'$ ) of the soil were 40° and 8.5 kN/m<sup>3</sup>, respectively.

Pipeline stresses and strains increased with decrease in pipeline clearance. Stresses and strains were also affected by the soil pipeline resistance force in the horizontal transverse direction and by gouge width. The internal pressure of the pipeline increased the stresses and strains developed. Maximum displacement and strain occurred at the gouge centerline, with some local maximum strains at about 16 m away from the gouge

centerline in the axial direction. See Figure 2-23 and Figure 2-24 for plots of the deformed pipeline shape and axial plastic strains for the decoupled model results.

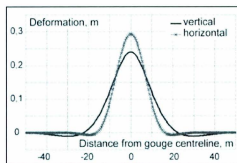


Figure 2-23- Pipeline deformed shape, decoupled model (Liferov et al., 2007)

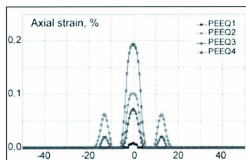


Figure 2-24- Pipeline axial plastic strains, decoupled model (Liferov et al., 2007)

### 2.9.2 Two-Dimensional Continuum Models

Due to limited computing power and finite element formulation constraints, the earlier ice gouge continuum models were developed with a plane strain assumption inside a Lagrangian framework. Lagrangian analyses were limited due to convergence issues caused by large mesh distortion inherent in these problems.

In order to test the validity of the finite element approach, to the ice gouge problem, a two-dimensional plane-strain model was developed to simulate the centrifuge tests describe by Lach et al. (1993) (Yang et al., 1994). The model keel's dimensions consisted of a 100 mm width, length of the horizontal bottom face of 50 mm and an attack angle of 15°. The elasticity of the soil was assumed to be linear and the plastic behaviour was defined by the extended Drucker Prager model described by Yang et al. (1994). Table 2-12 below lists some of the test parameters used for undrained and drained conditions.

Table 2-12- Material Parameters (Yang et al., 1994)

<b>Parameter</b>	<b>Undrained</b>	<b>Drained</b>
E (MPa)	5.73	5.00
$\nu$	0.49	0.30
c (kPa)	10.00	5.00
$\phi$ (degrees)	0.00	23.00
$\rho$ (kg/m <sup>3</sup> )	1700.00	700.00

The results at steady state for this analysis were compared to the average or maximum values recorded in the centrifuge tests. The average magnitudes of the horizontal and vertical forces recorded during the centrifuge tests were 328 N and 645 N respectively. For the undrained conditions, the steady state value demonstrated good correspondence with the physical model data with a horizontal force of 346 N. However, the vertical force experienced during the analysis was substantially higher during steady state, with a maximum value of 1096 N. Although the vertical force was considerably larger, this predicted the tendency of the iceberg to heave prior to reaching a steady state gouge depth.

The experimentally observed soil displacements were predicted in the numerical analysis. Formation of a frontal mound was observed as the material in the gouge was displaced forward and upward. Also, small backward horizontal soil displacements were predicted by the simulation. The numerical analysis yielded larger displacements but both studies indicated that horizontal movements are negligible at depths approximately three times the gouge depth.

A numerical model (Sayed and Timco, 2008) using a Particle-In-Cell (PIC) advection method was studied at the Canadian Hydraulics Centre. The simulations studied two dimensional soil deformations with the movement of a keel. The soil was moved with a forward velocity while the keel was held stationary. This was employed to simplify the velocity boundary condition. A reference case was used in order to study the effects of various parameters.

An initial simulation showed that soil deformations occurred along relatively narrow bands. The solids volume fraction was found to be highest in front of the rigid keel while relatively low values were found underneath the keel. This was due to the keel only having a forward velocity.

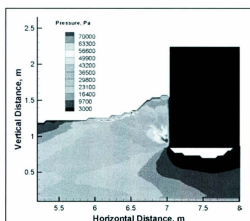


Figure 2-25 - Contour plot of pressure for reference case after 5 s (Sayed and Timco, 2008)

Analysis was done using a soil internal friction angle of  $\phi = 30^\circ$  for comparison with a base case of  $\phi = 40^\circ$ . The mean normal stresses were larger for a larger internal friction angle. The stresses predicted by the numerical model in front of the indenter were shown to be larger than that determined by passive earth pressure. The author attributes this to the inertia of the moving soil. Increasing keel velocity, while holding all other parameters constant, showed increases in soil mean stresses from 53 kPa for a velocity of 0.05 m/s to 167 kPa with a velocity of 0.25 m/s. Simulations were done using an initial solids volume fraction of 0.48, 0.55 and 0.58. Higher initial solids volume fraction corresponded to higher stresses experienced by the soil during the gouging event.

When comparing the simulation results to the experiments of Barker and Timco (2002), which studied the gouging of rigid ice blocks through sand and gravel, the numerical model gave noticeably higher stresses than the experimental model but followed a similar

trend. The higher stresses were considered to be due to the assumption of an infinitely wide keel for the numerical study. The experiments were done on an indenter of width 0.1 m which allowed the soil to be pushed around the indenter's sides. The experiments also took into account pore water pressure.

Velocity profiles showed that the velocity of the soil dropped with depth; from 0.15 m/s at the indenter base to 0.01 m/s at a depth of 0.25 m below the indenter. The soil velocity also showed exponential type decay. The horizontal normal stresses also dropped with an increase in depth.

The Pressure Ridge Ice Scour Experiment (PRISE) (Phillips et al., 2005) conducted research and development studies focused on the protection of marine pipelines and subsea facilities in environments subjected to seabed ice gouging. One of the main purposes of this program was to study the soil deformations experienced beneath the ice keel due to a gouging event. Two soil models were used in the PRISE investigations of soil response during a gouge event: elasto-plastic material with Drucker-Prager yield criterion and a Mohr-Coulomb soil model which was used for a parametric study of elastic modulus. A pure Lagrangian formulation was used for the soil mesh and a frictionless contact was assumed between the rigid keel and soil. The studies were conducted in ABAQUS/Standard. The preliminary study investigated seabed reaction forces, pore water pressures, soil displacements and plastic strain contours.

Horizontal movements of less than 50% of the gouge depth were obtained before numerical instability occurred, due to large element distortion during the gouge event.

The analysis did provide evidence that Lagrangian, 2D continuum FE modelling was reasonable for modeling the magnitude and distribution of subgouge deformation profiles.

Two-phase material behaviour based on a Cam-Clay model, finite strain formulation, and rigid surface interface elements to account for the ice keel-soil boundary effects were implemented to improve the model. Volumetric compression and strain hardening were found to increase the zone for subgouge deformations and stress fields.

In a study of dilatant soils, horizontal translations of 10 gouge depths were achieved. The parametric study conducted using the Mohr-Coulomb soil supported the magnitude and depth of subgouge deformations observed during the centrifuge tests. Plastic deformation extended to a few gouge depths and was consistent with other PRISE studies. It was also determined that the FEA was strongly influenced by the soil elastic modulus.

Lach and Clark (1996) utilized a detailed two phase material, using a Modified Cam-clay constitutive model, to analyse a free field gouge event. ABAQUS/Standard was the software package used in the development of model.

The soil was discretized using rectangular eight-node isoparametric elements with biquadratic displacement and bilinear pore pressure description. The soil parameters included the critical state stress ratio ( $M = 0.90$ ), the gradient of normal consolidation lines ( $\lambda = 0.25$ ), the gradient of the swelling lines ( $\kappa = 0.04$ ), the critical state reference specific volume ( $\Gamma = 3.44$ ), and a Poisson's ratio of ( $\nu = 0.33$ ). An UL formulation was

adopted in order to map the soil stress history and stress and strain states in the current deformed configuration. Solid continuum elements with a fully nonlinear formulation were used to model the soil.

The keel was modeled as an analytical rigid surface, through a connection of straight line segments. Contact between the rigid keel and soil was accomplished with the use of rigid interface elements. These interface elements formed part of the soil medium and allowed for contact between the keel and the soil. A standard Coulomb friction model was used with appropriate friction angles ( $\delta = 2.9^\circ$  to  $8.5^\circ$ ) to define the interaction at the keel/soil interface.

The numerical simulations were compared to three centrifuge tests (Lach and Clark, 1996); Test 04, Test 05, and Test 09. Magnitudes and profiles of pore pressures and soil displacements from the numerical model were shown to have good agreement with data obtained from physical Test 04 analysis. Horizontal forces predicted by the numerical model were in close agreement to the measured values obtained in the prototype. At low horizontal movements, the numerical model under predicted vertical forces, but closer correspondence was seen as horizontal movement increased (Figure 2-26).

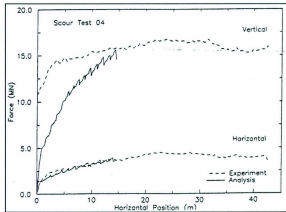


Figure 2-26- Test 04 comparison of measured and computed values of horizontal and vertical components of resultant force plotted against horizontal position (Lach and Clark, 1996)

The correspondence of the numerical tests with Test 05 and Test 09 was less satisfactory than Test 04 comparisons. The magnitude of the computed pore pressure field was in reasonable agreement with the experimental results, but the response did not show the same correspondence. The numerical analysis predicted greater values of horizontal and vertical forces than the Test 04 computed results, which was in agreement with the experimental predictions. The computed soil displacement patterns showed a similar trend to those of the Test 04 analysis. The computed vertical displacement magnitudes were comparable to lower bounds of the experimental data.

The initial state of the soil, and variation of test parameters such as keel angle of attack, was shown to have an effect on the mode of soil deformation. Plastic volumetric compression and strain hardening allowed for increased transmission of stresses and distribution of deformation over a greater depth of influence (Lach and Clark, 1996).

### ***2.9.3 Three-Dimensional Continuum Models***

LS-DYNA modeling software was used in developing a model to study both ice keel/soil interactions and ice keel/soil/pipeline interactions (Konuk and Gracie, 2004). The author looked at soil particle trajectories, with and without a pipe, and the effect of backfill of a trench with different soil parameters than the native soil.

The ice keel was modeled as a rigid indenter that was constrained in all rotational and translational degrees of freedom. Two main geometries of this keel were studied: sloped prism and cone with edge angle on the prism ranging from 45 degrees to 90 degrees. The ice ridge was modeled with rigid shell elements.

The soil was modeled with 8 node constant stress solid elements that were defined as Eulerian elements (nodes are fixed) due to large soil deformations experienced. A finer mesh was used where large strains and deformations were expected. The length of the model was sufficient enough to allow for steady state to be reached. An inviscid CAP clay constitutive model was used to model the soil properties.

The pipeline was discretized using shell elements. Depending on the study being conducted, the pipeline is either modeled as a rigid body or a deformable body.

The first study conducted was an ice keel/soil interaction where the soil particle trajectories were studied in both the plan and profile planes. Two types of weak clay were used in this analysis (soft clay and stiffer clay). It was determined that the soil moves in a boundary layer type fashion with the particles near the keel bottom having large

displacements while the particles inside the boundary layer experience decreasing displacements with increasing depth. Care should be used when examining the below figures as parameters used by Konuk and Gracie (2004) are not in line with parameters used in centrifuge experiments to develop C-CORE's PRISE function. Parameters such as: the attack angle was  $45^\circ$  for Konuk and Gracie (2004) compared to 15 to 30 for PRISE study, the soil strength was 2 kPa for Konuk and Gracie (2004) compared to 15+ kPa for PRISE study and a normally consolidated soil state was used by Konuk and Gracie (2004) compared to an overconsolidated soil state for the PRISE study.

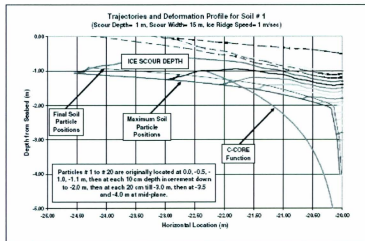


Figure 2-27- Particle trajectories for soft soil (Konuk and Gracie, 2004)

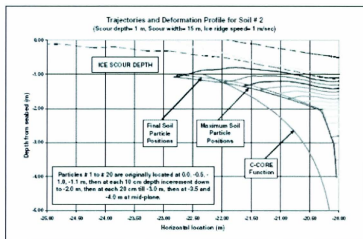


Figure 2-28- Particle Trajectories for stiffer soil (Konuk and Gracie, 2004)

The stiffer clay experiences smaller displacements than the soft clay in Zone 1 but in the subgouge regions the displacements are greater for the stiffer soil. This is attributed to the stiffer soil being able to carry a greater load therefore extending its displacements further into the subgouge region.

The soil particles move toward the berm during the gouge process. These results show that the trajectories are not affected greatly by keel cross section geometry but are influenced by the keel angle.

Konuk et al. (2005) studied the effect of trenching on the ice keel/soil/pipeline interaction, the backfill soils were taken to be softer than the native soil of the seabed. There were two soil types tested. The soil particle tracers experienced the same movement as those in the study of the native seabed soil except their movements were

much smaller and also showed boundary layer type behaviour as before. It was observed that the soil at the pipeline depth was pushed around the pipeline (either over or under). This protects the pipeline because minimal load is transferred if the soil is flowing around it. The stiffer the backfill soil the greater the load that would be transferred to the pipeline. The pipeline experiences a cyclic load pattern as the indenter passes over (loading and unloading). This cyclic load pattern cannot be modeled in a Winkler analysis.

A study on keel angle effects was conducted for a conical keel with attack angles varying from 15 to 45 degrees, with respect to the horizontal (Konuk et al., 2005). It was found that sub scour deformations are very sensitive to keel angle. Deformations increased as the attack angle decreased. The same holds for the vertical reaction force on the keel. Horizontal forces will be greater for higher angles of attack.

The three-dimensional model developed in Konuk and Gracie (2004) also tested the sensitivity of the following parameters: soil properties, clearance depth, pipeline diameter, gouge width, gouge depth, and gouge track orientation (Konuk and Yu, 2007a). It was determined that the soils cohesion had minimal effect on the pipeline displacements but increasing the soil hardening behaviour caused an increase in soil displacements.

As the gouge width increased, the pipeline displacements increased but the stresses did not follow the same trend. The von Mises stresses attained a minimum value at a 15 m gouge width, and showed significant increase at 10 m and 20 m with minimal change

when the gouge width exceeded 20 m. Also, the smaller the gouge width, the greater rebound experienced by the pipeline after the gouge process. These results did not agree with the Winkler model presented by Konuk and Fredj (2004). For the Winkler model, the pipeline stresses decrease when the gouge width increases. Increasing the gouge depth increased the vertical and horizontal displacements.

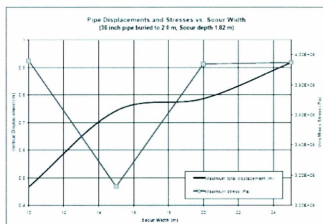


Figure 2-29- Maximum pipe displacements and stress for different scour widths, Continuum Model (Konuk and Yu, 2007a)

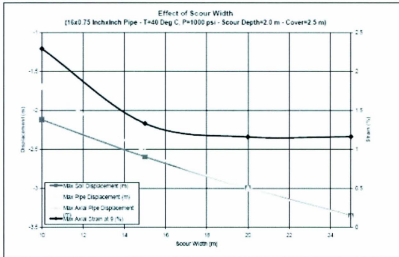


Figure 2-30- Maximum pipe displacements and strains for different scour widths, Winkler Model (Konuk and Fredj, 2004)

Analysis of the oblique gouge concluded that an oblique gouge is equivalent to a perpendicular gouge with a width calculated by the formula:

$$W_{perpendicular} = \frac{W_{oblique}}{\cos(\phi - 90)} \quad (2-12)$$

where  $\phi$  is the angle between the scour track and the pipeline axis.

The study of pipeline diameter indicated that pipeline displacements were a minimum for a 30 in. pipeline. The stresses seemed to remain relatively constant up to a 30 in. diameter and then were reduced for larger pipelines.

Kenny et al. (2005) developed a three dimensional continuum model using ABAQUS/Explicit. The soil was modeled using C3D8R (continuum three dimensional 8 node reduced integration) elements and the pipeline was modeled with S4R (shell 4 node

reduced integration) elements. These S4R shell elements have three degrees of freedom per node and are defined by linear shape functions. To eliminate boundary effects, the pipeline was extended for an additional 500 meters beyond the soil and was discretized using beam elements connected to spring elements. The penalty function approach was used to model the soil/pipeline and the keel/soil contact along with Coulomb friction criteria.

An Updated Lagrangian method with an adaptive mesh refinement was used. The soil that did not experience large deformations was left out of the adaptive mesh zone.

The keel was modeled as a rigid body with a conical geometry and an attack angle of 30°. von Mises yield criterion was used to model the soil as an elasto-plastic material. The soil parameters were that of an undrained clay material. Two soil types were selected for this analysis: medium clay and a cemented clay material. Trench soil was taken to be the same as the native soil. Kinetic and internal energies were monitored to ensure a quasi-static loading condition.

Analysis showed that pipeline deformations increased as the gouge depth increased (clearance decreased) from 1.0 m to 1.7 m (pipeline burial depth was 1.7 m). Pipeline deformations were also larger for the stronger soil ( $s_u = 100$  kPa). After the gouging event occurred, the pipeline stresses are not at their maximum levels due to some unloading. Maximum stress in the pipeline will occur at different stages of the gouging event but these do not differ greatly from the final stresses at steady state.

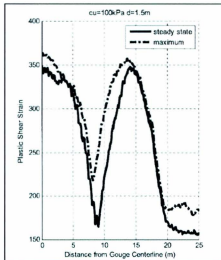


Figure 2-31- Comparison of maximum and steady state stress conditions (Nobahar, 2005)

Lateral soil deformations showed to be significantly greater than vertical deformations. This was attributed to the high attack angle ( $30^\circ$ ). This may differ if a smaller attack angle is used.

When compared to the Winkler type analysis, the continuum model showed lower pipeline deformations, strains and stresses with a similar pattern for pipeline deformation. The differences were most significant in terms of plastic shear strain. The lower soil reactions on the pipeline were partially contributed to the unloading during the gouging event and the reduced soil reaction due to combined loading. Soil fails at lower loads when it is loaded in various directions.

A numerical model was developed at J.P. Kenny (Jukes et al., 2008), which uses ABAQUS/Explicit with a CEL formulation to study the ice/soil/pipeline interactions. The

Eulerian domain has dimensions of 52 m long by 40 m wide by about 12 m high and is meshed with EC3D8R elements. The trench was also modeled in the Eulerian domain with a base of 1 m and a slope of 1:2. Velocity boundary conditions were applied to the outer extent of the Eulerian domain. The soil in this study was assumed to be one phase with loose and dense backfill, and a cap model was used. The velocity and angular velocity were set to zero in the perpendicular direction of the bottom and all side faces.

The pipeline was modeled as a 3D deformable body meshed with S4R elements with hour glass control. The pipeline's diameter was 12 in. with a wall thickness 0.7 in. The pipeline ends were restrained from translation and rotation in all directions.

The ice keel was modeled as a three dimensional rigid body meshed with C3D4 elements. Its attack angle was 20 degrees and the other three sides were 70 degrees. The analysis considered gouge depths of 2, 3, and 4 meters and general contact with a penalty formulation was used between the keel and the soil. The ice keel's velocity was set to 1 m/s.

The analysis studied the effects of gouge depth and trench back fill. Gouge depths of 2 m, 3 m, and 4 m were studied. Loose and dense sand were analysed as the trench backfill. The analysis determined that higher pipeline deflections are seen in dense backfills than in loose and with increasing gouge depth. Initially the pipeline is deflected downward due to the stresses built up in the soil. An unloading step occurs then where the pipeline rebounds upward as the keel moves over it.

Pipeline deflections occurred mostly in the horizontal direction. This may be attributed to the 30° angle of attack. Although higher deflections occur mostly in dense soils, sometimes looser backfill may cause higher bending moments due to limited boundary layer around the keel, which would lead to more concentrated loading on the pipe (Jukes et al., 2008).

The model (Jukes et al., 2008) was simplified to a keel/soil interaction in order to validate the subgouge deformations against available data. The results were compared to centrifuge experimental data (Lach and Clark, 1996), the empirical PRISE function (Woodworth-Lynas et al., 1996), and available numerical data in literature.

The subgouge displacements directly below the keel and for one to two gouge depths down are higher from this study than for the PRISE centrifuge results and PRISE subgouge displacement model. Although the displacements are much greater for this model, they tend to follow the same trend as the PRISE centrifuge results and the PRISE model.

Sensitivity studies were done to examine the effect of keel angle, keel geometry and also gouge depth. Small keel attack angles were found to result in larger subgouge soil displacements. Keel speed was set to 1 m/s with a gouge depth of 2 m. A study of gouge depth showed positive correlation between gouge depth and subgouge soil displacements.

For the study of keel geometry, the authors looked at two geometries: rectangular keels and conical keel. Soil displacements and berm formations were analysed. It was found

that conical shaped keels form higher berms than rectangular shaped keels. Also, steep keel angles form higher berms. It was also determined that the sharp edges of a rectangular keel produce higher stresses in the soil, just under the keel-soil contact, when compared to conical keels.

LS-DYNA was utilized in building a model for BMT Fleet (Fredj et al., 2008) using an ALE formulation. The dimensions of the model region were selected to ensure that boundary effects were negligible and that the model reaches a steady state.

The soil was defined using a two surface plasticity model, with friction and cohesion ( $c$ ) factors of  $17^\circ$  and 4.8 kPa respectively. The pipeline was modeled using reduced integration shell elements, with 5 integration point through the thickness.

The following loading sequence was used in the model: apply gravity for sufficient time, apply 30 MPa internal pipeline pressure, apply pipeline operating temperature of  $95^\circ\text{C}$  (from an initial temperature of  $15^\circ\text{C}$ ) and apply keel load.

The authors studied the effects of operating temperature and pressure, gouge width and trench bottom imperfections. Two cases for pipeline pressure and temperature were studied: Case 1 consisted of zero internal pressure with a differential temperature of zero (construction conditions) and Case 2 considered an operating temperature of  $95^\circ\text{C}$  and 30 MPa (operating conditions).

Case 1 was found to yield greater pipeline displacements in both the vertical and horizontal directions, along with a greater pipeline bending moment. The strain

experienced in the pipeline at operating conditions was four times as high as those experienced by the pipeline under construction conditions. At 7 m along the pipeline axis from the centreline, the pressurized pipeline experienced localized peak plastic strain

(See Figure 2-33).

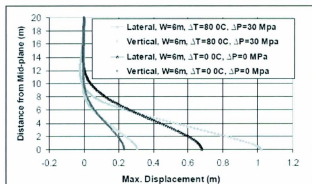


Figure 2-32- Pipeline displacements, Pressurized vs. Unpressurized (Fredj et al., 2008)

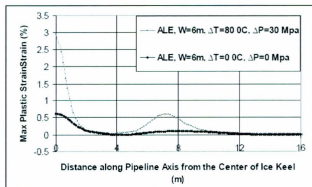


Figure 2-33- Pipeline plastic strain, Pressurized vs. Unpressurized (Fredj et al., 2008)

Gouge widths of 6 m, 8 m, and 10 m were studied. Maximum pipeline displacements increase with gouge width while the plastic strains did not follow the same trend. Maximum strain and bending moment occurred at a critical gouge width of 6 m.

An investigation into the forces produced during ice gouging was conducted by Fredj et al. (2008). The parameters considered in this study were gouge depths, widths, and their effects on the vertical and horizontal ice keel reaction forces. The effect of a pipe in soil scenario was also examined for its effect on ice keel reaction forces. Analyses were carried out using 3D continuum modelling with an Arbitrary Lagrangian Eulerian (ALE) formulation and a Smooth Particle Hydrodynamics (SPH) formulation. The platform used for the analysis was LS-Dyna 971. These results were validated with medium scale gouging tests conducted by Kioka et al. (2006).

The soil was modelled as dry soil, using a double hardening plasticity model and the ice keel was assumed rigid with an attack angle of  $15^\circ$ . The pipeline was discretized using reduced integration shell elements with 5 integration points through thickness. The pipeline was 1 km in length with an operating temperature of  $95^\circ\text{C}$  and a 30MPa operating pressure. The pipeline material was X70 steel with an assumed installation temperature of  $15^\circ\text{C}$ . Derating was applied to the material as per DNV, 2007.

The gouge depth was varied over three levels from 0.5m to 1.5m. The gouge width was also varied over three levels from 6m to 10m. Both the peak horizontal and vertical forces were seen to increase with and increase in gouge width and depth (See Figure 2-34 and

Figure 2-35). The ratio of vertical force to horizontal force ( $F_v/F_h$ ) ranged from 3.85 to 3.23.

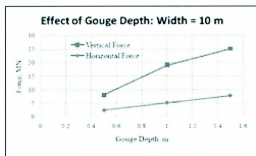


Figure 2-34 - Effect of gouge depth on ice keel reaction forces (Fredj et al., 2008)

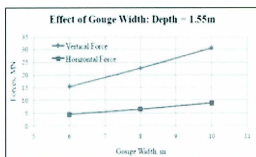


Figure 2-35 - Effect of gouge width on ice keel reaction forces (Fredj et al., 2008)

The peak forces were also seen to increase by approximately 5 to 10 % when a pipeline was introduced to the problem.

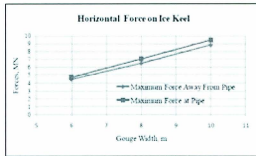


Figure 2-36 - Effect of pipeline on horizontal ice keel reaction force (Fredj et al., 2008)

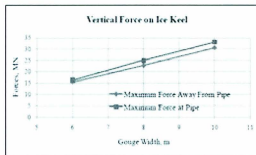


Figure 2-37 - Effect of pipeline on vertical ice keel reaction force (Fredj et al., 2008)

The study of trench imperfections consisted of a 12 inch pipeline buried with a 0.3 m vertical and lateral imperfection. At operating conditions, a burial depth of 2.23 m to the top of the pipeline was shown to prevent pipeline instability. The imperfection was shown to have small effect on the plastic strains experienced by the pipeline.

A numerical study conducted by Phillips et al. (2010) compared three different FEA techniques common to analysing the ice gouge problem; ALE and CEL formulations from ABAQUS/Explicit and ALE formulation from LS-DYNA which closely resembles the CEL formulation in ABAQUS (material flows through a fixed mesh in LS-DYNA).

The authors here extend the validation exercise to include gouge forces, frontal berm formation, seabed failure mechanisms, vertical SGD, and transverse SGD. The study consisted of six cases, shown below in Table 2-13. The program included three soil strengths of 25 kPa, 50 kPa, 100 kPa and two rigid keel geometries (trapezoidal and inverted truncated cone).

Table 2-13 – Keel-Seabed Cases (Phillips et al., 2010)

Case	Clay Strength ( $s_u$ ) (kPa)	Keel Shape	Keel Angle (Degrees)
1	50	Flat Face	15
2	50	Flat Face	30
3	50	Flat Face	45
4	25	Cone	30
5	50	Cone	30
6	100	Cone	30

The soil was modeled as clay using von-Mises criteria and constant undrained shear strength with depth was assumed. The Young's modulus (E) was taken as 60 times the undrained shear strength ( $s_u$ ), with a Poisson's ratio ( $\nu$ ), of 0.49. This gives a rigidity index ( $I_r$ ) of 20 which is appropriate for highly plastic overconsolidated clay (Phillips et al., 2010).

The three finite element procedures had comparable vertical and horizontal seabed reaction forces. The CEL analysis predicted slightly larger reaction forces than the other techniques. Figure 2-38 below shows the normalised horizontal reaction forces of all cases. The horizontal forces are normalised by the cross sectional area of the gouge and

the soil strength. The three conical cases normalize to the same line and are approximately 50% higher than that on the trapezoidal keel.

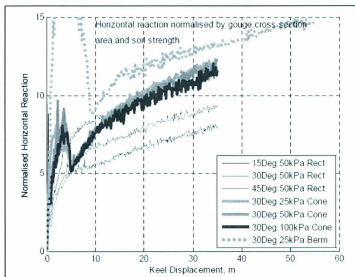


Figure 2-38 - Normalised horizontal keel reaction force development (Phillips et al., 2010)

Ratios of horizontal to vertical keel reaction forces are approximately 1 for a 45° attack angle and decreases to about 0.8 for a 30° attack angle and 0.6 for a 15° attack angle. These force ratios indicate a normal to the inclined face of about 0 to 15°. Unlike the forces, the force ratios are similar for the trapezoidal and inverted conical indenters (see Figure 2-39).

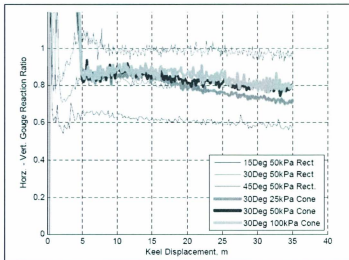


Figure 2-39 – Development of keel horizontal to vertical reaction force ratios (Phillips et al., 2010)

Figure 2-40 below shows the effect of keel angle on berm height. A trend of increasing berm height to keel angle was seen. However, the authors believe that the predicted berm heights are probably excessive due to the assumed cohesive strength of the soil.

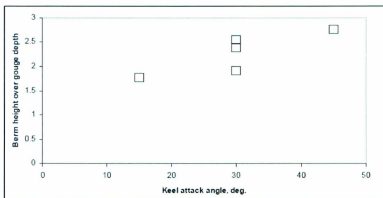


Figure 2-40 –Berm height versus keel attack angle (Phillips et al., 2010)

The SGD with changing keel attack angle was compared to the PRISE model (see Figure 2-41). Deformations within the top 0.5 m are strongly influenced by the shear discontinuity at the keel base due to constant strains in the 0.25 m high elements (Phillips et al., 2010).

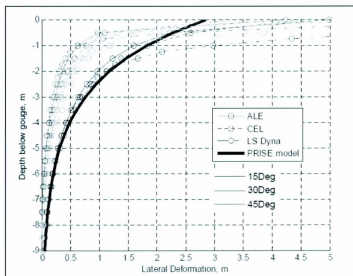


Figure 2-41 - Horizontal deformation comparison, Cases 1 to 3 (Phillips et al., 2010)

Vertical and transverse SGD were also considered against the PRISE model. The numerical analysis under predicted the results from the PRISE model for both vertical and transverse SGD. The lower deformations would mean lower bending strains developed in a pipeline when a keel passes over.

A parametric study was conducted at Memorial University (Pike et al., 2011) to examine the influence of attack angle and interface properties on soil behaviour and pipeline

mechanical response. This work utilized ALE formulations in LS-Dyna and CEL formulations in ABAQUS/Explicit to simulate both free field and coupled ice gouge events. The soil was discretized using an 8 node Eulerian elements with reduced integration (EC3D8R) and the pipeline with a four node reduced integration shell element (S4R).

The interface friction was modeled using a penalty-based coulomb friction model with the coefficient of friction set to one. The maximum interface shear strength was defined equal to the soil undrained shear strength and one-third the soil undrained shear strength.

The ice keel was represented as an inverted truncated cone with a gouge depth of 2 m, a gouge width of 20 m at the mudline, and attack angles of 15° and 30°. The ice keel was constrained to move only in the direction of gouge. The soil domain was a cohesive material with a mass density of 1600 kg/m<sup>3</sup>, elastic modulus of 10 MPa, Poisson's ratio of 0.49, and undrained shear strength of 30 kPa. For the coupled scenario and 18 in. grade X65 pipeline with a yield strength of 448 MPa and a diameter to thickness ratio (D/t) of 30 was used. The pipeline's mass density was 7850 kg/m<sup>3</sup>, with an elastic modulus of 210 GPa, and Poisson's ratio of 0.3. It was accounted for that the densities quoted above are dry and not submerged densities.

For the free field case with a keel attack angle of 15°, the ratio of vertical to horizontal seabed reaction forces was 5.5 in ABAQUS/CEL when the interface shear strength limit was 30 kPa. For the 30° keel attack angle case the ratio of vertical to horizontal seabed reaction forces was 2.7 in ABAQUS/CEL when the soil interface shear strength limit was

30 kPa and remained the same when the shear strength was reduced to 10 kPa. The equivalent force ratio of 2.7 can be explained by the issue with modeling the interface shear strength limit in ABAQUS/CEL. The difference between the seabed reaction force ratios presented by Pike et al. (2011) and those presented by Philips et al. (2010) can be explained by the rougher ice keel/soil interface assumption applied by Philips et al. (2010).

Figure 2-42 below displays the vertical profile of horizontal and subgouge soil deformations of a free field ice gouge event, for both 15° and 30° keel attack angles. The attack angle of the keel had significant effects on the displacement profiles of the soil. For shallow depths below the gouge base the displacements are greater for the 30° attack face, but the vertical extent of these displacements are greater for the 15° attack face.

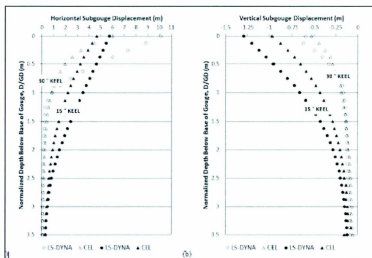


Figure 2-42 - Vertical Profile of Horizontal and Vertical Subgouge Soil Deformations, Free Field (Pike et al., 2011)

Introduction of a pipeline causes an interruption in the soil displacement field due to flow of the soil around the pipeline (see Figure 2-43). A discontinuity in the subgouge soil displacement fields develop at the crown of the pipe.

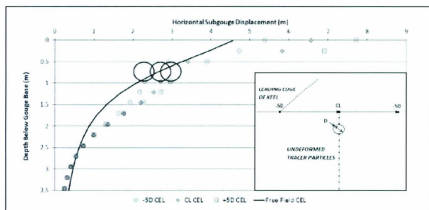


Figure 2-43 - Vertical profile of vertical subgouge soil deformations, pipe in soil (Pike et al., 2011)

Lateral subgouge soil deformations, perpendicular to the gouge path, were influenced significantly by the angle of attack where the 30° keel produces more of a dragging mechanism than the 15° keel, which produces greater subduction mechanism of the soil under the keel.

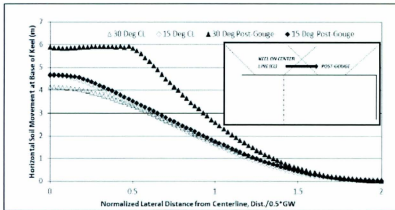


Figure 2-44- Plan view of lateral subgouge deformations at the ice gouge depth, free field (Pike et al., 2011)

In the 30° case the shearing mechanism in the gouge direction continued until a critical shear stress was reached, whereby further displacement, due to interface friction, had reached a peak causing sliding at the interface (Pike et al., 2011).

Preliminary analysis for drained gouging in sand was conducted, using finite element and validated against PRISE physical test data (Phillips and Barrett, 2011). The variables of interest in this study were mesh density, sand dilation, and stress effects due to scaling. A Drucker-Prager model is used with a friction angle of 32.6° and cohesion of 1.2 kPa. The elastic modulus was set to 3MPa with a Poisson's ratio of 0.3. The submerged density of the sand was 800kg/m<sup>3</sup>. The ice keel was modelled as a rough truncated conical indenter with 15 m minimum diameter, 30° attack angle, and a gouge depth of 1.5 m. A solution dependent variable was used to vary the dilation angle between 0° and 11°.

The mesh density study consisted of three mesh sizes, ranging from a coarse mesh to a fine mesh (See Table 2-14). The coarse mesh was considered to coarse for design purposes. The time to steady state was decreased by priming the frontal berm that builds in front of the keel by using an initial berm at the start of the gouge. Steady state conditions were achieved at approximately 20 gouge depths (about 30m).

Table 2-14- Mesh density parameters (Phillips and Barrett, 2011)

	<b>Coarse Mesh</b>	<b>Medium Mesh</b>	<b>Fine Mesh</b>
<b>Element Dimension (m) (gouge direction)</b>	1	0.5	0.5
<b>Element Dimension (m) (depth)</b>	1	0.25	0.125
<b>Element dimension (m) (lateral)</b>	1	0.5	0.25
<b>Degrees of Freedom (Millions)</b>	0.2	1.2	3.4
<b>Memory Required (GB)</b>	0.5	1.7	5.2
<b>CPU Time (hours)</b>	1	23	328

The coarse mesh over predicted the keel reaction forces while the medium and fine mesh had highly comparable results with a vertical to horizontal keel reaction force ratio of about 1.4.

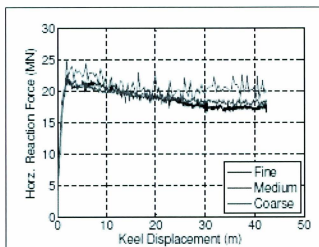


Figure 2-45- Horizontal keel reaction force (Phillips and Barrett, 2011)

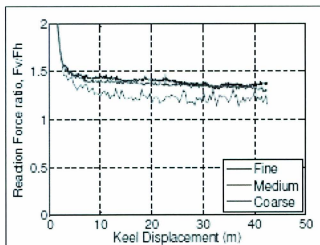


Figure 2-46- Vertical to Horizontal reaction force (Phillips and Barrett, 2011)

The subgouge deformation profile for the coarse mesh is essentially a smeared combination of that imposed by the thin shear discontinuity directly under the keel and

the underlying zone of plastic shear flow, while the fine and medium meshes are refined enough to separate these two components at about 0.3 D depth below the gouge (Phillips and Barrett, 2011).

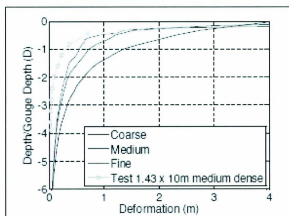


Figure 2-47 - Subgouge displacement profiles (Phillips and Barrett, 2011)

The keel reaction forces were seen to be sensitive to the assumed dilation conditions. For a dilation angle of  $6^\circ$  unrealistic keel reaction forces were seen and the analysis failed to converge at about 30 m keel displacement. Allowing the dilation to vary between  $0^\circ$  and  $11^\circ$  caused a 5% increase in the steady state reaction force when compared to that of a  $0^\circ$  dilation analysis.

### **3 PIPELINE SOIL INTERACTION: A REVIEW**

#### **3.1 General**

Pipelines are one of the most vital infrastructures used to transport hydrocarbons over vast distances. It is estimated that Canada's underground natural gas and liquids pipeline network (gathering, transmission and delivery lines) is 825,000 km in length (<http://www.cepa.com>). As most pipeline transportation systems are buried, it is important to consider and design against any geohazards that the pipeline can be subject to in its life. Some of these hazards to consider are: fault movements, liquefaction, thaw settlement, landslides, and ice gouging in offshore ice covered regions. Large ground deformations occurring during these events can be detrimental to pipeline serviceability and mechanical integrity with respect to leak and rupture. During these occurrences, the pipeline can be subjected to considerable stresses and strains, which can potentially result in pipeline failure causing environmental damage and financial loss.

Current engineering guidelines used to assess pipeline/soil interaction, such as PRCI (2004) (Honegger and Nyman, 2004), utilize a structural model to evaluate pipeline response. The pipeline is modeled using beam elements while the soil behaviour is modeled using discrete springs in three perpendicular directions (axial, lateral, and vertical). The soil load-displacement response is non-linear and can be approximated by hyperbolic functions and often simplified in engineering practice through bilinear relationships. In this structural method, the springs are independent and the procedures generally do not consider the possible coupling of loads in the different directions. This

assumption of independent slices of soil will not truly replicate the observed behaviour and will generally produce conservative designs (Kettle, 1984). Recent studies (Phillips et al., 2004a; and Daiyan et al., 2010a) have shown that there is a considerable increase in axial soil restraint when a lateral pipeline movement occurs simultaneously, therefore, stressing the importance to reevaluate the current state of practice and the necessity to consider the effect of load coupling during oblique pipeline movement on pipeline-soil interactions.

The subsequent sections review past research conducted on pipeline/soil interactions in various soil media, with the majority of the research presented relating to lateral, vertical, and oblique lateral-vertical pipeline/soil interaction in cohesive soil.

### 3.2 Analytical Models

Hansen (1961) implemented an analytical model to estimate the soil loads on pipelines subjected to lateral ground movements. This model was developed initially to predict the lateral capacity of rigid piles in soil with assumed rigid body rotation around a point at depth  $D_r$ . Dimensions of the passive failure wedge on a pile (or anchor) at moderate burial depths were calculated using Rankine passive earth pressure theory. The ultimate pressure per unit length at a depth  $z$  was given by:

$$P_{ult} = qN_\gamma D + s_u N_c D \quad (3-1)$$

where  $q$  is the vertical effective overburden pressure and  $N_\gamma$  and  $N_c$  are constants that are a function of angle of internal friction ( $\phi$ ) and burial depth to characteristic dimension ( $Z/D$ ). The constants  $N_\gamma$  and  $N_c$  are presented in Figure 3-1 and Figure 3-2, respectively.

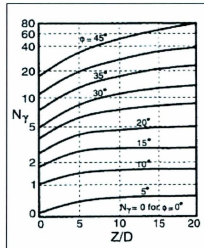


Figure 3-1 – Coefficient  $N_\gamma$  for laterally loaded piles (Prakash and Sharma., 1990)

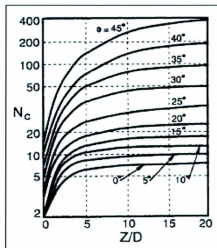


Figure 3-2 – Coefficient  $N_c$  for laterally loaded piles (Prakash and Sharma., 1990)

The Hansen (1961) model does not allow for the vertical movement of the buried structure. A buried structure when subjected to a lateral ground movement may move

upward; therefore, the additional constraint of restraining the vertical movement in the model would result in predicting higher loads on pipe than those expected in an actual situation.

Wantland et al. (1979) proposed that the lateral resistance due to pipeline movement is similar to that of the bearing capacity of a foundation; however, due to the geometry of the pipeline/soil interface and the position of the free boundary, it is somewhat more complex. The authors used a limit load analysis technique, along with the concept of perfect plasticity, to model the soil behaviour for this study. The least upper bound solution for the load-carrying capacity of a strip-footing restricted to short-term loading is given by

$$P = (2 + \pi)s_u b_f \quad (3-2)$$

where  $s_u$  is the undrained cohesion,  $b_f$  is the footing width, and  $P$  is the resistance to displacement per length of pipeline. If the soil is assumed weightless and incompressible and the effects of pipe curvature and geometric nonlinearities are neglected, the mechanism in Equation 3-2 can be adopted to a laterally moving pipe in an open trench, shown in Figure 3-3. Therefore,  $P$  should be maximized as a function of embedment ( $D$ ) at an embedment ratio ( $D/B$ ) equal to 2, where  $D$  is the embedment depth to the bottom of the pipeline and  $B$  is the diameter of the pipeline. This results in the formula given in Equation 3-3.

$$P_{ult} = 5.14s_u d \quad (3-3)$$

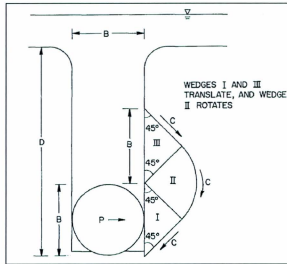


Figure 3-3 – Assumed flow pattern for pipe buried in an open trench (Wantland et al., 1979)

However, the authors recognize that an embedment greater than  $2D$  may be necessary to produce  $P_{ult}$ . Therefore, the authors suggest the modified formula as

$$P = N_c s_{u-avg} D \quad (3-4)$$

where  $N_c$  is the lateral bearing capacity factor and  $s_{u-avg}$  is the average undrained cohesion of the soil. The authors note that if  $D$  is less than  $H$  then the above equation is modified to

$$P = N_c s_{u-avg} H \quad (3-5)$$

### 3.3 Experimental Research

There are a number of physical studies conducted in various soil media that consider pipeline/soil interaction, with movement along one of the orthogonal axis within a vertical plane section, including lateral (e.g. Paulin et al., 1998), vertical (e.g. Trautmann

et al., 1985) and axial directions (e.g. Wijewickreme et al., 2009). Some experimental programs have been extended to incorporate oblique loadings such as axial-lateral pipeline/soil interactions (e.g. Daiyan et al., 2010a) and lateral-vertical (e.g. Nyman, 1982). Prior to physical studies conducted in the area of pipeline/soil interaction, researchers in this field utilized experimental work conducted on anchors, footings, and piles, to infer soil loads and failure mechanisms during pipeline/soil interaction events.

Mackenzie (1955) conducted small scale model tests on deadman anchors in cohesive soil to determine if the anchor strength would reach a limiting value with increasing cover depth. These experiments were also used to evaluate the application of passive earth pressure theories and the theory of Hansen (1948) on the dowel-like action of piles.

The tests were conducted in a steel tank filled with silty clay with a liquid limit of 92% and a plastic limit of 30%. The tests were conducted with soil at water contents of 63% ( $s_u = 2.5$  kPa and  $\gamma = 15.7$  kN/m<sup>3</sup>) and 45% ( $s_u = 21$  kPa and  $\gamma = 16.5$  kN/m<sup>3</sup>). The anchor was square in cross section with a width and breadth of 1 in. square and 10 in. length. To reduce end effects, lubricated steel plates were placed adjacent to the end of the anchor. A total of twenty tests were conducted with cover depths ranging from 0 to 17 in.

For shallow cover depths ( $H/D < 8$ ) the author observed a disturbed soil surface which indicated a passive wedge type failure. For deep cover depths ( $H/D > 10$ ) the failure surface was established as that of a deep failure mechanism with soil flow around the anchor. Passive wedge theory showed close agreement with the experimental results for shallow cover depths. Mackenzie (1955) suggested that a correction be applied to passive

wedge theory in order to fit to his experimental data. A correction which worked well was  $(D/H)^{1/2}$  which produced the following equation:

$$P_{ult} = \sqrt{\frac{D}{H} \left( \frac{\gamma H^2}{2} + 2Hs_u \right)} \quad (3-6)$$

where D is the anchor width and H is the depth of the soil to the bottom of the anchor,  $P_{ult}$  is the ultimate resistance per unit length of anchor. This equation should be used for depths up to approximately 200 mm. For deep burial depths (greater than 250 mm) the limiting condition was found to be

$$P_{ult} = 8Ds_u \quad (3-7)$$

At depths between 200 and 250 mm both equations over predict the ultimate capacity of the anchor. Mackenzie (1955) concludes that passive wedge theory can be used on horizontally loaded surface anchors in clay but does not apply to deadman anchors with a considerable cover as it will result in strengths that are on the unsafe side.

By reanalysing the data collected by Mackenzie (1955), Tschebotarioff (1973) plotted it in dimensionless form using the following equation

$$N_c = \frac{P_{ult}}{Ds_u} \quad (3-8)$$

where  $N_c$  is termed the breakout factor. In Figure 3-4,  $N_c$  is plotted against the embedment ratio  $(H/D)$  where H is the depth from the soil surface to the bottom of the anchor.

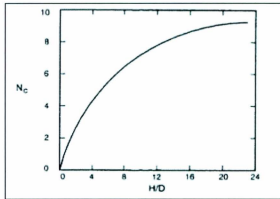


Figure 3-4 –  $N_c$  versus  $H/D$  for strip anchors in clay after Mackenzie (1955) (Das, 1990)

From Figure 3-4 it can be seen that  $N_c$  increases with increasing embedment up until it reaches a limiting breakout factor, termed  $N_c^*$ , at which point it remains relatively constant (Das, 1990). The embedment ratio at which this occurs is termed the critical embedment ratio,  $(H/D)_{CR}$  (Das, 1990). Anchors with an embedment ratio less than  $(H/D)_{CR}$  are considered shallow anchors and those at embedment ratios greater than the critical value are considered deep anchors (Das, 1990).

Audibert and Nyman (1977) conducted an experimental program to determine force-displacement ( $p$ - $y$ ) curves for a buried pipeline in sand. The authors investigated the influence of parameters such as: pipeline diameter, embedment ratio, and soil density. Three different pipeline diameters were studied: 25 mm, 60 mm, and 111 mm. The embedment ratios investigated were: 1, 3, 6, 12, and 24, for the 25 mm diameter pipeline, 1, 3, and 6 for the 60 mm pipeline, and 1 and 2 for the 111 mm pipeline. The tests were conducted in air dried medium Carver sand. The sand was spread in 25 mm layers using a

slumping technique to achieve a loose condition and dynamic compaction to achieve a dense condition.

One side of the test box was constructed from Plexiglas, which allowed the soil failure mechanisms to be observed. The authors noticed a front passive wedge bounded by a logarithmic spiral failure surface formed in front of the pipeline for small cover depths ( $H/D < 3$ ). For embedment ratios from 12 to 24 a confined zone of soil flow was observed to extend 1 diameter in front of the pipe for dense sand and 2 to 3 diameters for loose sand. Audibert and Nyman (1977) normalized their data with respect to the ultimate lateral soil pressure,  $P_{ult}$ , and the ultimate displacement,  $Y_{ult}$ , to achieve this pressure.

$$p_{norm} = \frac{p}{P_{ult}} \quad (3-9)$$

for  $p \leq P_{ult}$  and

$$y_{norm} = \frac{y}{Y_{ult}} \quad (3-10)$$

for  $y \leq Y_{ult}$ . The trend of the normalized curves could be described as

$$p_{norm} = \frac{y_{norm}}{0.145 + 0.855y_{norm}} \quad (3-11)$$

By rearranging Equations 3-9 to 3-11 the authors determined analytical formulae for predicting p-y curves.

$$p = \frac{y}{A' + B'y} \quad (3-12)$$

where

$$A' = \frac{0.145Y_{ult}}{q_{ult}} \quad (3-13)$$

and

$$B' = \frac{0.855}{q_{ult}} \quad (3-14)$$

and  $q_{ult}$  is the predicted ultimate lateral pressure acting on the pipeline. The authors found good agreement between their results for ultimate lateral pressure ( $P_{ult}$ ) and those predicted by Hansen (1961) and recommended that Hansen's method be used in estimating the ultimate lateral pressure in the above equations. The authors also recommended that a value for  $Y_{ult}$  equal to 1.5 to 2% of the embedment depth be used.

Audibert and Nyman (1977) also conducted a field test in a natural deposit of Carver sand with a unit weight of 16.8 kN/m<sup>3</sup> and a frictional angle of 35°. The pipeline was 2.36 m in length with a diameter of 229 mm and its springline was located at 80 cm below the soil surface. The test was used to assess their proposed method of developing p-y curves. The ultimate load calculated by their method was 6% less than measured in the field, while the calculated ultimate displacement was 10% lower than the field measurement. The authors determined that their method for developing p-y curves gave a good approximation to the curve obtained from the field data.

Wantland et al. (1979) conducted a series of laboratory and field tests of model pipelines in cohesive soils. These tests were conducted to determine the effects of pipe weight, pipe diameter, embedment depth, loading rate, and the effect of soil type on the resistance developed during pipeline lateral movement. The first series of tests were conducted in

the estuary of Cedar bayou in Harris County, Texas. The soil medium was under consolidated, highly plastic montmorillontic clay. The pipe sections were 20.5 ft long with diameters of 2.875 in. and 4.50 in. The pipes were tested at two weights: pipe empty and pipe with ballast inside. The pipes were placed directly on the soil without trenching and were allowed to settle. Once the pipelines settled to an equilibrium depth the pipelines were moved laterally with a winch at a constant rate of approximately 1 ft/min. A continuous load displacement record was created.

The second series of tests were conducted in the laboratory using kaolin clay kept at the liquid limit to model under consolidated conditions. The pipes used in the laboratory measured 22.75 in. in length and 1.50 in. and 3.00 in. in diameter. Embedment depths ranged from less than 1D to 6D were tested. The two rates of displacement used were: 0.014 and 0.070 in./min. The results of both test programs are shown in Figure 3-5. Given the plotted values a trend curve was fitted to represent typical results of  $N_{ch}$  with embedment ratio.

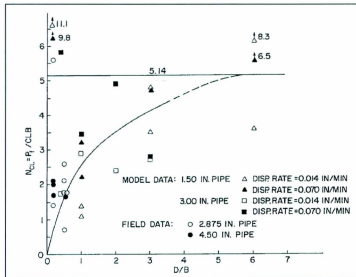


Figure 3-5 – Relationship between  $N_c$  and  $H/D$  (Wantland et al., 1979)

Equations 3-4 and 3-5 can be used in conjunction with Figure 3-5 to determine the ultimate lateral resistance of an uncovered pipe per unit length ( $P$ ) in a soft clay near the liquid limit. The authors report an upper limit of  $N_c$  to be approximately 5 or 6. Also, the lateral resistance was found to be independent of displacement rate within the range of displacement rates considered.

Wantland et al. (1979) also constructed normalized displacement to peak load versus embedment ratio from the tests conducted. It was observed that the displacements to failure were highest for the shallowest and deepest relative penetrations (see Figure 3-6). Shallow pipes appear to fail by surface sliding, causing a build up of material in front of the pipeline which increases the resistance with continued displacement. Deeply buried pipeline fail due to a flow mechanism, which may need considerable distance to fully

mobilize. Intermediate embedment fails due a passive wedge mechanism which requires less distance to fully mobilize than the other mechanisms.

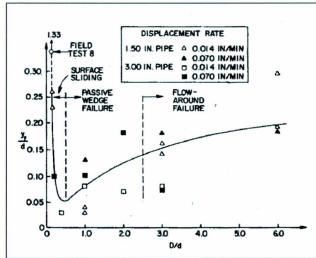


Figure 3-6 – Normalized relationship between displacement at failure and embedment ratio

Trautmann and O'Rourke (1985) conducted an experimental program in dry sand to analyse the effect of various factors on soil restraint to lateral pipe displacement. The testing program included 30 lateral force-displacement tests on pipes having outside diameters of 102 mm and 324 mm at H/D ratios of 1.5, 3.5, 5.5, 8, and 11. The tests were performed at initial dry unit weights of 14.8, 16.4, and 17.7 kN/m<sup>3</sup>, corresponding to loose, medium dense and dense sand, respectively. The goals of this research were: to determine the maximum lateral soil force as a function of pipe depth and soil density, evaluate the force-displacement behaviour with reference to soil density and embedment

ratio, and to establish a simple mathematical model to characterize the force-displacement behaviour.

The results presented in Figure 3-7 are plotted in terms of dimensionless force  $N_h$  in terms of embedment ratio.  $N_h$  is defined as

$$N_h = \frac{P_{max}}{\gamma H_s DL} \quad (3-15)$$

where  $P_{max}$  is the maximum measured force,  $\gamma$  is the soil unit weight,  $H_s$  is the depth to the pipe springline,  $D$  is the pipe diameter, and  $L$  is the pipe length. For dense sands the peak force was easily identifiable but for loose and medium sands the peak force was taken at the point where the force-displacement curve became linear.

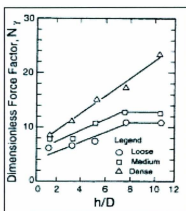


Figure 3-7 –  $N_h$  as a function of  $H_s/D$  for loose, medium, and dense sands (Trautmann and O'Rourke., 1985)

The displacements to peak force were seen to vary with density giving displacements of 0.13H, 0.08H, and 0.03H for dense, medium, and loose sands respectively. There were

four tests conducted at an H/D of 3.5 to assess the effect of surface roughness on  $N_b$ . The first two tests the pipeline was made rough by covering the pipes outer surface with sand paper and the last two tests the pipeline was covered with two layers of polyethylene plastic and coated with SAE 90 gear oil. It was seen that  $N_b$  for rough pipes was 10% higher than that for the smooth pipes. Therefore, for the burial depth tested the smooth coating has little effect in reducing lateral forces. The authors also compared the results of the 102 mm and 324 mm diameter pipes at identical embedment ratios and seen little variation of  $N_b$ . They concluded that for these test conditions a 102 mm pipe is representative of the behaviour of larger diameter pipes and can be extrapolated on to determine the performance of pipes with diameters larger than 300 mm.

The test results of Trautmann and O'Rourke (1985) agreed most closely with the data from Ovesen (1964) and Audibert and Nyman (1977). When compared to analytical models, the tests data compares most closely with Ovesen (1964) and Rowe and Davis (1982) models. However, these models do not predict the constant values of  $N_b$  for H/D greater than 8 in loose and medium sand, depicted in Figure 3-7. Because of the close agreement with Ovesen's (1964) analytical model the authors developed the plot in Figure 3-8.

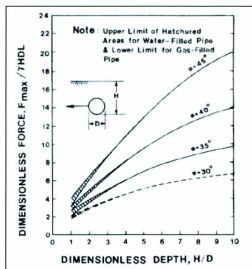


Figure 3-8 –  $N_h$  versus  $H/D$  for pipeline design (Trautmann and O'Rourke, 1985)

The authors determined that their data set followed a hyperbolic relationship between normalized force ( $F''$ ) and normalized displacement ( $Y''$ ) which can be expressed as

$$F'' = \frac{Y''}{(0.17 + 0.83Y'')} \quad (3-16)$$

where

$$F'' = \frac{P/(YHDL)}{(N_h)} \quad (3-17)$$

and

$$Y'' = \frac{Y/D}{(Y_f/D)} \quad (3-18)$$

Where  $P$  is the force measured at each increment of displacement of  $Y$ . This expression is similar to the hyperbolic expression recommended by Audibert and Nyman (1977). The authors also proposed a bi-linear representation of the force-displacement curve, which

consists of an initial constant-slope for the elastic portion followed by a constant plastic portion at the value of maximum force. The authors suggested that Figure 3-8 can be used to determine the maximum lateral force. The recommendation for the elastic stiffness was for the secant line to extend from the origin through a point  $0.7N_h$ . This is given by

$$K_{h70} = C_k N_h \gamma DL \quad (3-19)$$

where  $K_{h70}$  is the secant slope of the bilinear relationship defined at 70% of the maximum force.  $C_k$  is 20, 30, and 80 for loose, medium, and dense sand respectively.

Poorooshasb et al. (1994) conducted a series of centrifuge tests at the Laboratoire Central des Ponts et Chaussées (LCPC), Centre de Nantes. The study considered the effects of trench width and pipeline cover depth on pipe-soil interaction and the results were compared to the current state of practice (SOP) formulations of Hansen (1961) and Rowe and Davis (1982). The program consisted of two sets of tests: Test A and Test B. Four pipelines were tested during each test at an acceleration of 50g. Trenches were constructed at 1g and then backfilled to replicate construction procedures. The pipelines were considered rigid and were moved laterally through the overconsolidated kaolin clay at 1 mm/s which was sufficient for modelling undrained conditions. The pipelines were also free to move vertically during the test. Soil shear strength measurements were taken in flight using a cone penetrometer (CPT). Measured values of the soil shear strength were lower than that expected from empirical correlations for 100 % saturated kaolin clay resulting in no distinct difference in the strength of native and backfill soil.

Prior to consolidation in the centrifuge, the clay was one-dimensionally preconsolidated to a vertical effective stress of 160 kPa. The trench backfill soil was also kaolin clay, which was normally consolidated in the centrifuge. The pipelines were stainless steel with prototype dimensions of 0.95 m in diameter and 12.5 m in length. The cover depth above the pipeline crown was 0.92 m for shallow cover and 1.52 m for deep cover. The authors note that various degrees of desiccation occurred which resulted in a lack of certainty about the effective stresses in the region above the water table.

For test A, Pipelines 1, 2, and 3 were displaced at constant rates while Pipeline 4 was moved initially at a very slow rate then stopped for 30 min (52 days prototype scale) for stress relief to occur and then motion was reapplied. This was found to have negligible effect on pipeline loading. All pipelines were seen to increase to a peak load while still inside the trench with displacements to peak load occurring between 0.26 m and 0.63 m. Peak resistance normalized with respect to backfill shear strength ranged from 10.45 m to 11.3 m. The narrow trenches experienced lower values of peak load which is opposite to what is expected. Also, there was no conclusive result that deeper pipeline cover resulted in greater forces at peak load. For test B the pipelines were displaced at a more uniform speed and peak loads occurred between 0.21 m and 0.27 m. Normalised peak loads ranged from 9.47 m to 11.66 m. For the entire data set the authors represent the normalised peak resistance as  $10.86 \pm 20\%$  and the displacements to 90% peak resistance as  $0.18\text{m} \pm 39\%$ . When compared to the work of Hansen (1961) and Rowe and Davis (1982) the centrifuge results were usually greater than the current SOP predictions with

some cases in close agreement with the “no breakaway” condition proposed by Rowe and Davis (1982).

As part of Phase II of the NOVA Gas Transmission Limited experimental research program, Paulin et al. (1995) conducted a series of test to study the effect of various parameters on pipe/soil interaction. These tests investigated the effects of: nominal cover, deep cover, trench width, and interaction rate. Three tests were also conducted at 25g, 50g, and 100g to demonstrate the reliability of centrifuge modelling through the “modelling of models.” Rigid pipelines were installed into a soil mixture of 50% kaolin clay and 50% Sil-Co-Sil silt with a plasticity index (PI) of 13% and a specific gravity of 2.62. The trench backfill was the same material type but was subjected to a different stress history resulting in a weaker soil. In flight cone penetrometers tests measured the shear strength of the soil. Pipeline segments were 0.95 m in diameter with length ranging from 6.25 m to 17.5 m at prototype scale. The pipelines were pulled laterally but allowed to move in the vertical direction.

For undrained conditions, spaghetti strands installed in the soil below the pipeline indicated a well defined shear deformation zone extending approximately 0.5 pipeline diameters below the pipeline base. Spaghetti strands above the pipeline indicated plastic flow around the pipeline during displacement. For drained conditions, the failure mechanism was different with distinct failure surfaces in front of the pipeline extending from the pipeline toe to the surface at approximately 40°. The lateral force on the pipeline was seen to increase with increasing embedment ratio (H/D). However, the authors note

that for large  $H/D$  ratios the effect of embedment on lateral pipeline reaction force is not as noticeable. Trench width was seen to have little effect on pipe-soil interaction factor. Interaction rate had a significant effect on the interaction factors with velocities tending toward drained conditions having loads greater than those for undrained conditions. The authors suggest three different loading regimes: drained, partially drained, and undrained. The authors compared their results to that of Hansen (1961) and Rowe and Davis (1982) (see Figure 3-9). It was found that the results lied between the “immediate separation” condition of Rowe and Davis (1982) and Hansen (1961) model.

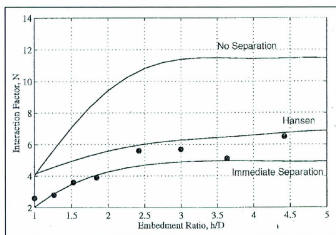


Figure 3-9 – Burial Depth Tests Data Comparison to Rowe and Davis and Hansen (Paulin et al., 1995)

Paulin et al. (1995) reconsidered the results of the tests conducted by Rizkalla et al. (1992) in Phase I of the program. Undrained shear strengths in Phase I were much lower than expected from empirical correlations and theoretical predictions. Paulin et al. (1995)

conducted additional cone penetrometers tests in kaolin clay to replicate Phase I test conditions and reassess the undrained shear strengths used. The repeat tests demonstrated higher undrained shear strengths and when used to normalize the data collected by Rizkalla et al. (1992) resulted in interaction factors that were in good agreement with Phase II data.

In addition to the series of test conducted by Paulin et al. (1995), three model tests were conducted by Paulin et al. (1996) to investigate the effects of interaction rate, preconsolidation stress and backfill type. The experimental test apparatus, instrumentation, and soil used were the same as that described in Paulin et al. (1995). Pipeline diameters used in these experiments were 0.95 m with a cover depth of 0.8 m, at prototype scale. There were four types of backfill used in the tests: clay slurry, chunks of backfill, remoulded backfill tamped in place and loose sand. The tamped in place remoulded backfill had the greatest resistance to pipeline movement while the pipeline buried in loose sand experienced the least load. After the pipeline buried in loose sand penetrated into the trench wall at a distance of 2.5 m (2.6D), it experienced a load that was approximately 67% less than that experienced by the other pipelines. Two pre consolidation pressures of 160 kPa and 400 kPa were tested. The pipeline experienced higher normalized interaction loads and smaller displacements to these loads for the lower pre consolidation stress. However, this could not be confirmed due to insufficient data.

As in the previous investigation spaghetti strands showed a well defined zone of shear deformation extending below the pipeline to approximately 0.5 to 0.75 pipeline diameters and plastic flow above the pipeline during pipeline displacement. Similar to previous test by Paulin et al. (1995) for drained conditions, failure surfaces were observed in front of the pipeline extending from the pipeline toe to the soil surface at an angle from 25 to 44° to the horizontal.

Through analysis of the centrifuge test program, Paulin (1998) derived empirical formulations for the ultimate normalized resistances ( $N_c$ ) based on four fits to the data set, shown in Figure 3-10. The fits include

$$N_c = 1.57 \frac{H}{D} + 2.38 \quad \text{for } \frac{H}{D} \leq 1.842 \quad (3-20)$$

$$N_c = -0.915 \left(\frac{H}{D}\right)^2 + 4.86 \left(\frac{H}{D}\right) - 1.13 \quad \text{for } \frac{H}{D} \leq 2.5 \quad (3-21)$$

$$N_c = 0.150 \left(\frac{H}{D}\right)^3 - 1.58 \left(\frac{H}{D}\right)^2 + 5.51 \left(\frac{H}{D}\right) - 1.59 \quad \text{for } \frac{H}{D} \leq 2.5 \quad (3-22)$$

$$N_c = 1.69 \frac{H}{D} + 0.928 \quad \text{for } \frac{H}{D} \leq 2.5 \quad (3-23)$$

where Equation 3-20 is a bilinear conservative bound, Equation 3-21 is a polynomial fit up to an embedment ratio of 2.5 followed by a constant interaction factor, Equation 3-22 is a polynomial fit through the data from the first two tests, and Equation 3-23 is a bilinear regression with the linear regression plotted through Test 01 and Test 02 data up to a constant interaction factor at an embedment ratio of 2.5. Equations 3-20 to 3-23 are for undrained tests.

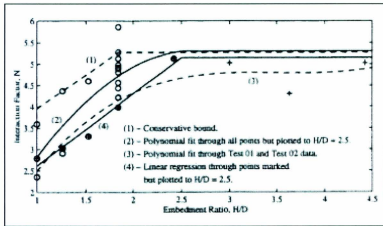


Figure 3-10 – Evaluated trends through undrained interaction factor data (Paulin, 1998)

Paulin et al. (1998) conducted full scale investigations into pipe/soil interactions for both sand and clay material. Loose (approximately 0% relative density) and dense (approximately 100% relative density) sand test beds were used for testing. For preparation of the loose sand test bed the sand was slumped from a container. The dense sand test bed was prepared by placing the sand into 100 mm layers and then compacting with a vibratory tamper. The clay used was kaolin clay with a liquid limit of 56%, a plastic limit of 31%, and a specific gravity of 2.66. The clay test bed was prepared by placing the soil loosely into 150 mm layers and then tamping them. This resulted in the tamped layer thickness of approximately 100 mm. Cone penetration, laboratory vane, and hand vane tests were conducted to characterize the clay. Undrained shear strengths of the clay were approximately 25 kPa to 35 kPa for soft soil and 65 kPa to 70 kPa for stiff soil. Once the test beds were prepared, internal displacement markers and vertical deformation

tubes were inserted. The rate of pipeline displacement in sand was about 10 mm/hr while in clay it was either 0.5 mm/hr or 10 mm/hr.

The relative density of sand had a significant effect on the interaction. Post peak lateral loads in dense sand were approximately 80% greater than those in loose sand while post peak axial loads in dense sand were 160% of those in loose sand.

Peak axial loads for the stiff clay were approximately 150% of the peak loads in the soft clay for the fast loading condition. For the displacement rates considered in clay, the peak loads from the slow tests were 25% larger than those from the fast tests. The post peak data during the soft slow tests tend to increase with increasing pipe displacement. Steady state values from the lateral stiff clay tests were approximately 100% greater than those from the soft clay tests.

Phillips et al. (2004b) conducted physical modelling experiments in a geotechnical centrifuge using the methodology used by Paulin (1998). The tests program studied the effects of: trench width, burial depth, backfill material, and mitigative effects of inclined trench walls. At prototype scale the pipelines were 0.95 m in diameter and 12.5 m in length. The native soil material was a mixture of 50% speswhite kaolin clay and 50% Sil-CoSil silt, which was the same combination as used by Paulin (1998). Undrained shear strength was measured both post and pre test using a hand vane at 1g. For a more accurate calculation of undrained shear strength in flight measurements were taken using a piezocone penetrometer. In all tests the undrained shear strength of the native material was approximately 40 kPa. Both sand and clay backfill were tested. For clay backfill the

same material was used as that for the native soil. The weaker clay backfill was made by adding water to some native soil that had been removed from the top of the test bed. The sand backfill consisted of two types: well graded sand and uniformly graded fine sand.

Lateral force and displacements were measured for each test. The force was normalized with respect to the undrained shear strength of the native material (40 kPa) and the pipe diameter. The pipe displacements were normalized using the pipe diameter. Normalised displacements to maximum load ranged from 0.2 to 1.5, which are higher than 0.03 to 0.05 suggested by Honegger and Nyman (2004). Interaction factors from the centrifuge tests are presented in Figure 3-11.

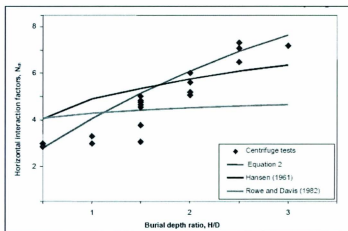


Figure 3-11 –Interaction Factor Comparison (Phillips et al., 2004b)

The factors are lower than those from Rowe and Davis (1982) up to about H/D of 1.5 and greater than those from Hansen (1961) above H/D of 2. The equation plotted in Figure 3-11 is generated from numerical predictions and is given by:

$$N_{ch} = \min \left( N_{ch}^* + \beta_h \frac{\gamma H_z}{s_u}, N_{ch}^{max} \right) \quad (3-24)$$

where:  $N_{ch}^*$  is the interaction factor associated with soil strength,  $\beta_h \gamma H_z / s_u$  accounts for the soil weight relative to the vertical stress at the pipe springline, and  $N_{ch}^{max}$  is the upper limit interaction factor for deep burial. This equation shows an acceptable bound for the data.

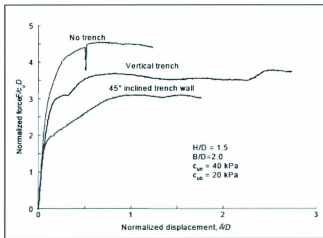


Figure 3-12 - Trench Effects (Phillips et al., 2004b)

Figure 3-12 illustrates that the presence of the trench reduces the force on the pipeline. The pipe reaches the vertical trench wall at 0.3 pipe diameters and the resistance increases slightly; however, it is still less than the case with no trench. The authors attribute this decrease to the upward movement of the pipe through the backfill. For the 45° degree trench wall at large displacements the force on the pipe is about 15% less than that of the vertical trench wall. For a 60° trench wall no significant decrease was shown compared to that of a vertical trench. A wider trench increased the displacement to peak

load for the same burial depth. Loose sand backfill rather than soft clay backfill had no significant effect on the pipe response for the tests conducted.

Phillips et al. (2004b) suggest a tri-linear p-y curve for a laterally loaded pipeline buried in a trench backfilled with a cohesive soil that is weaker than the native soil (see Figure 3-13).

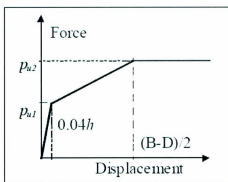


Figure 3-13 – p-y curve for laterally loaded trench pipeline (Phillips et al., 2004b)

The two load levels considered are  $p_{u1}$  and  $p_{u2}$  shown in the above figure and given by:

$$p_{u1} = s_{ub} N_{ch} D \quad (3-25)$$

where  $S_{ub}$  is the backfill strength, and

$$p_{u2} = s_{un} N_{ch} D \quad (3-26)$$

where  $S_{un}$  is the native strength. These loads are reached at displacements of  $0.04 h$  and  $(B - D)/2$ , respectively, where  $B$  is the trench width.

Oliveira et al. (2010) conducted a series of centrifuge tests to determine the resistance of the soft clay found in Guanabara Bay during the lateral movement of a pipeline. The main reason for this research program was an oil spill that occurred in Guanabara Bay in Rio de Janeiro due to the thermal buckling of a pipeline. The authors also conducted a set of 1g tests in order to observe, in more detail, the soil failure mechanisms.

Centrifuge experiments were conducted at 30g using a 15.2 mm diameter pipeline attached to a rigid shaft. The pipeline was dragged laterally by the rigid shaft and forces in both lateral and vertical directions were measured. Four strain gauges measured the lateral force while a load cell measured the vertical force. A pore pressure transducer located inside the soil monitored soil consolidation.

Clay from the accident site was used in the experiments. This clay is characterized as lightly overconsolidated highly compressible soft clay with water content close to the liquid limit. Vane and tri axial tests were used to measure the undrained shear strength of the in situ and laboratory clay. Almeida et al. (2001) described the undrained shear strength of the soil as

$$s_u = 0.126 + 1.373z \quad (3-27)$$

where  $z$  is the depth below the soil surface in m and  $s_u$  is in kPa. Consolidation of the soil in the centrifuge was conducted at 100g while the pipe displacements were carried out at 30g. Pore pressures were allowed to dissipate during the deceleration from 100g to 30g.

The pipeline was positioned by vertical penetration through the soil test bed. Due to the configuration of the pipeline and rigid bar the penetration phase could be used as a T-bar penetrometer test and the vertical loads could be used to estimate the undrained shear strength of the soil. The following equation was used to estimate the undrained shear strength

$$s_u = \frac{V}{N_b D^* L} \quad (3-28)$$

where V is the vertical force measured during penetration, L is the pipe length,  $N_b$  is a T-bar factor and  $D^*$  is a modified pipe diameter taken as the horizontal projection of the pipe soil contact area given by

$$D^* = 2\sqrt{H(D-H)} \quad (3-29)$$

where H is the burial depth from the soil surface to the bottom of the pipe and D is the pipe diameter. For deeper burial ( $H > D$ )  $D^*$  is equivalent to D. Numerical analyses was conducted to assess the T-bar factors as a function of embedment ratio (Oliveria, 2005) using an elastic perfectly plastic finite element code (Costa, 1984). Using  $N_b$  factors from the numerical analyses along with the results from the penetration tests Oliveira et al. (2006) proposed the following equation

$$s_u = 0.1002 + 1.283z \quad (3-30)$$

which was in good agreement with the in situ equation.

During the lateral displacement step, displacement rates were maintained at a level that allowed for undrained conditions. The lateral force was normalised using the following equation

$$N_h = \frac{F_h}{s_u D^2 L} \quad (3-31)$$

where  $F_h$  is the lateral force on the pipe and  $s_u$  is taken at mid depth of penetration or mid height for full penetration. Figure 3-14 plots the normalised values of the centrifuge tests.

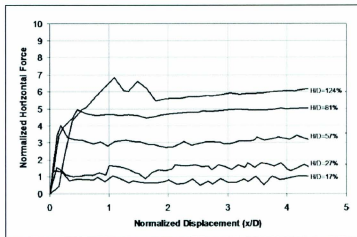


Figure 3-14 - Normalised horizontal force for centrifuge tests (Oliveira et al., 2010)

From 1g tests the authors observed a shallow failure mechanism for H/D ratios of 0.5, 1.0, and 2.0. The authors adopted a circular failure surface with a radius equal to 2.5D. From geometric considerations an analytical model capable of predicting the lateral interaction factor given in Equation 3-32 was proposed.

$$N_h = 5 \arctan\left(\frac{H}{D}\right) \quad (3-32)$$

This model is based on a shallow failure mechanism and is applicable up to  $H/D$  of 4. The authors found good correlation between the centrifuge experiments and the proposed analytical model.

### 3.4 Numerical Models

Rowe and Davis (1982) conducted a theoretical investigation into laterally and vertically oriented anchor plates in cohesive soil. The analyses utilized an elasto-plastic finite element model with the soil being assumed as saturated clay. Plane strain conditions with a rigid anchor plate were assumed. The factors analysed were: anchor embedment, layer depth, overburden pressure, breakaway condition, anchor roughness, thickness, and shape. Two breakaway conditions were used: "immediate breakaway," where the back of the anchor separates from the soil immediately and "no breakaway," where the anchor remains in contact with the soil.

Rowe and Davis (1982) describe two different failure mechanisms observed. For shallow embedment soil failure was characterized by a plastic flow to the surface while at deep embedment soil failure was characterized by a local flow around the anchor. Anchors could be considered deep at an embedment of 3 to 4 as increasing the embedment beyond this had no significant effect on anchor capacity.

The authors suggest that the applied pressure  $q_u$  required to cause undrained failure can be expressed as

$$q_u = s_u F'_c \quad (3-33)$$

where  $F_c'$  is the lower value given by

$$F_c' = F_c + \frac{sqh}{s_u} \quad (3-34)$$

or

$$F_c' = F_c^* \quad (3-35)$$

where  $F_c$  is the dimensionless anchor capacity factor corresponding to the case where the soil is initially stress free and the interface between the back of the anchor and soil is unbonded and  $F_c^*$  is the dimensionless anchor capacity factor corresponding to the case where the anchor and soil are fully bonded.  $q_h$  is the overburden pressure at depth  $h$  and  $s$  is a coefficient for the effect of overburden pressure on anchor capacity. Finite element analysis was performed to calculate the anchor capacity for a range of embedment ratios. The results of this analysis are plotted in Figure 3-15.

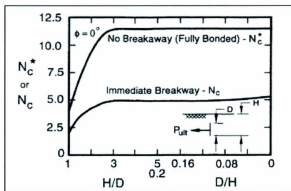


Figure 3-15 – Rowe and Davis (1982) anchor capacity for a vertical plate anchor in clay (Poulos, 1988)

The authors found that their results compared well with those by Mackenzie (1955). The authors state that their theoretical model provides reasonable limits for anchor plate behaviour in cohesive soils.

Popescu et al. (1999) developed two-dimensional plane strain finite element modeling procedures using ABAQUS/Standard. The soil was discretized using the plane strain element CPE8R (8-node biquadratic continuum element with reduced integration) and the pipeline with B22 beam structural elements. A contact surface approach was chosen to model the contact at the pipe-soil interface. Due to the fact that the soil was dry for the tests in sand and not fully saturated for the tests in clay, and the low rate of pipe displacement, drained behaviour was assumed for these tests.

The Modified Cam-Clay model was implemented to simulate clay material behaviour. The numerical model was calibrated against two clay tests (soft and stiff clay) from Paulin et al. (1998). The authors obtained the soil parameters by curve fitting the recorded force-displacement from the numerical model to that of the physical tests by means of a parametric study (Popescu, 1999). A Mohr-Coulomb plasticity model was implemented to simulate sand material behaviour. A non-associated Mohr-Coulomb model with no hardening was used to simulate dense sand. Peak soil strength parameters and interface friction coefficient were chosen based on direct shear tests.

The numerical model gave close predictions for the force displacement response in clay while only close predictions for peak loads were given in sands. Neither constitutive model exhibited softening after peak load was reached. The authors attribute the

discrepancies in the initial part of the analysis in sand on the high elasticity simulated by the constitutive model and the need to introduce a cohesion greater than zero. Observed shear induced plastic compaction was not properly simulated in the numerical model. The predicted shear zone in clay was seen to deviate upwards at an angle of about  $45^\circ$  in front of the pipe. Considering the limitations inherent in the classic plasticity models the numerical predictions were able to simulate the pipe-soil interaction relatively well. This model was later altered by Popescu et al. (2002b) to account for mobilization of the shear strength of soil with shear deformations and variation of the low strain deformation moduli with effective confining stress. This modification allowed for the model to capture the softening nature of dense sands subjected to large shear deformations.

Popescu and Konuk (2001) conducted three-dimensional finite element analysis of pipe-soil interaction to determine the effects of shear interaction in soil during translational and rotational movement of a pipe. The numerical model was developed using ABAQUS/Standard framework and an elastic-perfectly plastic soil constitutive model was employed to simulate undrained behaviour in a clayey soil. The undrained shear strength was taken as 50 kPa, the Young's modulus as  $100*s_u$ , Poisson's ratio as 0.49, and the equivalent shear stress limit as  $s_u/3$ . The contact surface approach in ABAQUS/Standard was used to simulate the pipe/soil interface. Two embedment ratios of 2.2 and 3.4 were analysed to study the mechanisms of shallow and deep cover. Three displacement cases were conducted at each cover depth: rigid lateral translation, rigid rotation, and flexible rotation of the pipeline.

For the rigid lateral case and deep cover, the normalised displacement to peak load was 0.18 resulting in a normalised peak load of 5.8. For shallow cover depths rigid lateral translation resulted in a normalised displacement to peak load of 0.12 and the normalised peak load was approximately 4.5.

The authors determined that for large cover depths ( $H/D > 3$ ), the forces experienced by the pipe are not significantly affected by pipe rotations or the deflected pipe shape. However, for shallow embedment ratios ( $H/D < 3$ ) lateral shear interaction between soil zones along the pipe axis are significant. For rigid pipes experiencing rotation, interaction forces can be reduced up to 25% compared to a pipe experiencing rigid translation. For flexible pipes the difference was found to range from -5% to 10%. Lower forces occur closer to the pipe's axis of rotation. For deep cover depths a local punching failure was observed and for shallow cover a general shear failure was seen. The authors also note that for deep cover the interaction forces continuously increased and did not level off which may result in larger forces than predicted by current guidelines.

Popescu et al. (2002a) extended the study conducted by Popescu and Konuk (2001) to assess the effects of soil stiffness, pipeline flexibility, and internal pipeline pressures on pipe/soil interaction forces. Two types of soil were analysed to observe soil failure mechanisms: very soft clay with undrained shear strength of 10 kPa and stiff clay with undrained shear strength of 100 kPa. For an embedment ratio of 3 the stiff soil experienced a shear failure while the soft clay experiences a flow around mechanism (see Figure 3-16).

Popescu et al. (2002a) also considered a range of shear strength plotted in Figure 3-17. They are compared to Hansen (1961) and Rowe and Davis (1982) models. There is an increase in normalized reaction forces with decreasing undrained shear strength which leads to the recommendation by the authors to alter the formula used to normalize the reaction loads to:

$$\frac{F_{ult}}{s_u D} = N_{ch} + \frac{\alpha}{s_u} \quad (3-36)$$

where  $\alpha$  is a factor including the effects of soil weight and type of soil failure mechanism. For the case analysed in this study the soil unit weight was  $18 \text{ kN/m}^3$  and the embedment ratio was 3 resulting in a suggested  $\alpha$  of 45 kPa.

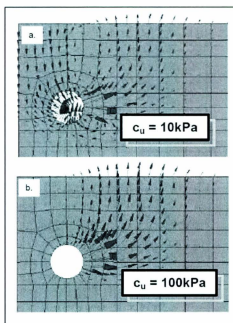


Figure 3-16 – Numerical results for lateral rigid pipeline displacement in clay: failure mechanisms (Popescu et al., 2002a)

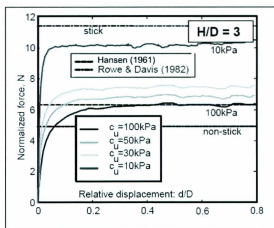


Figure 3-17 – Predicted and recommended interaction forces for lateral loading of a rigid pipeline in clay (Popescu et al., 2002a)

The authors also investigated the effects of internal pressure on pipe ovalisation and found that internal pressure has a significant effect on the ovalisation and collapse mechanisms of buried pipes subjected to moment loading. Two situations were analysed: no internal pressure and internal pressure inducing a hoop stress of 40% of the yield strength of the pipe. The location of collapse and buckling modes differed significantly for both cases. Also, predicted ovalisation under internal pressure was one order of magnitude smaller than that of a pipe with no internal pressure.

In addition to the centrifuge experiments, Phillips et al. (2004b) conducted plane strain finite element analysis using the model by Popescu et al. (2002b). A parametric investigation was performed to assess the effects of burial depth and soil properties on the interaction force for lateral pipeline displacement in soil. The results from various soil undrained shear strengths and embedment ratios is shown in Figure 3-18.  $N_{ch}$  increases with increasing embedment and undrained shear strength. However, for  $H/D > 4$ ,  $N_{ch}$  is reasonably constant for equivalent undrained shear strengths. For  $H/D > 2$ , the predicted numerical values are greater than those predicted by Hansen (1961) and the peak load at deep burials is approximately 35% to 76% higher than Hansen (1961). The change in interaction factor with burial depth is connected with a change in failure mechanism. For shallow burial soil weight from the passive weight contributes to the resistance to pipe displacement, while for deep burial there is little effect from soil displacement and Equation 3-24 is recommended to account for this change in mechanism.

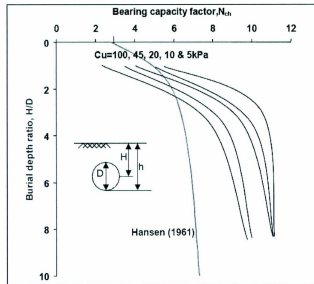


Figure 3-18 – Lateral bearing capacity factors (Phillips et al., 2004b)

An additional series of FEA was performed for undrained shear strength of 10 kPa and 20 kPa and each of the analyses were repeated assuming no soil weight and a soil weight of  $17.5 \text{ kN/m}^3$ . A value of 0.85 for  $\beta$  was seen to give the best fit to the data (see Figure 3-19).

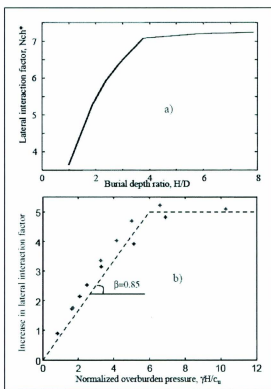


Figure 3-19 – Lateral interaction factor contributions, for 10 kPa and 20 kPa soils (Phillips et al., 2004b)

Phillips et al. (2004a) conducted a parametric investigation into the influence of embedment ratio, soil strength, axial-lateral pipe displacement angle, and the pipe-soil interface friction angle. The model used in the study was calibrated against large scale experimental data by Popescu et al. (2002b). The axial and lateral forces were normalized by the soil's undrained shear strength using

$$N_x = \frac{F_x}{s_u D L} \quad (3-37)$$

$$N_z = \frac{F_z}{s_u DL} = \alpha \pi \quad (3-38)$$

where  $\alpha$  is an adhesion factor and  $F_x$  and  $F_z$  are the maximum lateral and axial forces, respectively.

Both lateral and axial interaction factors increased with depth across the range of translation angles, shown in Figure 3-20 and Figure 3-21. The axial interaction factors were very low for pure axial displacement and a slight increase in interaction angle lead to a significant increase in the axial interaction factor. For the factors studied, an angle of approximately  $10^\circ$  resulted in the maximum axial interaction factor which is consistent with adhesion factors around 0.5. For angles greater than  $30^\circ$ , the peak axial forces gradually reduce due to failure of the soil on inclined planes while the mobilized lateral force increases (Phillips et al., 2004a).

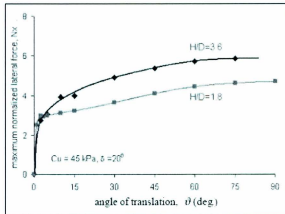


Figure 3-20 – Effect of burial depth on lateral interaction factor (Phillips et al., 2004b)

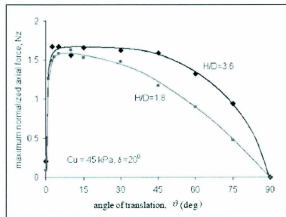


Figure 3-21 - Effect of burial depth on axial interaction factor (Phillips et al., 2004b)

Axial and lateral interaction factors are plotted in Figure 3-22 for the range of interaction angles. The axial resistance,  $N_x$  is controlled by sliding and friction along the pipe-soil interface for low translation angles. The axial resistance is controlled by shear through the soil mass at higher translation angles (Phillips et al., 2004b).

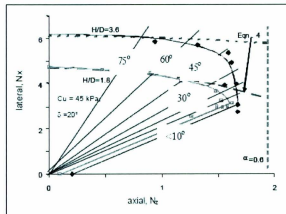


Figure 3-22 – Axial-lateral force interaction diagram (Phillips et al., 2004b)

The authors approximate the axial-lateral interaction envelope of Figure 3-22 as

$$N_x^2 + 3N_z^2 = N_{x90}^2 \quad (3-39)$$

where  $N_{x90}$  is the lateral interaction factor for pure lateral loading and  $N_z < \alpha x$ . The 3 is an analytical factor proposed by the authors to account for the difference between the shear and bearing stress limits associated with axial and lateral loading, respectively. Equation 3-39 is plotted in Figure 3-22 with  $N_z$  capped by an adhesion factor of 0.6. A study on the effect of undrained shear strength on axial and lateral interaction factors revealed that both factors decreased slightly with increasing soil strength. Interface friction angle was also seen to affect the interaction factors. Axial interaction factors increased with increasing friction angle while the effect of friction on lateral interaction factors was small.

Daiyan et al. (2009) conducted a parametric study to assess the oblique lateral-vertical pipe/soil interaction. The authors used a Response Surface Methodology (RSM) to analyse the results of the study and to obtain a response surface capable of predicting the response for various factor levels. Three dimensional finite element analyses were performed in ABAQUS/Standard. The soil was discretized using 8-node linear brick elements with reduced integration (C3D8R) and an elastic perfectly plastic von-Mises criterion was implemented to model the soil material behaviour. The pipe was assumed rigid and discretized using 4-node shell element with reduced integration and 5 degrees of freedom per node (S4R5). The interface between the pipe and soil was simulated using the contact surface approach available in ABAQUS/Standard and the coefficient of friction was set to 0.25. The factors considered in this study were: a range of embedment

ratios from 1 to 7, pipe diameters ranging from 0.4 m to 1.0 m, and undrained shear strength from 5 kPa to 95 kPa.

Examining the results of the numerical analysis using RSM for two non-dimensional parameters  $H/D$  and  $\gamma H/s_u$  resulted in the following equation describing the lateral interaction factor

$$N_{ch} = N_{ch}^* + \beta_h \frac{\gamma H}{s_u} \quad (3-40)$$

where

$$N_{ch}^* = 0.20 * \frac{H}{D} * \left(10.5 - \frac{H}{D}\right) + 2 \quad \text{for } \frac{H}{D} < 5 \quad (3-41)$$

or

$$N_{ch}^* = 7.5 \quad \text{for } \frac{H}{D} \geq 5 \quad (3-42)$$

and

$$\beta_h = 0.97 + 0.07 * \frac{H}{D} - 0.052 * \frac{\gamma H}{s_u} \quad (3-43)$$

where  $N_{ch}^*$  is the weightless term of the interaction factor and  $\beta_h$  determines the amount the soil weight that contributes to the lateral soil restraint on the pipeline. Equations 3-40 to 3-43 are valid for  $1 \leq H/D \leq 7$  and  $0.5 \leq \gamma H/s_u \leq 6.5$ . Figure 3-23 shows the contribution of the overburden ratio in the lateral interaction factor when varying  $H/D$  and  $\gamma H/s_u$ .

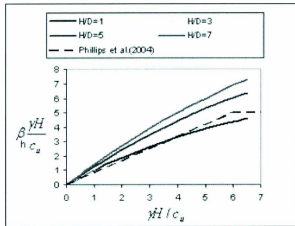


Figure 3-23 – Variations in the weight term of the lateral interaction factor with H/D and  $\gamma H/s_u$  (Daiyan et al., 2009)

RSM was also conducted on the results for vertical pipe/soil interaction which resulted in the following equations for the vertical interaction factor

$$N_{cv} = N_{cv}^* + \beta_v \frac{\gamma H}{s_u} \quad (3-44)$$

where

$$N_{cv}^* = 0.25 * \frac{H}{D} * \left( 11.2 - \frac{H}{D} \right) - 0.94 \quad \text{for } \frac{H}{D} < 5.5 \quad (3-45)$$

or

$$N_{cv}^* = 6.9 \quad \text{for } \frac{H}{D} \geq 5.5 \quad (3-46)$$

and

$$\beta_v = 1.034 + 0.039 * \frac{H}{D} - 0.06 * \frac{\gamma H}{s_u} \quad (3-47)$$

where  $N_{cv}^*$  is the weightless term of the interaction factor and  $\beta_v$  determines the amount the soil weight that contributes to the vertical soil restraint on the pipeline. Equations 3-44 to 3-47 are valid for  $1 \leq H/D \leq 7$  and  $0.5 \leq \gamma H/s_u \leq 6.5$ . Figure 3-24 shows the contribution of the overburden ratio in the lateral interaction factor when varying  $H/D$  and  $\gamma H/s_u$ .

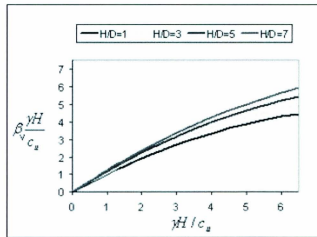


Figure 3-24 - Variations in the weight term of the vertical interaction factor with  $H/D$  and  $\gamma H/s_u$  (Daiyan et al., 2009)

Figure 3-25 and Figure 3-26 illustrates the effect of the overburden ratio on the lateral and vertical interaction factors, respectively. The interaction factors increase with increase in overburden ratio but the rate of increase is reduced up to a limiting point where the shallow mechanism changes to a deep one. For a constant embedment depth the soil failure mechanism can be shallow or deep depending on the overburden ratio.

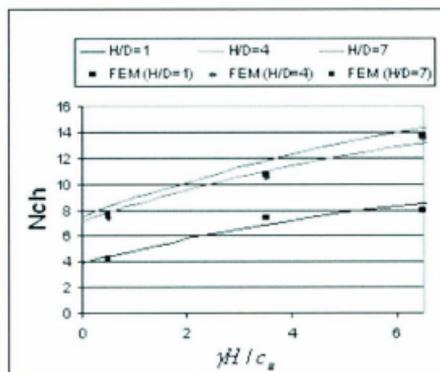


Figure 3-25 – Effect of overburden ratio on lateral interaction factor (Daiyan et al., 2009)

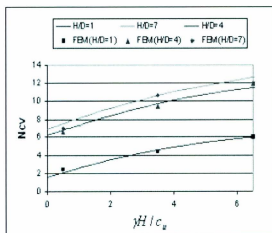


Figure 3-26 - Effect of overburden ratio on vertical interaction factor (Daiyan et al., 2009)

RSM was also conducted for oblique lateral-vertical pipe/soil interaction. The following equations were obtained

$$\frac{p}{p_u} = k(1.576 - 0.576k) \quad (3-48)$$

and

$$\frac{q}{q_u} = 1 - k(0.244 + 0.756k) \quad (3-49)$$

where

$$k = \frac{\theta}{90} \quad (3-50)$$

and  $p$  and  $q$  are the lateral and vertical loads, respectively, during a pipe displacement at an oblique angle  $\theta$ . The variables  $p_u$  and  $q_u$  are the loads during pure lateral and pure vertical displacement, respectively. The effects of  $H/D$  and  $\gamma H/s_u$  are not significant when using the normalized loads  $p/p_u$  and  $q/q_u$ .

Pike and Kenny (2011) studied pipe/soil interactions in clay using plane strain finite element analysis to examine the effects of embedment ratio and pipe direction of travel have on soil failure mechanisms. A Coupled Eulerian Lagrangian (CEL) approach was used for the analysis. The soil was modeled using the Eulerian element, EC3D8R which is an 8-node brick element with reduced integration. The pipeline was discretized using an 8-node linear brick element (C3D8R) and was assumed rigid. The contact at the pipe/soil interface was modeled using the general contact option available in ABAQUS/Explicit. The shear stress at the pipe/soil interface was capped by setting  $\tau_{max}$  equal to half the undrained shear strength.

The soil had a unit weight of  $17.5 \text{ kN/m}^3$  and undrained shear strength of  $45 \text{ kPa}$ . Embedment ratios of 1, 2, 4, and 6 were used to examine the effects of burial depth on

lateral interaction factor. Increase in the burial depth resulted in an increase in the lateral interaction factor and were bounded by an upper limit of 11 for deep burials, shown in Figure 3-27.

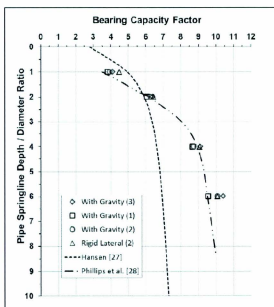


Figure 3-27 - Lateral interaction factors as a function of H/D

The authors also compared three different methods used to obtain peak loads for lateral interaction factor calculation: (1) the load value of the point of intersection of the tangents to the two straight line portions of the curve, (2) Terzaghi's definition, where the load at which the load-displacement curve passes into a steep straight tangent is taken, and (3) the maximum load with large displacement. These methods are highlighted in Figure 3-28. In Figure 3-27 method (1) exhibits the best correlation with Phillips et al. (2004b) data.

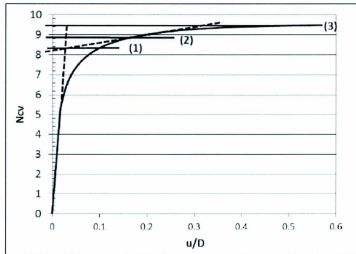


Figure 3-28 – Methods used to obtain peak loads for lateral interaction factors (Pike and Kenny, 2011)

Coupled response, during oblique lateral-vertical movements, was assessed at pipe embedment ratios of 2 and 6. Displacements to peak load occurred between 10% and 15% of the pipeline diameter with the upper bound lateral bearing factor of 8 and 9 for pure lateral displacement and 8 for pure vertical displacement. Significant increase in lateral soil strength mobilization was seen for attack angles greater than  $15^\circ$  from the vertical.

Seo et al. (2011) examined yield envelopes for axial-lateral oblique pipe/soil interactions in cohesive soils. Embedment ratios of 1.8 and 3.6 with oblique angles of movement ranging from  $0^\circ$  to  $90^\circ$  were used in the analysis. The soil had a unit weight of  $17.5 \text{ kN/m}^3$ , undrained shear strength of 45 kPa and was modeled using von Mises criterion.



For axial pipe movement, an annular shear zone around the pipe was seen (see Figure 3-30). For pure axial movement the axial interaction factor was approximately 0.69 for an H/D of 1.8 and 1.12 for an H/D of 3.6. The maximum axial interaction factor occurred at an oblique movement of 10°, relative to the axial direction, resulting in a value of 1.95 for the axial interaction factor.



Figure 3-30 – Soil failure mechanisms for axial pipe/soil interaction, H/D = 1.8 (Seo et al., 2011)

Borges and Oliveira (2011) conducted finite element analysis on the lateral-vertical oblique movement of a pipeline buried in clay. The soil was modeled using both von-Mises and Mohr-Coulomb criteria. The undrained shear strength of the soil was characterized by:

$$s_u = 1.424z + 3.0 \quad (3-51)$$

where  $z$  is the depth below the soil surface. The submerged unit weight of the soil was taken as  $5.45 \text{ kN/m}^3$ . The Young's modulus was obtained from:

$$E = 550s_u \quad (3-52)$$

The shear strength at the pipe/soil interface was taken to be half the undrained shear strength. The pipe had a diameter of 0.6 m and wall thickness of 0.0254 m. The Young's modulus of the pipe was 206 GPa and yield stress was 358 MPa. Embedment ratios ranging from 0.25 to 2.0 and oblique angle ranging from 0° to 180° were assessed. The angles of displacement were defined at 0° for pure vertical upward movement and 180° for pure vertical downward movement.

Failure envelopes plotted in Figure 3-31 indicate an increasing trend of interaction factors with burial depth. The failure envelopes are not symmetrical around the horizontal plane because of the increasing undrained shear strength with depth. Also, the interaction factors are significantly greater for movement that occur in the lateral-vertical downward direction. This can be attributed to the increase in soil mass involved during downward pipe displacements.

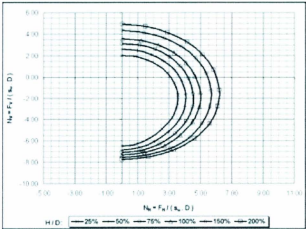


Figure 3-31 – Normalized failure envelopes (Borges and Oliveira, 2011)

In addition to the failure envelopes plotted in Figure 3-31, the authors normalized the maximum lateral and vertical forces with respect to their maximum values. The maximum horizontal force assumed for each H/D ratio was the value associated with  $\theta = 90^\circ$ . For the maximum vertical force, the values associated with  $\theta = 0^\circ$  and  $\theta = 180^\circ$  were adopted for the upward and downward movements, respectively. Figure 3-32 plots the normalized force values and Equation 3-53.

$$\left(\frac{F_H}{F_{Hmax}}\right)^2 + \left(\frac{F_V}{F_{Vmax}}\right)^2 = 1 \quad (3-53)$$

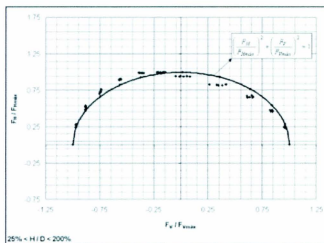


Figure 3-32 - Failure envelopes normalized by their maximum values (Borges and Oliveira, 2011)

### 3.5 Current Engineering Guidelines

#### 3.5.1 Guidelines for the Seismic Design and Assessment of Natural Gas and Liquid Hydrocarbon Pipelines

These guidelines were prepared by Honegger and Nyman (2004) for the Pipeline Research Council International (PRCI). These guidelines were intended to be an update of the 1984 ASCE guidelines relating to buried pipelines transporting natural gas and liquid hydrocarbons, since there has been considerable advancements since the ASCE (1984) guidelines were published.

Incorporated in these guidelines are analysis procedures to assess pipeline performance during movement in a soil medium. Recommendations for modelling pipe/soil interaction using finite element procedures are given. The recommended approach is to represent the pipeline with pipe or beam elements and the soil loading on the pipeline with discrete nonlinear spring elements. Figure 3-33 illustrates the idealized representation of the soil with discrete springs.

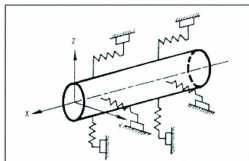


Figure 3-33 - Idealized representation of soil with discrete springs (Honegger and Nyman, 2004)

The equations for maximum soil spring force are based on laboratory and field experimental investigations on pipeline response, as well as general geotechnical approaches for related structures such as piles and anchor plates. The equation for axial soil spring force is:

$$T_u = \pi D \alpha c + \pi D H \gamma \left( \frac{1+K_0}{2} \right) \tan \delta \quad (3-54)$$

where  $T_u$  is the axial soil spring force,  $D$  is outside pipe diameter,  $c$  = soil cohesion representative of the soil backfill,  $H$  = depth to pipe springline,  $\gamma$  = effective unit weight of soil,  $K_0$  is coefficient of pressure at rest,  $\alpha$  is adhesion factor,  $\delta$  is interface angle of friction at the pipe soil interface,  $\phi$  is internal friction angle of the soil and  $f$  is coating dependent factor relating the internal friction angle of the soil to the friction angle at the soil-pipe interface. The equation for lateral soil spring force is:

$$P_u = N_{ch} s_u D + N_{qh} \bar{\gamma} H D \leq Q_d \quad (3-55)$$

where  $N_{ch}$  is the horizontal bearing capacity factor for clay (0 for  $c = 0$ ) and  $N_{qh}$  is the horizontal bearing capacity factor for sand (0 for  $\phi = 0^\circ$ ) and are given by

$$N_{ch} = a + bx + \frac{c}{(x+1)^2} + \frac{d}{(x+1)^3} \leq 9 \quad (3-56)$$

and

$$N_{qh} = a + bx + cx^2 + dx^3 + ex^4 \quad (3-57)$$

where  $x$  is equal to  $H/D$  and  $a, b, c, d, e$  are based on  $\phi$  and can be found in tabular form in the guidelines. The equation for vertical uplift soil spring force is:

$$Q_u = N_{cv} s_u D + N_{qv} \bar{\gamma} H D \quad (3-58)$$

where  $N_{cv}$  is the vertical uplift factor for clay (0 for  $c = 0$ ) and  $N_{qv}$  is the vertical uplift factor for sand (0 for  $\varphi = 0^\circ$ ) and are given by

$$N_{cv} = 2 \left( \frac{H}{D} \right) \leq 10 \text{ for } \left( \frac{H}{D} \right) \leq 10 \quad (3-59)$$

and

$$N_{qv} = \tan \varphi \left( \frac{\varphi}{44} \right) \left( \frac{H}{D} \right) \leq N_q \quad (3-60)$$

where

$$N_q = e^{\pi \tan \varphi} \tan^2 \left( 45 + \frac{\varphi}{2} \right) \quad (3-61)$$

The equation for vertical bearing soil spring force is:

$$Q_d = N_c s_u D + N_q \bar{\gamma} H D + N_\gamma \gamma \frac{D^2}{2} \quad (3-62)$$

where  $\gamma$  is the total unit weight of the soil and  $N_c$ ,  $N_q$ ,  $N_\gamma$  are bearing capacity factors given by

$$N_c = \cot(\varphi + 0.001) \left[ e^{\pi \tan(\varphi + 0.001)} \tan^2 \left( 45 + \frac{\varphi + 0.001}{2} \right) - 1 \right] \quad (3-63)$$

and

$$N_\gamma = e^{(0.18\varphi - 2.5)} \quad (3-64)$$

The equations provided for the parameters  $N_{qh}$ ,  $N_{ch}$ ,  $N_{qv}$ ,  $N_{cv}$ ,  $N_c$ ,  $N_q$  and  $N_\gamma$  are developed from empirical curves found in the literature (see Figure 3-34 to Figure 3-38).

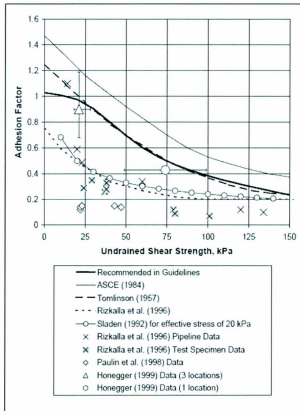


Figure 3-34 - Plotted Values for the Adhesion Factor,  $\alpha$  (Honegger and Nyman, 2004)

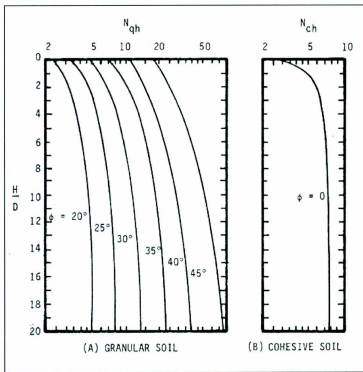


Figure 3-35 - Values of  $N_{qh}$  and  $N_{ch}$  (Hansen, 1961)

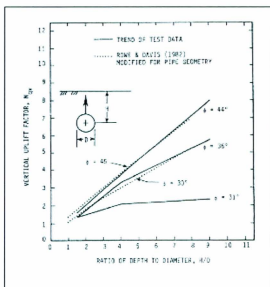


Figure 3-36 - Ranges for values of  $N_{qv}$  (Trautmann and O'Rourke, 1983)

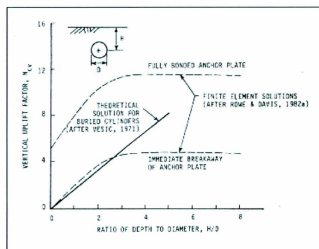


Figure 3-37 - Ranges for values of  $N_{cv}$  (Trautmann and O'Rourke, 1983)

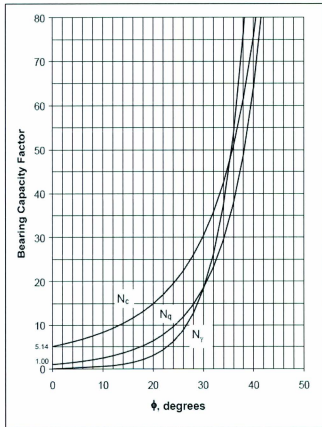


Figure 3-38 - Plotted values of bearing capacity factors ( $N_q$ ,  $N_c$ , and  $N_\gamma$ ) (Honegger and Nyman, 2004)

These guidelines use independent structural springs to represent the soil response in the axial, lateral, downward and upward directions and do not account for potential cross effects between the various directions. However, current research has shown that cross effects occur and need to be considered in pipeline design.

### ***3.5.2 Guidelines for the Design of Buried Steel Pipe***

This guide was prepared for the American Lifelines Alliance (ALA), by a group of civil and mechanical engineers, to develop design provisions to evaluate the integrity for buried pipe. The provision apply to: buried carbon or alloy steel pipe fabricated to ASTM or API specifications, welded pipe joined by techniques permitted by ASME code or API standards, and piping engineered in accordance with ASME B31 pressure piping code.

This guide also includes methods of evaluating pipe/soil relative displacements using finite element procedures. These procedures are the same as those described by Honegger and Nyman (2004), where the pipe is discretized using pipe or beam elements and the soil is represented by nonlinear springs. The equations that represent the soil spring forces and the non-dimensionalized interaction factors are the same as those presented by Honegger and Nyman (2004) in the PRCI guidelines.

## **4 PROJECT DESCRIPTION**

### **4.1 Scope of Work**

The research conducted here consists of the development of related but separate finite element modelling procedures examining the effects of large ground movement events on soil loads, deformations, and failure mechanisms. The first part is to develop advanced three-dimensional, continuum finite element modeling procedures capable of predicting the free-field subgouge soil response to an ice gouge event. The second part considered the application of the finite element method to predict soil response and load transfer mechanisms during pipeline/soil interaction. The commercial software package ABAQUS will be used to build and analyse the models. This finite element program can handle a broad range of materials, various element types, complex contact conditions, and solution strategies; such as Arbitrary Lagrangian Eulerian (ALE) and Coupled Eulerian Lagrangian (CEL) formulations. The advance of ALE and CEL methods have provided the required engineering tools for the analysis of complex, nonlinear large deformation geotechnical failure mechanisms, pipeline/soil interaction events and pipeline failure mechanisms.

The first study focused on the effects of ice keel profile and soil constitutive model, on soil response. Numerical modelling procedures were developed in ABAQUS/Explicit using ALE modeling procedures. Measurements of subgouge deformations and seabed reaction forces were taken. The main focus here was on intermediate gouge depths (~ 1.5 m) using a finite element approach. This gouge depth was selected as in the ALE

environment, ice gouge events with deeper keel depths and widths tended to experience numerical instability due element distortion with gouge travel (i.e. increased solution time). The study also details the relationship between ice geometry and the gouge profile geometry through measurements of berm height, height of frontal mound, and extent of plastic deformation below the gouging keel.

The primary calibration exercise was for free field gouge events characterizing the soil failure mechanisms and subgouge soil deformations for ice keel/seabed interaction events. The numerical model was calibrated against data obtained by Lach (1996).

The second part of the study consisted of the development and calibration of a pipeline/soil interaction model capable of predicting the soil load-displacement response and soil failure mechanisms during oblique ground movement events with a rigid pipeline. As in the first study, numerical modeling procedures were developed using an ALE formulation.

The model was used to study pipeline movements in lateral-vertical oblique directions with a range of different angles. Measurements of the peak load and pipeline displacement to peak load were taken for all interaction angles. The study also incorporated the effects of cover depth and undrained shear strength on the response. Qualitative data was also collected on soil failure mechanisms for various pipeline displacements and cover depths.

The primary calibration exercise for the pipeline/soil interaction model was to match peak load and peak displacements to Phillips et al. (2004b) centrifuge data. Two tests from this program were used as benchmarks for the numerical calibration.

The analyses described above are highlighted in the subsequent chapters. Calibration of numerical modelling procedures was considered for both analyses and the importance in accounting for correct soil representation was discussed. The studies were extended to analyse various parameters of importance to both ice keel/soil and pipeline/soil interactions. It is important to gain insight into ice keel/soil and pipeline/soil interactions in order to develop improved numerical modeling procedures capable of accurately predicting soil response. This knowledge can be transferred to help aid in the calibration of more complex ice keel/soil/pipeline interaction models.

## **5 ASSESSMENT OF ICE/SOIL INTERACTIONS: CONTINUUM MODELING IN CLAYS**

In this study, soil failure mechanisms and subgouge soil deformations for ice keel/seabed interactions are examined. Consideration of soil constitutive model, ice-soil interface contact mechanics and the assumed ice keel geometry and their effects on soil response are discussed. While notable progress has been made in this field, large uncertainty remains in the use of advanced simulation tools to adequately capture specific aspects of this complex phenomenon. In this study, difficulties on robust calibration of numerical modelling procedures, with respect to available experimental datasets, and questions on realistic numerical simulation of ice keel/seabed interface properties and contact mechanics are addressed.

This paper has been accepted for publication at the 22<sup>nd</sup> International Ocean and Polar Engineering Conference in Rhodes, Greece. As the principal investor and first author, I was responsible for conducting the numerical investigation, analyzing the data, and reporting it inside this paper. The second author, Dr. Shawn Kenny, was responsible for supervision of the investigation and guidance on data analysis.

Authors: Christopher Rossiter and Shawn Kenny

### **5.1 Introduction**

Various hazards that need to be acknowledged when developing oil and gas facilities offshore in cold regions are: waves, icebergs, freezing spray, sea ice, pressure ridges and characteristics of the seabed. Ice masses, such as pressure ridges, are of utmost concern to buried pipelines in arctic regions. Pressure ridges are created by the build up of sea ice

and can have keels which extend well below the water surface. These ridges are driven primarily by ocean currents and secondarily by wind, wind generated currents, and by direct loading from other ice. Potentially, these ice masses can be carried into water where the keel depth is sufficient to ground. When a floating ice mass moves into shallower water and comes into contact with the seabed, it causes surficial and subgouge soil deformations. Subgouge soil deformations pose a serious threat to buried pipelines. If an ice feature passes over a pipeline, the soil displacements can be large enough to interact with the pipeline and cause failure, even if the pipeline is buried well beneath the maximum gouge depth.

Due to the complexity of the ice gouge problem and the significant cost of field programs and large scale experiments, the examination of ice keel/seabed/pipeline interaction scenarios have been conducted using analytical, numerical and reduced scale physical modeling techniques. Physical modeling techniques (Porooshab et al., 1989; Paulin, 1992; Lach, 1996) have been the most popular option for the investigation into the gouge problem, especially centrifuge modeling with its increased accuracy corresponding to large scale field observations. But recent advancements in computer hardware and software technology have provided a technical framework to develop advanced numerical tools for the simulation of ice gouge events and a cost-effective approach for conducting these investigations. Eulerian based formulations, such as Arbitrary Lagrangian Eulerian (ALE) and Coupled Eulerian Lagrangian (CEL), have proved to be adequate in modeling the large deformation and strain inherent in the ice/soil interaction as demonstrated by: Konuk and Gracie (2004), Phillips et al. (2010) and Pike et al. (2011a,b).

CEL is capable of modelling realistic design scenarios for pipelines in ice gouge environments; such as backfill/native soil interface and multiple interfaces with compliant materials. When considering large deformation problems the CEL formulation in ABAQUS/Explicit offers a more computationally friendly framework than that of its ALE counterpart. By employing an Eulerian mesh, which is fixed in space, the analysis is capable of handling large deformation problems without mesh distortion affecting solution convergence. However, some limitations inherent in the CEL framework are discussed in subsequent sections.

While notable progress has been made, large uncertainty remains in the use of advanced simulation tools to capture many aspects of this complex phenomenon. Typically, calibration exercises are conducted by validating the numerical model against subgouge displacements from physical test data. A comprehensive dataset that provides a technical basis to establish a validated simulation tool of coupled ice keel/seabed/pipeline events, across a range of practical design scenarios does not exist. The lack of full scale dataset on extreme design ice gouge events is a technical gap. Further assessment of the numerical simulation tools capabilities and technical constraints is needed (Pike et al., 2011a). Extending the calibration and validation exercise to investigate the significance of other parameters; such as ice keel shape, ice keel compliance and failure envelopes, soil state and constitutive behaviour, interface mechanics and pipeline interference effects, on soil subgouge deformations, soil failure mechanisms and pipeline mechanical response is necessary to reduce model uncertainty (Kenny et al., 2000; Pike et al., 2011a, b).

The predicted soil response is dependent on the chosen constitutive soil model, ice-soil interface contact mechanics and the assumed ice keel shape, amongst several other factors. Analysing these factors through sensitivity studies can disclose the importance in choosing more realistic conditions when examining the value of numerical modelling to supplement physical test programs.

This study highlights the importance of choosing a proper soil model and interface contact conditions when calibrating against a physical data set. The calibration exercise is extended to incorporate matching seabed reaction forces and berm heights in addition to subgouge soil displacements. In addition to the calibration exercise a parametric study was conducted which considered keel geometry in terms of attack angle and width and the effects of these parameters on soil response.

## **5.2 Previous Numerical Models**

A number of studies have been conducted on the finite element modeling of ice gouging using Eulerian based approaches. Most of this modeling has been conducted in clays, within total stress analysis, due to the complexity of modeling sand constitutive behaviour and dilatant nature under shear.

Konuk and Gracie (2004) developed an ice gouge model using ALE procedures in LS-Dyna. ALE methods in LS-Dyna are comparable to that of CEL used in ABAQUS/Explicit, where a material is allowed to flow through a fixed Eulerian mesh. Their study was conducted in relatively soft clays and horizontal and lateral soil particle trajectories were measured. The authors also analysed two soil types to study the effects

of soil representation. This was done by increasing the soil's elastic parameters while maintaining the plastic parameters unchanged. The stiffer clay experienced smaller displacements than the soft clay, in regions just below the gouge depth, but in the subgouge regions the displacements are greater for the stiffer soil. Konuk et al. (2005) extended the model to consider keel attack angle, with angles ranging from  $15^\circ$  to  $45^\circ$ . It was found that subgouge deformations are very sensitive to keel angle, with deformations increasing with decreasing attack angle. Konuk and Yu (2007) tested the sensitivity of the following parameters: soil properties, clearance depth, pipeline diameter, scour width, scour depth, and scour track orientation. It was determined that the soils cohesion had minimal effect on the pipeline displacements but increasing the soil hardening behaviour cause an increase in soil displacements. Konuk and Yu (2010) examined the effects of depth dependent soil strength profile on seabed reaction force, pipeline trajectories and pipeline stresses. The soil mass consisted of a stiff clay with linear varying strength versus depth profile, overlain by a soft clay with a constant strength profile. This study also considered effects of reworking of the upper layer of the soft clay. It was found that a hard lower soil layer causes a reduction in pipeline stresses and displacements.

Numerical modeling procedures were developed at J.P. Kenny (Jukes et al., 2008) that used ABAQUS/Explicit with a CEL formulation. The analysis studied the effects of scour depth and trench back fill. Scour depths of 2m, 3m, and 4m were studied and loose and dense sand were analysed as the trench backfill. The analysis determined that higher pipeline deflections are seen in dense backfills than in loose and with increasing scour

depth. The model (Jukes et al., 2008) was simplified to a keel/soil interaction in order to validate the subgouge deformations against available data. The results were compared to PRISE centrifuge experimental data (Lach and Clark, 1996), and the empirical PRISE function (Woodworth-Lynas et al., 1996). Sensitivity studies were done to examine the effect of keel angle, keel geometry and also scour depth. Small keel attack angles were found to result in larger subgouge soil displacements.

A numerical study conducted by Phillips et al. (2010) compared three different FEA techniques common to the ice gouge problem: ALE and CEL formulations from ABAQUS/Explicit and ALE formulation from LS-DYNA. The authors extended the validation exercise to include gouge forces, frontal berm formation, seabed failure mechanisms, vertical subgouge displacements, and lateral subgouge displacements. The soil was modeled as clay using von-Mises criteria and constant undrained shear strength with depth was assumed. The three finite element procedures had comparable vertical and horizontal seabed reaction forces with the CEL analysis predicting slightly larger reaction forces than the other techniques. Ratios of horizontal to vertical keel reaction forces are approximately 1 for a 45° attack angle and decreases to about 0.8 for a 30° attack angle and 0.6 for a 15° attack angle.

A parametric study was conducted at Memorial University (Pike et al., 2011b) to examine the influence of attack angle and interface properties on soil behaviour and pipeline mechanical response. This work utilized ALE formulations in LS-Dyna and CEL formulations in ABAQUS/Explicit to simulate both free field and coupled ice gouge

events. The maximum interface shear strength was defined equal to the soil undrained shear strength and one-third the soil undrained shear strength. For the free field case with a keel attack angle of  $15^\circ$ , the ratio of vertical to horizontal seabed reaction forces ranged from 5.5 in ABAQUS to 6.3 in LS-Dyna when the interface shear strength limit was 30 kPa. A reduction in the vertical to horizontal seabed reaction forces to 3.4 was seen when the interface shear strength was reduced to 10 kPa. For the  $30^\circ$  keel attack angle case the ratio of vertical to horizontal seabed reaction forces ranged from 2.5 to 4.0 when the soil interface shear strength limit was set to 30 kPa. By reducing the shear strength to 10 kPa the ratio of vertical to horizontal seabed reaction forces decreased to 2.7 in LS-Dyna but remained the same in CEL. The attack angle of the keel had significant effects on the displacement profiles of soil. For shallow depths below the gouge base the displacements are greater for the  $30^\circ$  attack face, but the vertical extent of these displacements are greater for the  $15^\circ$  attack face.

These studies and other investigations (e.g. Kenny et al., 2007a; Pike and Kenny, 2012) have indicated that the magnitude and extent of subgouge soil deformations is dependent on soil strength properties and state variables. In addition, gouge geometry and shape, interface properties, and soil strength profile have been shown to affect subgouge soil deformations.

The current study was initially focused on using the CEL formulation due to the robust modelling capabilities to analyse practical ice gouge scenarios. However, in this study, from analysis of the contact stress developed at the ice keel/seabed interface, it was

observed that the interface frictional forces did not correctly account for the equivalent shear stress limit ( $\tau_{max}$ ). The shear stresses developed to a value much lower than the defined  $\tau_{max}$ , which resulted in greater clearing and subduction of the soil, causing incorrect estimation of the seabed reaction forces. This is a significant issue with respect to the correct simulation of interface mechanics that is not presently captured by the numerical modelling procedures in CEL. Although ABAQUS CEL numerical models have been partially calibrated with reduced-scale centrifuge data, the numerical modelling procedures may not be valid, outside this domain, with respect to clearing mechanisms, interface conditions and contact mechanics. This uncertainty has been identified in this study for ice gouge scenarios with respect to a parameter study on variation in ice keel/seabed interface shear strength limits. Thus, when using current ABAQUS CEL modelling procedures, there exists an uncertainty in the capability of the numerical simulations to predict the correct mechanisms that could develop during an ice gouge event. Consequently, this study was conducted within an ALE framework in order to properly account for the equivalent shear stress limit at the ice keel/seabed interface.

### **5.3 Physical Experiments**

Centrifuge modeling at high simulated gravity has an advantage over physical experiments carried out at single gravity, as it is capable of accurately modeling the soil stress field. These experiments have become the primary validation exercise for numerical procedures. Konuk and Gracie (2004) and Philips et al. (2010) compared their results to the PRISE function described by Woodworth-Lynas et al. (1996). Jukes et al

(2008) and Pike et al. (2011a, b) validated their numerical models against Lach (1996) centrifuge data. Jukes et al (2008) also validated against the PRISE function.

Lach (1996) conducted a series of tests at the Cambridge Geotechnical Centrifuge, in Cambridge England. The experimental program considered nine tests conducted in overconsolidated clays, in which the test variables included: the prescribed soil stress history, attack angle and width of the model keel, and the scour depth attained during steady state. Test 05 was the base case for the experimental program where the keel attack angle was set to 15°, keel width was 100 mm (10 m at prototype scale) and the steady state gouge depth attained was 12.1 mm (1.21 m at prototype scale). The corresponding berm elevations averaged about 4.3 mm (0.43 m at prototype scale) above the original surface level. The average magnitudes of the horizontal and vertical force, during steady state, were 5.0 and 16.9 MN (prototype scale) respectively. The maximum vertical and horizontal displacements immediately below the scour base were 0.88 m and 1.29 m respectively (prototype scale). The maximum depths below the base of the scour at which vertical and horizontal displacements measured were 6.2 m and 3.0 m, respectively, at prototype scale.

Woodworth-Lynas et al. (1996) developed empirical relationships to predict subgouge deformations in soft and stiff clays for a flat faced indenter with a rectangular gouge cross section. The data used to derive these equations was from PRISE centrifuge tests conducted in C-CORE's geotechnical centrifuge. The empirical relationships had four elements: an equation for horizontal subgouge displacements at the base of the keel; an

equation for the decay of horizontal displacements with increasing depth; an equation for the decay of vertical displacements with increasing depth; and an equation to compute horizontal displacements in the transverse direction.

## **5.4 NUMERICAL MODELLING PROCEDURES**

### **5.4.1 Overview**

Numerical instability is usually encountered when modeling large deformation processes with methods such as Lagrangian and Updated Lagrangian. More recently, ALE and CEL processes have been used to analyse large deformation structural mechanics and soil/structure interaction problems (Kenny et al., 2007; Pike et al., 2011a, b).

ALE and CEL formulations in the software package ABAQUS/Explicit were utilized here to simulate free-field ice gouge events. These methods are suitable for modelling the large deformations and strains inherent in ice-soil interactions. ALE is an adaptive meshing technique which combines features of both Lagrangian and Eulerian analyses. ALE adaptive meshing allows the mesh to move independently of the material, therefore maintaining high mesh quality. However, this adaptive method maintains mesh topology, which limits its ability to maintain a high quality mesh during extreme deformations.

In an Eulerian analysis, nodes are fixed in space, and material flows through elements that do not deform. Eulerian material can interact with a Lagrangian body through Eulerian-Lagrangian contact; these simulations are referred to as CEL simulations. Because the mesh is fixed, CEL procedures are capable of modeling extreme deformations.

#### **5.4.2 Numerical Model Definition**

In ALE the soil was discretized using C3D8R (solid three dimensional eight node with reduced integration) elements. The soil was modeled as an isotropic elastic perfectly plastic material with von-Mises failure criterion.

The soil domain was 140 m long, 18 m deep and 50 m wide. At the planes defining the outer extent of the domain, the nodal displacements in the normal direction were set to zero in ALE and normal nodal velocities were defined as zero in CEL. Biased meshing was used in all three directions in order to improve solution time. The maximum element length was 2.0 m at the edge of the boundary and decreased to 0.25 m where the ice keel was thought to reach steady state. The mesh region where gouging was to reach steady state was refined by elements with dimensions 0.25 m by 0.25 m by 0.25 m to increase accuracy in this area. Soil deformations were tracked at each increment using tracer particles.

The ice keel was assumed to be a rigid indenter with a trapezoidal geometry. The keel is modeled with a shell section and discretized with S4R (shell four node reduced integration) elements. The ice keel was constrained to only move in the direction of gouging.

The analysis consisted of three steps. The initial step was a geostatic step which established the in-situ stress state of the soil. The second step displaced the keel vertically to the required gouge depth. In the third step the keel was advanced in the gouging direction at a rate of 1 m/s.

## 5.5 NUMERICAL ANALYSIS

### 5.5.1 Calibration/Sensitivity Exercise

The results of the numerical procedures were compared to centrifuge data from ice gouge events within an overconsolidated speswhite kaolin clay test bed (Lach, 1996). The calibration exercise also examined the sensitivity of soil response to soil and interface contact definitions.

The over consolidation ratio (OCR) profiles (see Figure 5-1) with depth and plasticity index (PI) of 31 that Lach (1996) quoted for his soil specimens were used to calculate the rigidity index ( $I_r$ ) for the clay used in this study. Keaveny and Mitchell (1986) present a correlation based on anisotropically-consolidated triaxial compression test data that expresses  $I_r$  in terms of OCR and PI. The following is the empirical formulation which represents this correlation:

$$I_r = \frac{\exp\left(\frac{137-PI}{23}\right)}{\left[1 + \ln\left\{1 + \frac{(OCR-1)}{26}\right\}\right]^{3.2^{0.8}}} \quad (5-1)$$

The correlation above is based on  $G_{50}$  (50 % of  $\tau_{max}$ ). Taking the values obtained from Equation 5-1 above and considering the shear strength ( $s_u$ ) profiles with depth from Lach (1996) Test 05, the shear modulus ( $G$ ) can be obtained from the following equation:

$$G = I_r s_u \quad (5-2)$$

The elastic modulus (E) can then be determined from:

$$E = 2G(1 + \nu) \quad (5-3)$$

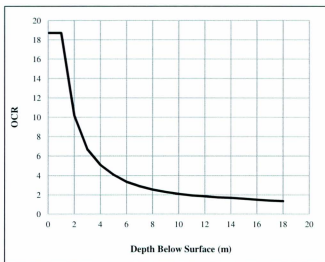


Figure 5-1 - OCR profile used in study

Sensitivity of the soil was also considered to determine if the soil strength would be affected by remoulding. The speswhite kaolin clay from Lach (1996) had a PI of 31 with a plastic limit (PL) of 38. This gives an activity (A) of approximately 0.48 and a clay fraction (CF) of 65%. This suggests that the clay will be affected by remoulding. A study by Andersen et al. (2004) which used a centrifuge to test penetration of suction anchors in soft clay measured the sensitivity of speswhite kaolin clay to be 2.2 with a standard deviation of 0.5. Doyle et al. (2004) quoted the sensitivity of speswhite kaolin clay to be 1.7 to 1.8 with highs of 2.2. For purposes of the current study a sensitivity of 2.0 was used. This suggests that the remoulding strength will be half the shear strength of the soil.

## 5.6 Model Calibration

Four calibration exercises were conducted in order to determine the sensitivity of soil response to soil constitutive model (see Table 5-1). The soil in all cases was modeled as undrained clay (Poisson's ratio ( $\nu$ ) of 0.49) and assumed to be an elastic perfectly plastic material. The analysis cases included soil shear strength as a constant (Case 1) and varying (Case 2) profile with interface shear strength equal to the undrained soil shear strength. Case 3 examined reduced soil shear strength at the ice keel/seabed interface. The last case (Case 4) looked at the effect of keel geometry.

For Case 1 the soil shear strength was taken as an average  $s_u$  value of 28 kPa and elastic modulus ( $E$ ) was taken to be  $300*s_u$  (based on an average OCR of 2.5). The maximum interface shear strength ( $\tau_{max}$ ) was taken to be equal to  $s_u$  for Case 1. For Case 2 and Case 3,  $E$  was obtained from the calculations highlighted in Equations 5-1 to 5-3. For Case 2,  $\tau_{max}$  was set equal to 28 kPa. Case 3 considered the effects of soil sensitivity and remoulding where the soil sensitivity was taken as 2, which gives  $\tau_{max}$  equal to  $0.5*s_u$  ( $s_u$  taken at the gouge depth 1.2 m below the surface).

Table 5-1 - Calibration Study Cases

	<b>Shear Strength</b>	<b>Elastic Modulus</b>	<b>Interface Shear Strength</b>
<b>Case 1</b>	28 kPa ( $s_u$ )	3.36 MPa ( $300*s_u$ )	28 kPa ( $s_u$ )
<b>Case 2</b>	Varying with depth	Based on Ir Calculations	28 kPa ( $s_u$ )
<b>Case 3</b>	Varying with depth	Based on Ir Calculations	10.5 kPa ( $0.5*s_u$ )
<b>Case 4</b>	Varying with depth	Based on Ir Calculations	10.5 kPa ( $0.5*s_u$ )

Case 4 was conducted using the same soil model as Case 3, however, a keel with the same dimensions as that in Lach (1996) was used to test the sensitivity of soil response due to the shape chosen for keel cross section. Due to the short length of the inclined keel face, in Lach (1996), the clearance from the front face of the keel and the seabed was very small. Once the berm developed to a certain height it would start pushing up over the front face of the keel (see Figure 5-2).

Seabed reaction forces along with subgouge soil deformations were compared to centrifuge results obtained from Lach (1996) Test 05 and PRISE empirical formulas (Woodworth-Lynas et al., 1996). Contact history output and contact field output were specified to monitor normal and frictional stresses developing on the keel.

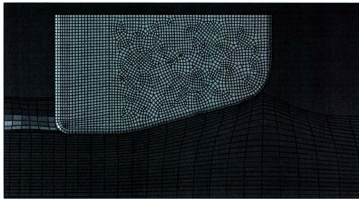


Figure 5-2 - Case 4 with Lach (1996) Keel

Table 5-2 summarizes the vertical and horizontal seabed reaction forces for the calibration tests. For Case 1 the interface shear strength of 28 kPa is too large and doesn't allow for enough subduction of soil beneath the keel. However, for this case, if  $\tau_{\max}$  was reduced an increase in vertical forces would occur. This would suggest that a constant  $s_u$  of 28 kPa is not accurate for this event. Case 2 uses a  $s_u$  profile which causes a significant decrease in vertical reaction forces, but the high  $\tau_{\max}$  doesn't allow for enough subduction beneath the keel, leading to higher horizontal forces. Case 3 and Case 4 consider the remoulded strength of soil at the interface and have the most appropriate matches for seabed reaction forces, with V/H ratios of 3.6 and 3.5 respectively.

Table 5-2 - Seabed Reaction Forces for Calibration Study

	Vertical Seabed Reaction Force (MN)	Horizontal Seabed Reaction Force (MN)	V/H
Case 1	17.6	8.1	2.2
Case 2	14.8	5.8	2.6
Case 3	15.4	4.3	3.6
Case 4	15.1	4.3	3.5
Lach 05	16.85	5.12	3.3

Figure 5-3 plots the FE results against Lach (1996) data set. It can be seen that the data presented here for vertical to horizontal force ratio is consistent with data obtained by Lach (1996).

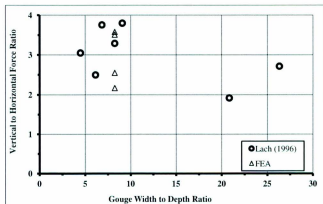


Figure 5-3 - V/H comparison of Lach (1996) to FE study

Figure 5-4 and Figure 5-5 plot horizontal and vertical subgauge deformations, respectively. Horizontal deformations extend beyond the 1 m shown in Figure 5-4; however, the 1 m is chosen to compare the results below one gauge depth. The numerical

model utilizes constant strain elements and therefore those elements just below the keel experience large unrealistic strains and in turn larger than normal deformations.

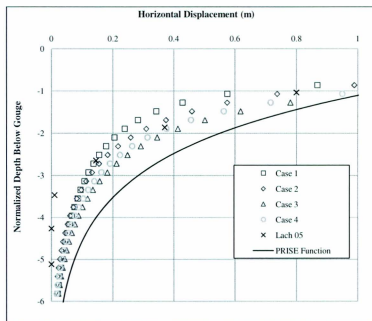


Figure 5-4 - Horizontal subgouge deformations for Calibration Tests

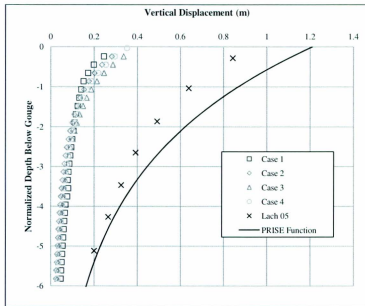


Figure 5-5 - Vertical Subgouge Deformations for Calibration Tests

All cases show similar results at and below four gouge depths. However, only good correlation is seen between Cases 2, 3, and 4 and Lach (1996) at depths between one and three gouge depths, with the best match seen in Case 4, which potentially suggests that clearing mechanisms influenced the soil behaviour. None of the tests conducted here match well with Lach (1996) data below three gouge depths. This could suggest that stiffer soil parameters may need to be used at these depths. Also, the soil bed in Test 05 of Lach (1996) was equipped with model pipelines which could affect the results as there is a significant influence and discontinuity from the pipe on soil behaviour (Kenny et al., 2007). This would be consistent with what was reported by Pike et al. (2011b), in which the pipeline caused an interruption in soil displacement field.

All calibration exercises conducted under predict vertical subgouge deformations. This is consistent with Phillips et al. (2010) and Pike et al (2011a). The extent of subgouge deformations travel below the depth at which the tracer particles were placed in the numerical model, however, it can be seen from the results that vertical soil displacements for Case 1 are greater than all other cases at greater depths and less than all other cases at depths closer to the soil surface, which is expected. This can be contributed to the constant  $s_u$  profile, resulting in a stiffer soil.

Gouge geometries such as berm height and frontal mound width appear to be highly sensitive to soil properties and interface contact conditions specified for the numerical model (see Table 5-3 and Figure 5-6). The frontal mound width decreases slightly due to a decrease in soil strength and an even greater decrease is seen with weaker interface properties. Frontal mound elevation is seen to decrease with decreasing soil strength but relatively unaffected by interface shear strength. For the ice keel attack angles investigated, the side berm elevations were not as sensitive to changes in  $s_u$  and  $\tau_{max}$  with only slightly decreasing trends for decreasing values of these properties. These results suggest:

- Higher strength soils have higher frontal mound elevation and less material being cleared to side berms. Also, high strength soils have a larger amount of material building in front of the gouging keel.
- Weaker soils have less resistance to subduction and clearing mechanisms and therefore have less material developing in front of the gouging keel.

- Weaker interface properties allow for greater subduction below the keel and therefore result in less material building in front of the keel.

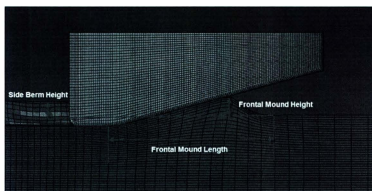


Figure 5-6 - Method of berm measurements

Table 5-3 - Frontal Mound and Side Berm Geometries

	<b>Frontal Mound Length (m)</b>	<b>Frontal Mound Elevation (m)</b>	<b>Side Berm Elevation (m)</b>
<b>Case 1</b>	17.6	2.1	1.46
<b>Case 2</b>	16.4	1.47	1.44
<b>Case 3</b>	14.9	1.32	1.30
<b>Case 4</b>	14.1	1.46	1.20
<b>Lach 05</b>	N/A	N/A	0.4

Good correlation for side berm elevations was not seen, with elevations calculated in the numerical model 3-5 times higher than that in Lach (1996). The soil model assumes perfect plasticity (von Mises criterion), and does not account for the effects of tension

cracking and the development of blocks of soil material being formed and cleared during gouge events. Options are available in ABAQUS to establish failure criterion to address this mechanism and treat the blocks as discrete rigid body kinematic particles.

### 5.7 Parametric Study

A gouge parameter study was conducted to assess the effects of gouge width and keel attack angle on soil response. The soil constitutive model, sensitivity parameters, and interface parameters used in the parametric study were the same as those from Case 3. Four cases were conducted with varying width to depth ratios (see Table 5-4). For Cases 5 to 8 the attack angle of the keel was set to 15°. The attack angle of the keel for Cases 9 to 10 was 30°, which is consistent with the mean keel angle of 26.6° given by Timco and Burden (1997) for first year ice ridges. For all cases the gouge depth was set to 1.5 m

Table 5-4 - Gouge Parameter Test Matrix

	<b>Keel Attack Angle</b>	<b>Width to Depth Ratio</b>	<b>Gouge Width (m)</b>
<b>Case 5</b>	15	5	7.5
<b>Case 6</b>	15	10	15
<b>Case 7</b>	15	15	22.5
<b>Case 8</b>	15	20	30
<b>Case 9</b>	30	10	7.5
<b>Case 10</b>	30	10	15

A number of items were considered that were affected by varying the keel width and angle of attack, such as: horizontal and vertical seabed reaction forces, horizontal and vertical subgouge deformations, maximum extent of vertical and horizontal subgouge

deformations, extent of plastic strain zone, frontal mound elevation and width, and side berm elevation.

There is an increasing trend of horizontal subgouge deformations with respect to increasing gouge width. Assessment of Figure 5-7 indicates that at larger gouge widths there is less of an increase in horizontal subgouge deformations. For Case 7 and Case 8 the maximum displacements at the keel base are 16.3 m and 18.0 m, respectfully. This evidence suggests that at large gouge widths, the model could tend to a plane strain condition where a limiting value of gouge width may exist. The vertical extent of both horizontal and vertical deformations was seen to increase with increasing keel width; however, this same limiting trend was not seen for vertical subgouge deformations.

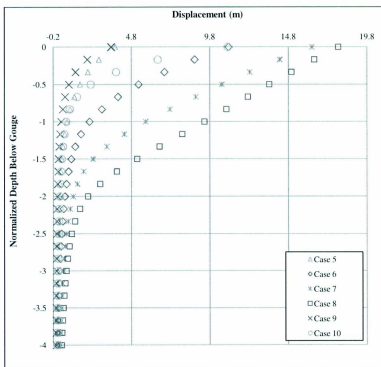


Figure 5-7 - Horizontal subgouge deformations for varying gouge widths

Table 5-5 - Seabed Reaction Forces for Case 5 to Case 9

	Vertical Seabed Reaction Force (MN)	Horizontal Seabed Reaction Force (MN)	V/H
Case 5	12.3	3.3	3.73
Case 6	29.3	8.6	3.41
Case 7	48.5	14.4	3.37
Case 8	70.1	21.2	3.31
Case 9	9.2	3.4	2.71
Case 10	19.3	8.4	2.30

The seabed reaction forces increase with increasing keel width and maintain the same vertical to horizontal force ratios. By increasing the keel attack angle to  $30^\circ$  the vertical to horizontal force ratio drops, due to an increase in horizontal forces and a decrease in vertical forces, which is expected. These ratios are consistent with Pike et al (2011b) for reduced shear strength at the ice-soil interface.

Figure 5-8 presents contour plots of equivalent plastic strain. It can be seen from the figure that the plastic strain zone extends to the end of the mound in front of the keel. For both cases in Figure 5-8, the zone of failure exhibits similar logarithmic curvature. This suggests that a relationship may exist between the vertical extent of plastic strain contours and the frontal mound width. These features are plotted against each other in Figure 5-9. The extent of plastic strain was measured in ABAQUS/CAE setting the lower limit of plastic strain to 10%. Further analysis suggests that there is a potential increasing trend across the data set. From measurement of the frontal mound width it could be possible to estimate the depth to which the plastic strain contours reach.

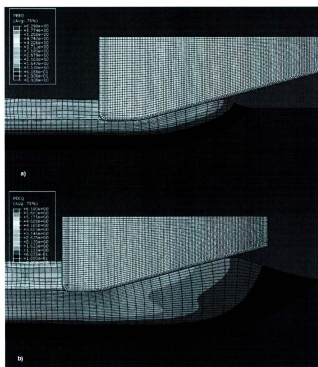


Figure 5-8 - Plot of  $\epsilon_{eq}$  contours for a) Case 5 and b) Case 8

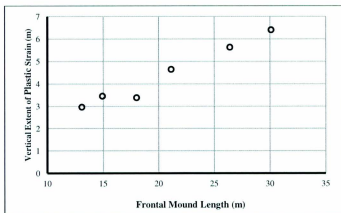


Figure 5-9 - Vertical extent of  $\epsilon_{eq}$  versus width of frontal mound

Another apparent trend which exists is that between the width of the frontal mound and the horizontal seabed reaction force. From Figure 5-10 the frontal mound width appears to increase linearly with increasing reaction force.

From studying berm geometries it is apparent that keels with a small width exhibit greater relative clearing to side berms as can be seen in Figure 5-11. As the keel becomes wider it increases the resistance to soil movement from the gouge centreline out to side berms. There is minimal change in ratio when considering keel's with a W/D of 15 and 20. This can be attributed to a limiting condition to where the soil clearing becomes independent of keel width. This trend is not apparent in the 30° keels studied, however, only limited analysis was done for this attack angle.

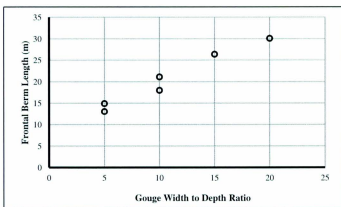


Figure 5-10 - Frontal mound width versus horizontal seabed reaction force

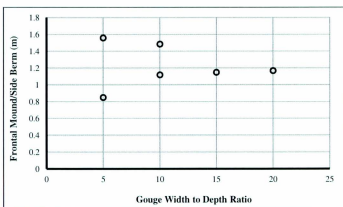


Figure 5-11 - Frontal Mound Height/ Side Berm Height versus W/D

## 5.8 Conclusions

This paper illustrates the importance of soil representation and interface conditions on the soil response. A calibration exercise was conducted in cohesive soil in which various interface strengths were considered along with a varying undrained shear strength profile. The soil clearing mechanisms were found to be sensitive for changes in interface contact conditions which could lead to an incorrect estimation of soil reaction and in turn an inaccurate calibration. Improved correlation was seen between the FE model and Lach Test 05 when considering reduced soil interface strength, variation in undrained strength with depth, and the OCR.

The model was also extended to assess the effects of gouge width and keel attack angle on soil response and to identify key parameters affected and relationships that exist between these parameters. Horizontal to vertical force ratios were within the range of Lach (1996) and PRISE centrifuge data. Plots of horizontal subgouge deformations

revealed an increase in deformation with increase in keel width, however, there is a potential trend seen in the data which suggests a limiting keel width as the model tends to a plane strain type condition.

This study utilized an ALE framework to examine ice keel/seabed interaction events. The CEL framework would be the preferred technical approach for simulating ice gouge events due to the more robust simulation capabilities. During this study, however, several technical issues were identified with the mathematical simulation procedures defining interface shear strength behaviour and contact mechanics within the ABAQUS/CEL modelling framework. These investigations raise questions on the validity of CEL simulations that involve large shear forces and deformations across multiple material interfaces. From this perspective there is significant uncertainty on how the ABAQUS/CEL simulation tool can be extended outside the calibration dataset when examining free-field or fully coupled ice gouge events. Although, the CEL formulation is the preferred modelling framework to address practical pipeline engineering design solutions for ice gouge environments, the current technical issues must first be resolved prior to conducting further rigorous calibration and validation studies.

## 5.9 References

- Andersen, K.H., Jeanjean, P., Luger, D., and Jostad, H.P. (2004). "Centrifuge tests on installation of suction anchors in soft clay." *Ocean Engineering*, Vol 32(7), pp. 845-863.
- Doyle, E.H., Dean, E.T.R, Sharma, J.S., Bolton, M.D, Valsangkar, A.J., and Newfin, J.S. (2004). "Centrifuge Model Tests on Anchor Piles for Tension Leg Platforms." *Proc., Arctic Technology Conference, OTC-16845*, 21p.
- Jukes, P., Eltahir, A., Abdalla, B. and Duron, B (2008). "The design and simulation of arctic subsea pipelines – Ice gouging formulations." *IBC Oil and Gas in Arctic and Cold Waters*, 11p.
- Keaveny, J. and Mitchell, J.K. (1986). "Strength of fine-grained soils using the piezocone." *Use of In-Situ Tests in Geotechnical Engineering*, GSP 6, ASCE, Reston/VA, 668-685.
- Kenny, S., Palmer, A. and Been, K. (2007a). "Design challenges for offshore pipelines in arctic environments." *Proc., IBC Arctic Oil and Gas*, 15p.
- Kenny, S., Barrett, J., Phillips, R. and Popescu, R (2007b). "Integrating geohazard demand and structural capacity modelling within a probabilistic design framework for offshore arctic pipelines," *ISOPE-2007-SBD-03*, 9p.
- Konuk, I.S. and Gracie, R. (2004). "A 3-dimensional Eulerian FE model for ice scour," *IPC04-0075*, pp.1911-1918.
- Konuk, I.S., Yu, S. Gracie, R. (2005). "An ALE FEM model of ice scour." *IACMAG*, Vol.3, pp.63-70.
- Konuk, I.S. and Yu, S. (2007). "A pipeline case study for ice scour design." *Proc., OMAE2007-29375*, 7p.
- Konuk, I.S. and Yu, S. (2010). "Design of pipelines against ice scour: effects of seabed geology." *Proc., OMAE2010-50578*, 7p.
- Pike, K and Kenny, S (2012). "Advanced Continuum Modeling of the Ice Gouge Process: Assessment of Keel Shape Effect and Geotechnical Data." *Proc., ISOPE*, 6p.
- Kenny, S., Phillips, R., McKenna, R.F. and Clark, J.I. (2000). "Response of Buried Arctic Marine Pipelines to Ice Gouge Events." *Proc., ETCE/OMAE 2000 Joint Conference*, Paper OMAE00-5001, 8p.

- Lach, R.P., and Clark, J.I. (1996). "Numerical Simulation of Large Soil Deformation Due to Ice Scour." *Proceedings of the 49th Canadian Geotechnical Conference of the Canadian Geotechnical Society*, St. John's, Newfoundland, pp. 189-198.
- Pike, K, Kenny, S. and Hawlader, B (2011a). "Advanced Numerical Simulations of Ice Gouge Events and Implications for Engineering Design." Proc., *POAC11-100*, 10p.
- Pike, K., Seo, D. and Kenny, S (2011b). "Continuum Modelling of Ice Gouge Events: Observations and Assessment." Proc., *Arctic Technology Conference, OTC-22097*, 12p.
- Paulin, M.J. (1992). "Physical Model Analysis of Iceberg Scour in Dry and Submerged Sand." *M. Eng Thesis*, Memorial University of Newfoundland, St. John's, Newfoundland, 183 p.
- Poorooshasb, F., Clark, J.I., and Woodworth-Lynas, C.M.T. (1989) "Small Scale Modelling of Iceberg Scouring of the Seabed." *POAC89*, Lulea, Vol. 1, pp. 133-145.
- Phillips, R., Barrett, J. and Al-Showaiter, A. (2010). "Ice keel-seabed interaction: Numerical modeling validation." OTC2010-20696, 13p.
- Timco, G.W and Burden, R.P. (1997). "An analysis of the shapes of sea ice ridges." *Cold Regions Science and Technology*, pp.65-77.
- Woodworth-Lynas, C.M.T., Nixon, J.D., Phillips, R., and Palmer, A.C. (1996). "Subgouge deformations and the security of arctic marine pipelines." OTC-8222 pp.657-664.

## **6 EVALUATION OF LATERAL-VERTICAL PIPE/SOIL INTERACTION IN CLAY**

Pipeline systems are vital infrastructure components used for the transport of hydrocarbons that may be subject to geohazards. Current engineering guidelines used to assess pipeline/soil interaction utilize a structural model to evaluate pipeline response that does not consider the effects of load coupling. This paper examines pipe/soil interaction events during oblique lateral-vertical soil movements using plane strain finite element analysis. The results from this study provide a technical framework to assess the effects of geotechnical loads on buried pipelines, highlight key parameters influencing soil yield envelopes, and identify soil failure mechanisms for oblique pipe/soil interaction events that can be used in the design of buried pipelines for large deformation geohazards. The implications that this work has on modelling ice keel/seabed/pipeline interaction and model verification are also discussed.

This paper is to be submitted to the 2<sup>nd</sup> Arctic Technology Conference in Houston, Texas. As the principal investor and first author, I was responsible for conducting the numerical investigation, analyzing the data, and reporting it inside this paper. The second author, Dr. Shawn Kenny, was responsible for supervision of the investigation and guidance on data analysis.

Authors: Christopher Rossiter and Shawn Kenny

## **6.1 Introduction**

Pipeline systems are one of the most efficient means of transporting products and goods, such as hydrocarbons, over long distances. As a means of protection, pipelines situated both onshore and offshore are usually buried. However, these pipelines can be subject to large ground deformation geohazards which can be detrimental to the pipelines integrity. Some of these hazards include fault movements, liquefaction, thaw settlement, landslides, and ice gouging in ice covered regions. During these events, the pipeline can be subjected to considerable stresses and strains which can potentially result in pipeline failure causing environmental damage and financial loss. Therefore, it is important to design against potential geohazards that the pipeline can be subject to.

Current engineering guidelines used to assess pipeline/soil interaction (i.e. Honegger and Nyman, 2004; ALA, 2002) utilize a structural model to define soil response, represented by nonlinear load-displacement relationships, and evaluate pipeline response. The expressions for ultimate maximum soil spring force are based on laboratory and field experimental investigations on pipeline response, as well as geotechnical approaches for structures such as piles, embedded anchor plates, and strip footings. The pipeline is modeled using beam elements while the soil behaviour is modeled using discrete springs in three perpendicular directions (axial, lateral, and vertical). However, these structural models do not account for potential coupling effects between directions. For example, recent studies (Phillips et al., 2004a; Daiyan et al., 2010a) have shown that there is a considerable increase in axial soil restraint when a lateral pipeline movement occurs simultaneously. This is due to an increase in the normal pressure on the pipeline surface.

There is a need for a reevaluation of the current state of practice and a requirement to consider the effect of oblique pipeline movement on pipe-soil interactions.

Recent advancements in computer hardware and software technology have provided a technical framework to develop advanced numerical tools capable of simulating large deformation events. These improvements allow for a cost effective approach in conducting parametric studies to assess parameters significant to pipe/soil interaction problems. Numerical formulations, such as Arbitrary Lagrangian Eulerian (ALE) and Coupled Eulerian Lagrangian (CEL), have proved effective in modeling large deformation and strain ice/soil interaction events, as demonstrated by: Phillips et al. (2010), Pike and Kenny (2011, 2012) and Rossiter and Kenny (2012). Validation of numerical pipe/soil interaction models is needed to provide confidence in these more complex problems such as ice keel/soil/pipeline interactions. If an acceptable level of certainty can be achieved in each constituent model (e.g. pipeline/soil interaction), then a higher level of certainty can be obtained for the more complex coupled problem (e.g. coupled ice keel/seabed/pipeline interaction).

Pipeline/soil interaction is a complex scenario which involves interplay of various factors such as: soil strength, soil effective weight, soil strain localization, pipe/soil interface contact mechanics, pipeline embedment depth, and pipeline displacement path among others. Generally, when modelling undrained conditions in clay, the shear strength of the soil is assumed to be constant. This assumption is not entirely representative for most practical design scenarios. For shallow embedment depths where the soil failure

mechanism is characterized by a passive failure wedge and soil surface heave, an assumption of constant shear strength can lead to an overestimation of the lateral interaction factor. The issue of modeling undrained shear strength as a constant, for particular design scenarios, is addressed in this study.

This investigation analyses the effects of a strength profile and oblique pipeline movements over a range of embedment depths and soil undrained shear strengths for lateral-vertical pipeline displacements in cohesive soil. Figure 6-1 illustrates the lateral-vertical interaction scenario. The numerical modeling procedures were developed in ABAQUS/Explicit with an ALE formulation and calibrated against available physical data. The implications that proper validations of pipe/soil interaction models have on ice keel/soil/pipeline events are discussed and the importance of selecting a suitable simplification of force-displacement curves are considered.

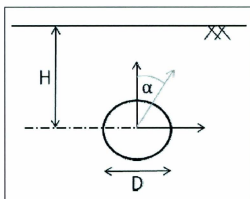


Figure 6-1 - Schematic illustration for lateral-vertical pipeline/soil interaction

## 6.2 Previous Investigations

There is a large volume of data which exists in the public domain for pipe/soil interaction events using buried rigid pipelines. This data has been collected through centrifuge testing (Phillips et al., 2004), large scale laboratory tests (Paulin et al., 1998), and numerical modeling simulations (Daiyan et al., 2009; Pike and Kenny, 2011). Current engineering guidelines (Honegger and Nyman, 2004 and ALA, 2002) define the maximum lateral force per unit length of pipeline for a cohesive soil with no internal angle of friction as

$$P_u = N_{ch}s_uD \quad (6-1)$$

where  $N_{ch}$  is the lateral interaction factor dependent on burial depth ratio,  $s_u$  is undrained shear strength, and  $D$  is the pipeline outside diameter. The equation for the parameter  $N_{ch}$  is developed from empirical curves found in literature (e.g. Hansen, 1961) and is a function of pipeline embedment ratio. Similarly the maximum vertical uplift load per unit length of pipeline can be expressed as

$$Q_u = N_{cv}s_uD \quad (6-2)$$

where  $N_{cv}$  is the vertical uplift factor and is also given by empirical curves.

The lateral interaction factor increases with increasing embedment ratio ( $H/D$ ) and accounts for the change in mechanism from a shallow burial ( $\sim H/D < 2$ ) to a deep burial mechanism ( $\sim H/D > 3$ ). For shallow embedment, a passive failure wedge extends from the pipeline toe up to the soil surface, whereas for deep embedment the soil failure is

characterized by local plastic flow around the pipe. Wantland et al. (1982) addressed these two mechanisms and assessed the effect of increasing embedment has on increased pipeline displacement too ultimate load.

Phillips et al. (2004) conducted plane strain finite element to assess the effects of burial depth and soil properties on the interaction force for lateral pipeline displacement in soil. Based on the work of Rowe and Davis (1982) the authors recommend using Equation 6-3 to account for the change in mechanism from shallow to deep burial.

$$N_{ch} = \min (N_{ch}^* + \beta_n \frac{\gamma H}{s_u}, N_{ch}^{max}) \quad (6-3)$$

where  $N_{ch}^*$  is the interaction factor associated with a zero stress state in the soil,  $\beta_n \gamma H/s_u$  is the factor to account for the soil weight relative to the vertical stress level at the pipe springline and  $N_{ch}^{max}$  is the upper limit for the lateral interaction factor associated with deep burial. A value of 0.85 for  $\beta_n$  was seen to give the best fit to the author's data.

Daiyan et al. (2009) conducted a parametric study using ABAQUS/Standard to assess the oblique lateral-vertical pipe/soil interaction. A Response Surface Methodology (RSM) was used to analyse the numerical results and obtain a response surface capable of predicting the interaction force for various factor levels. Equation 6-3 was adopted to express the lateral interaction factor and it was found that for a constant embedment depth the soil failure mechanism can be shallow or deep depending on the value of  $\gamma H/s_u$ . The amount of overburden ratio contribution ( $\beta_n$ ) to the interaction factors was seen to vary with depth and with  $\gamma H/s_u$ .

Pike and Kenny (2011) studied pipe/soil interactions in clay using plane strain finite element analysis to examine the effects of embedment ratio and pipe direction of travel have on soil failure mechanisms. To assess the effects of the passive wedge weight term on the lateral interaction factor, the analysis was conducted with and without gravity. It was determined that the passive wedge weight term did influence the lateral interaction factor. Increase in the burial depth resulted in an increase in the lateral interaction factor and were bounded by an upper limit of 11 for deep burials. Displacements to peak load occurred between 10 and 15% of the pipeline diameter. For oblique pipeline displacements, significant increase in lateral soil strength mobilization was seen for attack angles greater than  $15^\circ$  from the vertical.

Borges and Oliveira (2011) conducted finite element analysis on the lateral-vertical oblique movement of a pipeline buried in clay. The soil was modeled using both von-Mises and Mohr-Coulomb. The undrained shear strength of the soil was characterized by a linear increasing strength profile with depth. The tests incorporate oblique pipeline displacements in both the lateral-vertical upward and lateral-vertical downward direction. The interaction factors are significantly greater for movement that occur in the lateral-vertical downward direction. This trend was also observed in numerical studies conducted by Cocchetti et al. (2009) and Calvetti et al. (2004).

Using a limit equilibrium approach, Nyman (1982) investigated the effects of lateral-vertical pipeline movements based on a Meyerhof analysis of incline anchor plates. The relationship was defined as

$$p_{u\theta} = (1 - \beta)q_{u0} + \beta p_{u90} \quad (6-4)$$

where  $p_{u\theta}$  is the maximum load for an oblique movement at angle  $\theta$ ,  $q_{u0}$  is the ultimate vertical soil load,  $p_{u0}$  is the ultimate soil load, and  $\beta$  is the interaction factor defined by

$$\beta = \frac{0.25\theta}{90 - 0.75\theta} \quad (6-5)$$

where  $\theta$  is the oblique angle of movement measured from the vertical axis. The analysis assumed the pipe displacement vector was in-line with the oblique load vector.

Guo (2005) developed an alternate analytical model capable of predicting interaction factors for later-vertical oblique movements in clay. The authors proposed an elliptical failure envelope for the model given by

$$\left(\frac{p}{p_{u0}}\right)^2 + \frac{q}{q_{u0}} = 1 \quad (6-6)$$

where  $p_{u0}$  and  $q_{u0}$  are the maximum forces corresponding to pure horizontal and vertical upward pipe movements, respectively.

Several numerical investigations (e.g. Phillips et al., 2004a,b; Guo, 2005; Pike and Kenny, 2011) have indicated that continuum finite element modeling provides a reliable tool to solve pipeline/soil interaction problems. The current FE model was calibrated against data collected by Phillips et al. (2010) and the results of the current investigation are compared with the elliptical failure envelope adopted by Guo (2005) and results obtained by Pike and Kenny (2011).

### 6.3 Numerical Model

In this study, plane strain finite element procedures were developed in ABAQUS/Explicit utilizing an ALE framework to assess the effects of embedment ratio, shear strength profile, and direction of pipeline travel. The soil domain was discretized using 4-node plane strain elements with reduced integration (CPE4R) and was characterized by an elastic perfectly plastic von-Mises criterion. In the area of large deformation the elements size was set to 0.1m and biased meshing was used outside this region to decrease solution time. The unit weight of the soil ( $\gamma$ ) was taken to be 15.7kN/m<sup>3</sup> and the elastic modulus (E) was equal to 100\*s<sub>u</sub>. At the planes defining the outer extent of the soil domain, the nodal displacements in the normal directions were set to zero. The soil surface was not constrained by displacement boundary conditions and was free to move in both directions. The initial geostatic stress state of the soil was prescribed prior to the analysis to decrease computational time.

The pipeline was meshed with CPE4R elements and was assumed to be rigid. The pipeline was displaced at a constant velocity equal to 0.1 m/s. In the numerical simulation procedures contact at the pipe/soil interface was defined using a contact pair approach with a penalty algorithm. The pipe-soil interface contact conditions were assumed to follow the Coulomb friction model and capped at an equivalent shear stress limit ( $\tau_{max}$ ) equal to half of the undrained shear strength of the soil (s<sub>u</sub>).

The results of the numerical procedures were compared to centrifuge data from pipe/soil interaction events in overconsolidated clay, conducted by Phillips et al. (2004b). Phillips

et al. (2004b) conducted two baseline tests in uniform soil with approximate undrained shear strength of 40kPa and embedment ratios of 1.5 and 3.0. The remainder of the tests were conducted to evaluate trench geometry and associated mitigative effects on laterally loaded pipelines. A comparison of the current FEA study and the baseline tests from Phillips et al. (2004b) for H/D of 1.5 and 3.0 are shown in Figure 6-2 and Figure 6-3 respectively.

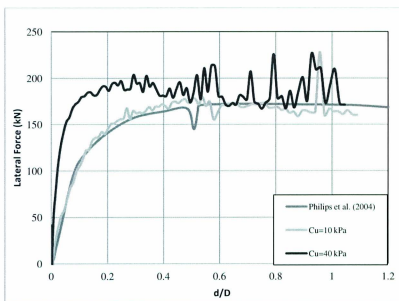


Figure 6-2 - Numerical comparison of FEA and Phillips et al. (2004b) data for H/D of 1.5

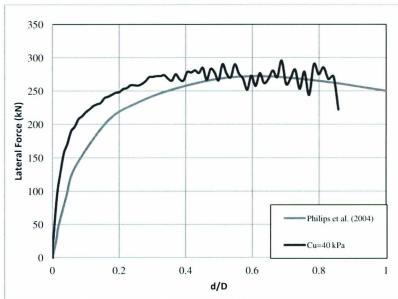


Figure 6-3 - Numerical comparison of FEA and Phillips et al. (2004b) data for H/D of 3.0. Initially, the comparison between the numerical model and Phillips et al. (2004b) for H/D of 1.5, the undrained shear strength of the soil was taken to be 40kPa for the numerical model, which was the average undrained shear strength of the soil for the centrifuge data. However, for this soil strength the response was too stiff and over predicted the values for peak lateral force. Undrained shear strength of 10kPa was chosen to simulate the centrifuge test, and was seen to give a more acceptable result, with predictions of peak lateral force being within 4% of the centrifuge data. The ultimate lateral force was approximately 190kN for the 40kPa soil compared to approximately 175kN for the 10 kPa. The weight of soil wedge for this shallow burial has an effect on the ultimate lateral force which causes both forces to be similar. Agreement with the elastic and peak load response with the weaker constant strength soil suggests the soil strength profile may

vary with the test bed depth. Weaker soil layers will be present near the soil surface and the soil strength would increase with increasing depth.

For H/D of 3, assuming a constant soil strength profile in the numerical simulation, there was agreement between the numerical model and centrifuge data (Phillips et al., 2004) with respect to the peak load and displacement at peak load. The numerical model predicts a peak load of 280 kN and normalized displacement to peak load of approximately 0.55 in. comparison with the centrifuge test peak load of 270 kN and normalized displacement to peak load of 0.6. The numerical model exhibited a relatively stiff elastic response, in comparison with the centrifuge data, which can be attributed to the assumption of a constant elastic modulus and soil undrained shear strength profile with depth.

#### **6.4 Effect of Burial Depth on Yield Envelopes**

Studies have shown that coupling effects occur during lateral-vertical pipe/soil interaction events (Guo, 2005; Daiyan et al., 2009). During large deformation ground movement events, such as ice gouging, oblique pipeline/soil interaction may occur due to non-orthogonal crossing angles of the ice keel over the buried pipeline and pipeline curvature in response to the ground deformation field (Kenny et al., 2007). Calibration of numerical procedures simulating oblique soil loads on buried pipelines will provide improved understanding on pipeline/soil interaction events, load transfer mechanisms and aid in the refinement of new procedures to assess the effects of ground movements on pipeline response. Furthermore, proper calibration and validation exercises for pipeline/soil

interactions are necessary to develop confidence in the capability of numerical modelling procedures to correctly simulate complex loading events such as ice keel/seabed/pipeline interactions.

A parameter study was conducted to examine the influence of pipeline diameter, burial depth, soil strength, and relative load attack angle on the soil response, with respect to peak load and displacement to peak load response. Pipeline/soil interactions were evaluated at various embedment ratios oblique angles undrained soil shear strengths and pipeline diameters, summarized in Table 6-1.

Table 6-1 - Parameters for burial depth study

H/D	1, 2, 4, 10
$\theta$	0° (pure vertical) to 90° (pure lateral)
$s_u$	25 kPa and 50 kPa
D	609 mm (24 in.) and 914 mm (36 in.)

The lateral and vertical force at peak load and the corresponding displacements to peak load were monitored for each attack angle. Well defined peaks for the force-displacement curve allowed measurements to be taken at peak pipeline response. These peak forces were normalized using Equations 6-1 and 6-2. Yield envelopes defined by interaction factors for the 609 mm (12 in.) pipeline are presented in Figure 6-4 and Figure 6-5. These results are in good agreement with Guo (2005) and Pike and Kenny (2011). Failure envelopes presented here are characterized by an elliptical curve for shallow embedment, which is more consistent with Guo (2005), and a circular curve, for deep embedment. Shallow failure mechanisms were characterized by surface heave with a passive wedge

extending from the pipeline to the soil surface. For deep burials the mechanism shifts to a plastic flow around the pipe with minimal surface heave.

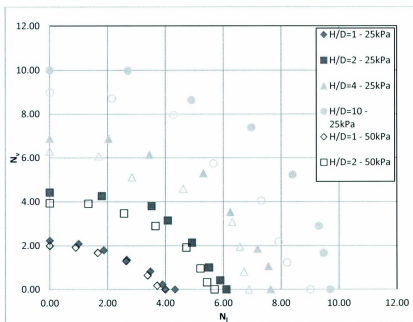


Figure 6-4 - Lateral-vertical interaction factors for pipeline with D = 24 in.

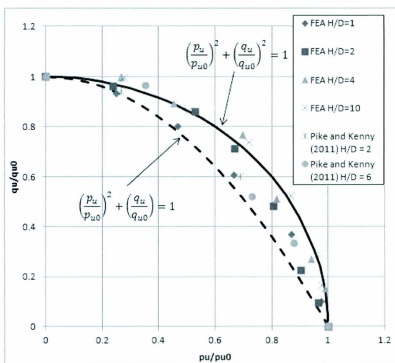


Figure 6-5 - Lateral-vertical limit load interaction forces as a function of embedment ratio (H/D) and attack angle

Yield envelopes plotted in Figure 6-4, for the two shear strengths analysed, do not normalize to the same trace for equivalent embedment ratios. Increasing the soil shear strength results in decreased normalized interaction forces, which is consistent with Popescu et al. (2002). For shallow burials the values are within an acceptable range and the difference is magnified with increasing burial depth. The same trend for the normalized forces was not observed when considering equivalent shear strengths and different pipeline diameters of 609 mm (24 in.) and 914 mm (36 in.) as shown in Figure 6-6. The interaction forces normalized to comparable values except for cases with

embedment ratios of 4 and 10 and oblique attack angles greater than 45°. At these oblique angles and burial depths the 36in. diameter pipeline experienced greater normalized forces and there exists an apparent change in mechanism when transitioning from the 45° to the 60° angles. At embedment ratios greater than 4, oblique pipeline movements of less than 45°, experience mainly surface heave and a passive wedge failure. For angles greater than 45°, the soil experiences more of a plastic flow around mechanism. From Figure 6-7 the larger diameter pipeline the soil experiences a greater zone of plastic deformation and greater surface heave expression.

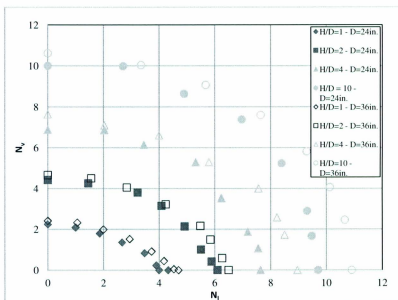


Figure 6-6 - Lateral-vertical interaction factors for 25 kPa soil

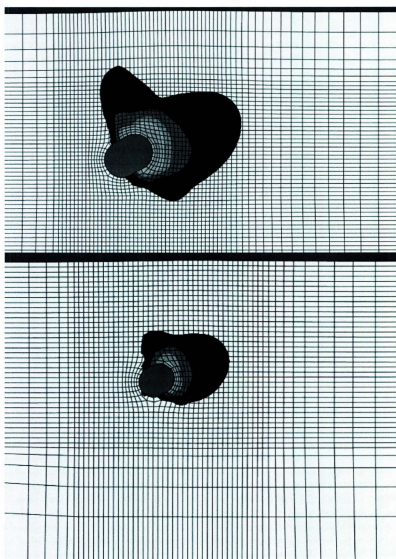


Figure 6-7 - Plot of plastic strain contours for  $H/D = 4$  and  $s_u = 25$  kPa: a)  $D = 24$  in. b)  $D = 36$  in.

These evolutions in the failure mechanisms with increasing burial depth may account for the variation in normalized forces as shown in Figure 6-4 to Figure 6-6.

### **6.5 Effect of Soil Strength Profile on Yield Envelopes for Oblique Loading Events**

When designing against large deformation geohazards, site specific data must be considered in order to accurately account for potential pipeline loading due to soil movements. Soil properties are a parameter of utmost importance when analysing pipe/soil interactions and must be correctly accounted for during the design process. However, it is important to note that the variability of soils along a pipeline route will never be fully defined as this would be too costly over the large distances involved. When modelling in clay, it is common practice to assume average soil shear strength for the soil medium and employ appropriate constitutive models with this assumed shear strength. This is an acceptable practice for design scenarios where the pipeline is trenched and backfilled and uniform soil properties may be expected. However, backfill may be uniform but different than native soil and pose different design challenges if the pipeline moves into the native soil. Also, backfill can experience consolidation over time and result in a variation in soil properties with depth. For instances where the pipeline is installed through horizontal directional drilling (HDD) a variation in shear strength above the pipeline is expected. A limited investigation was conducted in this study which highlights the importance of properly accounting for changes in soil undrained shear strength with depth.

A linear varying shear strength profile was considered and was described by the following equation

$$s_u = 10 + 6.25z \text{ kPa} \quad (6-7)$$

where 10 kPa is the undrained shear strength at the soil surface and  $z$  is the depth below the soil surface in meters. Analysis was conducted for embedment ratios of 2 and 4 and a pipeline diameter of 609 mm (24 in.). The results were compared to the constant shear strength results discussed in the previous section (Figure 6-8). For embedment ratios of 2 and varying shear strength with depth, the shear strength at the pipe springline was 17.5 kPa, which lead to a significant decrease in the interaction factors. For embedment ratios of 4 and varying shear strength with depth, the shear strength at the pipe springline was 25 kPa. Here, interaction factors for oblique attack angles greater than  $45^\circ$  (tending towards lateral bearing) experienced comparable values to those of the constant strength case. However, for oblique movements between  $0^\circ$  and  $45^\circ$  (tending toward vertical punching), the interaction factors were considerably less for the varying shear strength with depth cases, as the pipeline was moved into weaker soil zones.

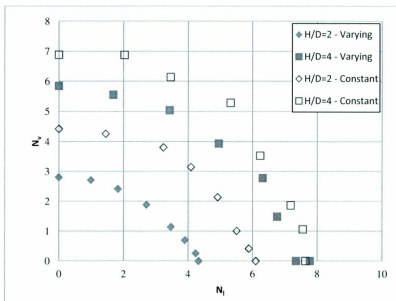


Figure 6-8 - Failure envelope comparison for constant and varying soil shear strengths with depth

### 6.6 Effect of Overburden Pressure on Lateral Pipeline Response

Previous investigations have illustrated the importance of considering soil overburden pressure during pipeline/soil interactions (e.g. Rowe and Davis, 1982; Phillips et al., 2004; Daiyan et al., 2009). To assess the effect of overburden pressure on normalized interaction forces lateral pipeline/soil analyses were conducted for various undrained shear strengths (25, 50, 75, 100kPa) and embedment ratios (1, 2, 4, 6, 8, 10). During these investigations the pipeline was prescribed to move laterally and vertical movement was permitted. As highlighted previously and observed by Popescu et al. (2002), Figure 6-9 illustrates that an increase in undrained shear strength results in a decrease in normalized lateral interaction forces.

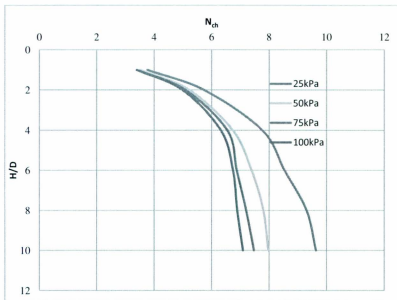


Figure 6-9 -  $N_{ch}$  as a function of  $H/D$  for various undrained shear strengths

Equivalent plastic strain contour plots at peak load, for 25 kPa and 100 kPa undrained shear strengths, are presented in Figure 6-10 and Figure 6-11, to determine if soil failure mechanisms were altered for different soil shear strengths. The area affected by plastic strain is significantly smaller for the 25 kPa soil than that observed for the 100 kPa soil. Evaluation of the area exposed to plastic strain was estimated by an elliptical shape. The enclosed area of equivalent plastic strain at peak load for the 25 kPa soil strength case was 72% of the enclosed area for the 100 kPa soil strength analysis case. Displacement measurements revealed that greater distance to peak load was needed for the 100kPa soil. Displacements to peak loads were 0.170 m and 0.251 m for the 25 kPa and 100 kPa soils, respectively. This suggests that not only should failure mechanisms be accounted for when transitioning from shallow to deep burials, they should also be accounted for with

reference to soil shear strength. There potentially exists a coupled relationship between displacement to peak load, soil strength and failure mechanism.

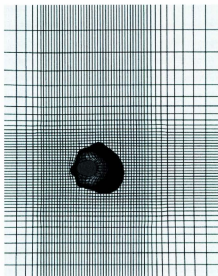


Figure 6-10 - Effect of undrained shear strength on plastic strain contours for H/D of 10 and 25 kPa

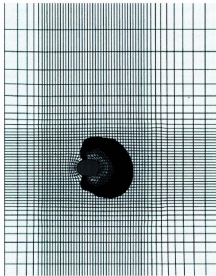


Figure 6-11 - Effect of undrained shear strength on plastic strain contours for H/D of 10:  
100 kPa

The analyses were repeated to isolate the relative importance of soil strength effects by ignoring the work done due to soil lifting during the interaction event by defining zero gravity condition (Figure 6-12). Over the range of shear strengths tested, the  $N_{ch}^*$  values were seen to follow a similar trace with a slight decrease in interaction factors with increasing shear strength. This suggests that the interaction forces which occur due to strength are scalable with respect to undrained shear strength.  $N_{ch}^*$  values increased to approximately 6.25 at an embedment ratio of 6 for all strengths tested and remained constant at greater depths. This value of  $N_{ch}^*$  is slightly less than the 7.5 derived by Daiyan et al. (2009) and 7.0 derived by Phillips et al. (2004b). For the cases considering soil weight in Figure 6-9, there was no observed limiting interaction value, however, the

increase in normalized interaction factors decreased after an embedment of 4, which is consistent with Phillips et al. (2004b).

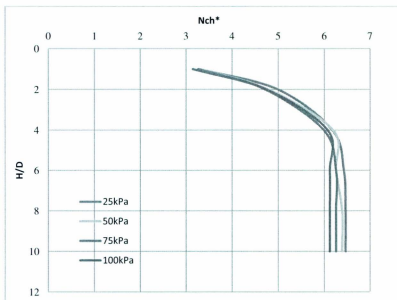


Figure 6-12 -  $N_{ch}^*$  as a function of  $H/D$  for various undrained shear strengths

Plots of  $N_{ch}$  were constructed using a trial and error approach to determine an acceptable value for  $\beta_h$ . Figure 6-13 illustrates this process for a 25 kPa soil.  $\beta_h$  values were chosen to give an approximate fit of Equation (6-3) to the  $N_{ch}$  values obtained from the analysis conducted with gravity. In Figure 6-13, an appropriate choice of  $\beta_h$  would give Equation 6-3 (dashed line), following a similar trace to  $N_{ch}$  (solid line). This process was repeated to give  $\beta_h$  values for all soil strengths studied.  $\beta_h$  values were then plotted in Figure 6-14 with a trendline fitted to the data, resulting in the following equation for determining  $\beta_h$ :

$$\beta_n = 0.001s_u + 0.86 \quad (6-8)$$

where  $s_u$  is in kPa. Equation 6-9 below was obtained by curve fitting the results over a range of shear strengths and embedment ratios.

$$N_{ch}^* = \begin{cases} 0.0299 \left(\frac{H}{D}\right)^3 - 0.4844 \left(\frac{H}{D}\right)^2 + 2.7024 \left(\frac{H}{D}\right) + 1.0156 & \text{for } \frac{H}{D} < 6 \\ 6.25 & \text{for } \frac{H}{D} \geq 6 \end{cases} \quad (6-9)$$

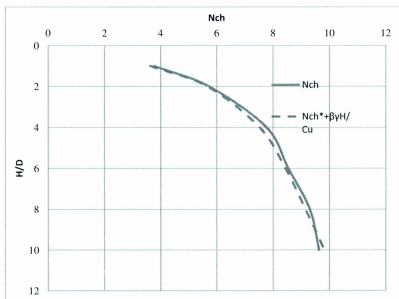


Figure 6-13 - Comparison of numerical results for soil weight study for 25 kPa soil

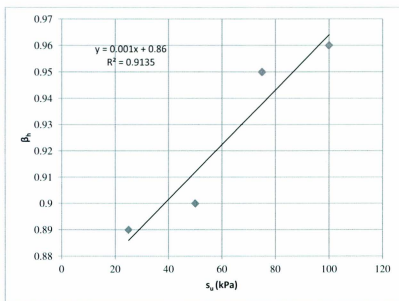


Figure 6-14 -  $\beta_n$  as a function of undrained shear strength

Equations 6-8 and 6-9 along with Equation 6-3 can be used to obtain values of  $N_{ch}$ . The  $\beta y H / s_u$  term in Equation 6-3 accounts for the effects of soil weight, overburden pressure, and change in soil failure mechanism for various soil shear strengths.

Further analysis need to be conducted for greater overburden pressures to assess the effects of deeper burials and where the  $N_{ch}^{\max}$  term is achieved.

### 6.7 Bi-linear Representation of Force-Displacement Curve

Structural finite element analysis is the state of practice for assessing pipeline response to imposed ground movements. Soil loading on the pipeline is represented by discrete nonlinear springs which are commonly defined by a bi-linear force displacement curve.

These bi-linear representations are constructed using peak force and displacement to peak force data.

To define the ultimate load on the pipeline from force-displacement curves various methods are adopted in literature. Five methods are illustrated in Figure 6-15. The load (1) is defined as the point of intersection of the tangent to the upper part of the curve and the vertical axis. This method was used by Neely et al. (1973) to investigate the interaction of vertical anchor plates in soil. Wantland et al. (1982) defined the failure load as the load value of the point of intersection of the tangents to the two straight line portions of the curve (2). Terzaghi's definition was described as the load at which the load-displacement curve passes into a steep straight tangent (3). Rowe and Davis (1982) proposed a failure load which corresponds to an apparent stiffness of one quarter of the elastic stiffness which is called the  $k_4$  method (4). The ultimate load given by (5) in Figure 6-15 is the peak load observed during the test. Depending on the soil response this load can occur at much greater pipeline displacements than the other methods described and result in higher reaction forces experienced by the pipeline.

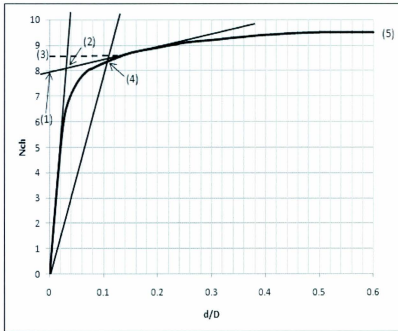


Figure 6-15 - Methods of determining peak load

For the purposes of this investigation the peak load for method (5) was taken as the interaction load between the pipe and soil. Unlike investigations conducted within an implicit analysis, ABAQUS/Explicit ALE capabilities allow for the large mesh distortion, inherent in the pipe/soil interaction problem, to be improved through mesh smoothing algorithms and allow for the peak load described by (5) to be reached.

Lateral force-displacement measurements were taken for a 0.6 m diameter pipeline at an embedment ratio of  $H/D$  of 4 in a soil medium with undrained shear strength of 25 kPa and are presented in Table 6-2 . Method (4) as used by Rowe and Davis (1982) gives the closest match to (5) for normalized displacement and peak load. Current guideline by

ALA (2002) and Honegger and Nyman (2004) give normalized peak force as 6.63 which are consistent with method (3) but underestimates methods (4) and (5). Displacements to peak load suggested by the current guidelines are between 10 to 15% of the pipeline diameter.

Table 6-2 - Normalized values for lateral pipeline/soil interaction using various measurement methods

Method	Normalized Displacement	Normalized Peak Load
3	0.06	6.62
4	0.22	7
5	0.42	7.7

An oblique movement of 70° for the same size pipeline, embedment ratio, and soil properties was assessed and good agreement was observed between method (4) and (5), with method (3) giving a substantial underestimation of normalized displacement and force (see Table 6-3). Good agreement was also observed between method (4) and (5) for a shallow embedment of H/D of 2 and oblique movement of 15°. Normalized forces were 1.45 for method (5) and 1.28 for method (4) with normalized displacements of 0.18 and 0.12 respectfully.

Table 6-3 - Normalized values for 70° oblique pipeline/soil interaction using various measurement methods

Method	Normalized Displacement	Normalized Peak Load
3	0.045	5.35
4	0.23	6.75
5	0.34	7.18

The values obtained here by the  $k_4$  method, proposed by Rowe and Davis (1982), were seen to give consistent results between Terzaghi's definition and the load measured at peak force. Lateral loads calculated using current engineering guidelines resulted in lower values of lateral force and displacement, which could lead to conservative designs. Depending on the angle of oblique movement, current guidelines can overestimate the forces transferred to the pipeline. Although the  $k_4$  method of measurement was seen to give adequate results for this analysis, measurement and bi-linear representation may have to be case specific. For example, a very strong soil may experience a brittle type failure which would lead to a very short response to peak load and the  $k_4$  method may not be applicable. Measurement of peak load would have to be used in this instance. In soft soils a peak load may only be experienced at undesirable design displacements, and a method such as the  $k_4$  would most likely be employed.

Normalized displacements at peak load for the lateral pipeline displacement study are plotted in Figure 6-16. Both the  $k_4$  method and distance to ultimate load were used to determine the values of displacement for each case. A general trend of increasing displacement to peak load with increasing embedment ratio was seen. This trend was also observed by Wantland et al. (1982). Variations in the trends plotted can be attributed to noise in the numerical solution at peak displacements, making the choice of peak load arbitrary to some extent. The data was unable to disclose any pattern between displacement to peak load and undrained soil shear strength. The  $k_4$  method gives significantly lower values for displacement when compared to peak displacement.

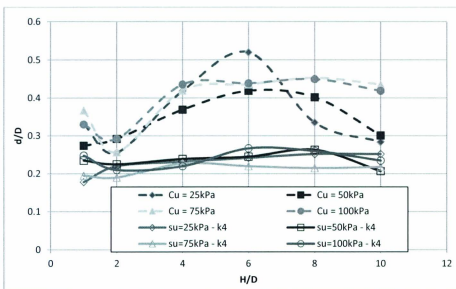


Figure 6-16 - Normalized pipeline displacement to peak load for lateral pipeline/soil interaction

## 6.8 Conclusion

Lagrangian analyses encounter problems with mesh distortion and convergence at large displacements. This mesh distortion can be controlled by employing ALE formulations along with mesh smoothing algorithms inside an explicit framework. The analysis conducted in this numerical investigation has demonstrated the ability of the ALE formulation to accurately model pipeline/soil interaction events. Results obtained from this study were consistent with other investigations (Phillips et al., 2004b; Guo (2005); Pike and Kenny (2011)).

This study examined parameters imperative to pipeline/soil interaction and the importance of proper simplification when conducting structural finite element analyses for pipeline design. Key observations during the numerical analysis were:

- Failure envelopes expand with increasing embedment while also transitioning from an elliptical to a circular surface.
- Failure envelopes were affected by incorporating a soil shear strength profile with depth, particularly at shallow embedment and oblique angles greater than  $45^\circ$  for deeper embedment.
- Normalized loads are dependent on undrained shear strength ( $s_u$ ) and pipeline diameter ( $D$ ).
- Pipeline/soil interaction forces derived from soil strength (no gravity case) were noticed to be scalable with undrained shear strength. However, when soil weight is incorporated a decrease in normalised interaction forces occurred with increasing shear strength. This decrease can be attributed to the soil failure mechanism experienced at various overburden pressures and be accounted for by employing an appropriate factor of  $\beta_b$  to the overburden ratio term.

Further investigations are needed and should incorporate the effects of:

- Soil overburden pressures
- Pipeline displacement rate and drained versus undrained conditions

- Soil consolidation with pipeline displacement
- Soil pore-pressures

From curve fitting, equations are proposed to estimate the normalised interaction forces; however, further analysis needs to be conducted to properly address the effects of overburden pressure. Daiyan et al. (2009) has illustrated that soil failure mechanisms are complex and depend not only on embedment ratio, but also overburden ratio.

The current investigation along with previous experimental (Daiyan et al., 2010) and numerical investigations (Daiyan et al., 2009; Pike and Kenny, 2011; Seo et al., 2011; Borges and Oliveira, 2011) have illustrated the importance of considering oblique pipeline movements in soil. Depending on the scenario, current guidelines are capable of incorrectly predicting the interaction loads during oblique pipeline movements in soil. It is important to address the issues raised above in greater detail in order to derive more applicable models capable of predicting pipeline/soil interaction for specific design scenarios.

Extending numerical pipeline/soil interaction outside the scope of developing structural finite element models can support the validation of more complex problems of ice keel/seabed/pipeline interaction scenarios. The validity of expanding the scope of pipeline/soil interaction models to enhance more complicated models is uncertain but is significant to examine. Along with additional ice keel/seabed numerical validation the

uncertainty of the complete problem can be reduced and understanding of the complex mechanisms occurring can be achieved.

## 6.9 References

- American Lifeline Alliance (ALA) (2002). Guidelines for the design of buried pipe. <[www.americanlifelinealliance.org](http://www.americanlifelinealliance.org)>.
- Borges, R.G. and Oliveira, J.R.M.S. (2011). "Multidirectional analysis of pipeline-soil interaction in clay." *Journal of Frontiers in Offshore Geotechnics II*, pp. 773-778.
- Calvetti, F., Prisco, C., and Nova, R. (2004). "Experimental and numerical analysis of soil-pipe interaction." *Journal of Geotechnical and Geoenvironmental Engineering*, Vol. 130(12).
- Cocchetti, G., Prisco, C., Galli, A. (2009). "Soil-pipeline interaction along unstable slopes: a coupled three-dimensional approach. Part 2: Numerical analyses". *Canadian Geotechnical Journal*. Volume 46, pp. 1305-1321.
- Daiyan, N., Kenny, S., Phillips, R. and Popescu, R. (2009). "Parametric study of lateral-vertical pipeline/soil interaction in clay." *Proceedings of the 1<sup>st</sup> Engineering Mechanics and Materials Specialty Conference*, St. John's, Newfoundland and Labrador, Canada.
- Daiyan, N., Kenny, S., Phillips, R. and Popescu, R. (2010). "Investigation of axial/lateral interaction of pipes in dense sand." *International Conference on Physical Modeling in Geotechnics*, Zurich, Switzerland.
- Guo, P. (2005). "Numerical modeling of pipe-soil interaction under oblique loading." *Journal of Geotechnical and Geoenvironmental Engineering*, Volume 131(2): 260-268.
- Hansen, J. B. (1961). "The ultimate resistance of rigid piles against transversal forces." *Bulletin No. 12*, Danish Geotechnical Institute, Copenhagen, Denmark, 5-9.
- Honegger, D.G., and Nyman, J. (2001). "Manual for the Seismic Design and Assessment of Natural Gas Transmission Pipelines." Pipeline Research Council International Project PR-268-9823.
- Honegger, D.G., and Nyman, J. (2004). "Guidelines for the seismic design and assessment of natural gas and liquid hydrocarbon." Pipeline Research Council International, Falls Church, Va. No. L51927.
- Kenny, S., Barrett, J., Phillips, R., and Popescu, R. (2007a). "Integrating Geohazard Demand and Structural Capacity Modeling within a Probabilistic Design Framework for Offshore Arctic Pipelines." *Proceedings of the 17th International Offshore and Polar Engineering Conference*, Lisbon, Portugal.

- Neely, W.J., Stuart, J.G. and Graham, J. (1973). Failure load of vertical anchor plates in sand. *Journal of the soil mechanics and foundations division, ASCE*, 99(9), 669-685.
- Nyman, K.J. (1982). Soil response against the horizontal-vertical motion of pipes. Preprint 82-534, Presented at ASCE National Convention, New Orleans.
- Paulin, M. J., Phillips, R., Clark, J.I., Trigg, A., and Konuk, I. (1998). A full-scale investigation into pipeline/soil interaction. *Proceedings of the International Pipeline Conference*, p779-788, Calgary, AB
- Phillips, R., Barrett, J. and Al-Showaiter, A (2010). "Ice keel-seabed interaction: Numerical modeling validation," OTC2010-20696, 13p.
- Phillips, R., Nobahar, A., and Zhou, J. (2004a). "Combined axial and lateral pipe-soil interaction relationships." *Proceedings of the 5<sup>th</sup> International Pipeline Conference*, Calgary, Canada., 5p.
- Phillips, R; Nobahar, A.; Zhou, J. (2004b). "Trench effects on pipe-soil interaction." *Proceeding of IPC2004*, International Pipeline Conference, Calgary, Alberta, Canada
- Pike, K. and Kenny, S. (2011). "Advancement of CEL procedures to analyze large deformation pipeline/soil interaction events," *Offshore Technology Conf.*, Houston, TX, USA. 10p.
- Pike, K. and Kenny, S. (2012). "Lateral-axial pipe/soil interaction events: numerical modelling trends and technical issues," *IPC2012-90055*, 5p.
- Popescu, R., Konuk I., Guo, P., Nobahar, A. (2002). "Some aspects in numerical analysis of pipe-soil interaction." *Proceedings of the 2nd Canadian Specialty Conference on Computer Applications in Geotechnique*, Winnipeg, Canada, pp. 290-297.
- Rossiter, C.P.A. and Kenny, S.P. (2012). "Assessment of Ice/Soil Interactions: Continuum Modeling in Clays" Proc., ISOPE2012, 8p.
- Rowe, R. K., and Davis, E. H. (1982). "The behaviour of anchor plates in clay." *Geotechnique*, 32(1), 9-23.
- Seo, D., Kenny, S., Hawlader, B. (2011). "Yield envelopes for oblique pipeline.soil interaction in cohesive soil using ALE procedure." *Proceedings of the 14<sup>th</sup> Pan-Am CGS Geotechnical Conference*, Toronto, Canada, 7p.
- Wantland, G.P., O'Neill, M.B., and Coelogyne, E.H., Reese, L.C. (1982). "Pipeline lateral stability in soft clay," *Journal of Petroleum Technology*, Vol. 34, No.1, pp. 217-220.

## 7 SUMMARY AND CONCLUSIONS

This thesis investigated the validity of using finite element analysis to assess ice keel/soil interaction and the pipeline/soil interaction problems. Initially, the test program was to conduct a comparison of ALE and CEL modeling procedures in ABAQUS/Explicit for ice keel/soil and ice keel/soil/pipeline interactions; however, problems were encountered with CEL's ability to properly account for the defined equivalent shear stress limit ( $\tau_{eq}$ ) at the ice keel/soil contact interface. This caused the scope of work to be modified and to incorporate both ice keel/soil and pipeline/soil interactions.

The current study considered both the calibration and assessment of both ice keel/soil and pipeline/soil interaction models using a total stress analysis and assuming undrained conditions in clay. A total stress analysis is usually used in modelling soil response due to the complexity of modelling two phase soil behaviour using a one phase ALE soil model. Both numerical models were developed within an ALE framework using ABAQUS/Explicit and calibrated against available physical data. Once calibrated, these models were extended to assess parameters important to both interactions. The ice keel/soil study investigated parameters such as undrained shear strength profile, interface contact mechanics, soil sensitivity and assumed ice keel geometry. The pipeline/soil interaction analysis considered pipeline diameter, embedment ratio, direction of pipeline travel, and undrained shear strength profile.

Calibration of the numerical ice keel/soil interaction model revealed that soil reaction forces and subgouge deformation patterns are sensitive to soil stress state, ice keel/soil

interface strength, and assumed ice keel profile. Numerical predictions were in best agreement with Lach (1996) when using reduced interface strength corresponding to soil sensitivity and varying strength profile of the soil medium. Acceptable correlation was seen between seabed reaction forces and horizontal subgouge deformations. A correlation between vertical subgouge deformations of the numerical procedures and the physical tests was not observed. A correlation proposed by Keaveny and Mitchell (1986) relating the soil rigidity to its over consolidation ratio and plasticity index to calculate the soil elastic properties along with measured undrained shear strength from Lach (1996) gave acceptable results when predicting soil response.

A gouge parameter study was conducted to assess the effects of gouge width and keel attack angle on soil response. There was an increasing trend of horizontal subgouge deformations with respect to increasing gouge width observed, with less of an increase in horizontal subgouge deformations at larger gouge widths. This evidence suggests that at large gouge widths, the model could tend to a plane strain condition where a limiting value of gouge width may exist. Assessment of berm geometries revealed that keels with a small width exhibit greater relative clearing to side berms than keel with larger widths. As the keel becomes wider it increases the resistance to soil movement from the gouge centreline out to side berms causing less build up of soil to the flanks of the gouge. There is minimal change in side berm elevation to frontal mound elevation ratio when considering keel's with a W/D of 15 and 20. This can also be attributed to a limiting condition to where the soil clearing becomes independent of keel width. It was also found that there is a potential relationship between the length of the frontal mound and the

extent to which the plastic strain contours reach. Further analysis is necessary to confirm this observation.

Calibration of the numerical pipeline/soil interaction model disclosed that the interaction force-displacement curve is dependent upon assumed undrained shear strength of the soil. Different undrained soil shear strengths had to be used at the two embedment ratios used in the calibration study. The calibration data along with the analyses of a linear increasing undrained strength profile revealed that strength profile should be considered when designing for pipeline response during displacement in a soil medium. Direction of pipeline travel was also observed to be significant in pipeline response and is not considered in current guidelines. Yield envelopes followed a circular trend for shallow embedment conditions and transitioned into a circular yield surface at deeper depths.

An investigation of lateral pipeline response for a range of embedment ratios and undrained soil shear strengths demonstrated a decrease in normalized interaction forces with an increase in undrained soil shear strength. This result was also observed by Rowe and Davis (1982) and Popescu et al. (2002). Lateral pipeline studies were also conducted within a zero gravity condition. This allowed for evaluation of the effect that the gravity term and initial stress state of the soil have on the pipeline/soil interaction. It was determined that a stress free soil over a range of undrained shear strengths normalized to the same value, suggesting that normalization issues arise from initial soil stress state and soil failure mechanisms. Future numerical analysis should isolate the work done by

displacing the soil during pipeline movement and determine the individual effects that soil weight and soil stress state have on pipeline/soil interactions.

Displacement to peak load was observed to increase with increasing embedment. However, displacements at embedment ratios of 2 were less than those measured at an embedment ratio of 1. The fit to the experimental data presented by Wantland et al. (1979) suggested a low point at an embedment ratio of approximately 0.5 (burial depth measured to bottom of pipe), with the displacement to peak load response increasing for embedment ratios less than and greater than 0.5. The variation in data presented here can be potentially due to human error when choosing the peak load point. However, a trend of sharp increase in displacement to peak load for intermediate embedment and levelling off of the curve at deeper embedment conditions was observed, which is consistent with the data reported by Wantland et al. (1979).

Evaluation of various methods to obtain peak load measurements was also considered. Consistent results for normalized force were seen between the  $k_4$  method, proposed by Rowe and Davis (1982), and peak normalized force. However, a discrepancy was seen between displacements to peak loads for these two methods, with the  $k_4$  method giving significantly smaller displacements. Bi-linear representations of force-displacement curves used for import into structural FEA models should be problem specific and may not be able to rely on one specific method of obtaining peak loads, depending on the soil state in question.

Much calibration is needed before numerical modeling procedures can be globally accepted in predicting ice keel/soil/pipeline interactions. There are various accepted models representing the soil state numerically depending on the soil conditions. For undrained conditions it is acceptable to use a total stress analysis incorporating a von Mises failure criterion based on the undrained shear strength of the soil. The first study extended the calibration to assess soil sensitivity and OCR which resulted in closer agreement of the numerical procedures with the physical experiments conducted by Lach (1996). Undrained soil shear strength profile also played a key role in calibration of the numerical procedures. This was also seen in the second study for shallow embedment and when the pipeline moved vertically into weaker soil.

Calibration should also be extended outside of matching seabed reaction forces and horizontal subgouge displacements for ice keel/soil interactions. Good correlation of berm heights was not observed and is attributed to the inherent nature of the von-Mises criterion. The soil model assumes perfect plasticity (von Mises criterion), and does not account for the effects of pore pressures, soil friction, tension cracking and the development of blocks of soil material being formed and cleared during gouge events. Options are available in ABAQUS to establish failure criterion to address this mechanism and treat the blocks as discrete rigid body kinematic particles. Further analysis is needed to assess various failure criterions against the failure models used here.

Parametric studies for both ice keel/soil and pipeline/soil interaction models established important parameters to consider in future analysis and highlighted potential relationships

between these parameters. An extensive study which incorporates physical modelling techniques and is complimented by extensive calibrations of numerical modeling procedures while considering the factors imperative to these interaction models is needed to aid in the development of numerical modelling tools. Consideration of important factors needed for proper numerical calibration prior to undertaking physical experimentation would be valuable when calibrating numerical models against physical data sets.

## 8 REFERENCES

- Abdalla, B., Pike, K., Eltaher, A., Jukes, P., and Duron, B. (2009). "Development and Validation of a Coupled Eulerian Lagrangian Finite Element Ice Scour Model," *Proceedings of the ASME 28th International Conference on Ocean, Offshore and Arctic Engineering*, Honolulu, Hawaii.
- Abdelnour, R., and Graham, B. (1984). "Small Scale Tests of Sea Bottom Ice Scouring," *Proceedings of the Ice Symposium*, International Association for Hydraulic Research, Hamburg, West Germany, pp. 267-279.
- Abdelnour, R., Lapp, D., Haider, S., Shinde, S.S., and Wright, B. (1981). "Model Tests of sea Bottom Scouring," *Proceedings of the 6<sup>th</sup> International Conference on Port and Ocean Engineering under Arctic Conditions*, Quebec City, Quebec, pp. 688-705.
- Almeida, M. S. S. (1982). "The undrained behaviour of the Rio de Janeiro clay in the light of critical state theories." *Soils and Rocks*, 5(2), pp. 3-24.
- Almeida, M. S. S., et al. (2001). "Pipeline failure on very soft clay." *Proceedings of the 3<sup>rd</sup> International Conference on Soft Soil Engineering*, Balkema, Hong Kong, pp. 131-138.
- American Lifeline Alliance (ALA) (2002). "Guidelines for the design of buried pipe." <[www.americanlifelinealliance.org](http://www.americanlifelinealliance.org)>.
- Andrier, B. (1981). "E.T.P.M. in Pipelaying and Burying Activities." *Proceedings, Symposium on Production and Transportation Systems for the Hibernia Discovery*, St. John's, Newfoundland, pp. 270-278.
- Audibert, J.M.E and Nyman, K.J. (1977). "Soil restraint against horizontal motion of pipes." *Journal of the Geotechnical Engineering Division*, ASCE, Vol. 103, No. GT10, pp. 1119-1142.
- Barker, A. and Timco, G.W. (2003). "The friction coefficient of a large ice block on a sand/gravel beach," *Proceedings of the 12th Workshop on the Hydraulics of Ice Covered Rivers*, CGU HS Committee on River Ice Processes and the Environment, Edmonton, AB, 15p.
- Barnes, P.W., McDowell, D., and Reimnitz, E. (1978). "Ice-Gouging Characteristics: Their Changing Patterns from 1975-1977, Beaufort Sea, Alaska." United States Geological Survey Open-File Report 78-730.
- Been, K., Kosar, K., Hachey, J., Rogers, B.T., and Palmer, A.C. (1990). "Ice Scour Models." *Proceedings of the 9th International Conference on Offshore Mechanics and Arctic Engineering*, Vol. 5, pp. 179-188

- Been, K., Sancio, R., Ahrabian, D., van Kesteren, W., Croasdale, K., and Palmer, A. (2008). "Subscour Displacement in Clays from Physical Model Tests." Proceedings of the 7<sup>th</sup> International Pipeline Conference, Calgary, Alberta.
- Beketsky, S.P. and Astafiev, V.N. (1997), "Morphology of hummocks in the Sea of Okhotsk," *Proceedings of the 14<sup>th</sup> Okhotsk Sea and Sea Ice Symposium*, Monbetsu, Japan, pp.42-47
- Beketsky, S.P., Astafiev, V.N. and Truskov, P.A. (1997),"Design parameters for hummocks and grounded hummocks in the Sea of Okhotsk," *The Proceedings of The 7<sup>th</sup> International Offshore and Polar Engineering Conference*, Honolulu, USA, Vol.2, pp.487-493
- Borges, R.G. and Oliveira, J.R.M.S. (2011). "Multidirectional analysis of pipeline-soil interaction in clay." *Journal of Frontiers in Offshore Geotechnics II*, pp. 773-778.
- Brown, R.J., and Palmer, A.C. (1985). "Submarine Pipeline Trenching by Multipass Ploughs." *Proceedings of the 17<sup>th</sup> Offshore Technology Conference*, Houston, Houston, Texas, Vol. 2, pp.283-288.
- Caines, J.V.M. (2009). "Engineering Assessment of Ice Gouge Statistics from the Canadian and American Arctic Oceans." *M. Eng Thesis*, Memorial University of Newfoundland, St. John's, Newfoundland, 267 p.
- Calvetti, F., Prisco, C., and Nova, R. (2004). "Experimental and numerical analysis of soil-pipe interaction." *Journal of Geotechnical and Geoenvironmental Engineering*, Vol. 130(12).
- Chari, T.R. (1975). "Some Geotechnical Aspects of Iceberg Grounding." *Ph.D. Thesis*, Memorial University of Newfoundland, St. John's, Newfoundland, 181 p.
- Chari, T.R., and Muthukrishnaiah, K. (1978). "Iceberg Threat to Ocean Floor Structures." *Proceedings of Symposium on Ice Problems*, International Association for Hydraulic Research, Lulea, Sweden, pp. 421-435.
- Chari, T.R., and Green, H.P. (1981). "Iceberg Scour Studies in Medium Dense Sands." *Proceedings of the 6<sup>th</sup> International Conference on Port and Ocean Engineering under Arctic Conditions*, Quebec City, Quebec, Vol. 2, pp. 1012-1019.
- Cocchetti, G., Prisco, C., Galli, A. and Nova, R. (2009a). "Soil-pipeline interaction along unstable slopes: a coupled three-dimensional approach. Part I: Theoretical formulation." *Canadian Geotechnical Journal*. Vol. 46, pp.1289-1304.

- Cocchetti, G., Prisco, C., Galli, A. (2009b). "Soil–pipeline interaction along unstable slopes: a coupled three-dimensional approach. Part 2: Numerical analyses." *Canadian Geotechnical Journal*. Vol. 46, pp. 1305-1321.
- Comfort, G., Gilbert, C, and Ferregut, C. (1990). "Analysis of Subscour Stresses and Probability of Ice Scour-Induced Damage for Buried Submarine Pipelines, Vol. I, Database of Key Ice Scour Parameters." *Panel for Energy Research & Development and Canada Oil and Gas Lands Administration - Energy Mines and Resources Indian and Northern Affairs*, March.
- Comfort, G. and Graham, B. (1986). "Evaluation of Sea-Bottom Ice Scour Models." Environmental Studies Revolving Funds Report No. 037, Ottawa, Ontario, 71 p.
- Costa, A. M. (1984). "Application of computational methods and rock mechanics principles in excavation of underground mines (in Portuguese)." *D.Sc. Thesis*, COPPE–Federal University of Rio de Janeiro, Brazil.
- Daiyan, N., Kenny, S., Phillips, R. and Popescu, R. (2009). "Parametric study of lateral-vertical pipeline/soil interaction in clay." *Proceedings of the 1<sup>st</sup> Engineering Mechanics and Materials Specialty Conference*, St. John's, Newfoundland and Labrador, Canada.
- Daiyan, N., Kenny, S., Phillips, R. and Popescu, R. (2010a). "Investigation of axial/lateral interaction of pipes in dense sand." *International Conference on Physical Modeling in Geotechnics*, Zurich, Switzerland.
- Daiyan, N., Kenny, S., Phillips, R. and Popescu, R. (2010b). "Numerical investigation of oblique pipeline/soil interaction in sand." *Proc., IPC2010-31644*, 6p.
- Daiyan, N., Kenny, S., Phillips, R. and Popescu, R. (2011). "Investigating pipeline-soil interaction under axial-lateral relative movements in sand." *Canadian Geotechnical Journal*, Vol. 48(11), pp. 1683-1695.
- Daiyan, N., Kenny, S., Phillips, R. and Popescu, R. (2011). "Numerical investigation of axial-vertical and lateral-vertical pipeline/soil interaction in sand." *Proceedings of the 14<sup>th</sup> Pan-Am CGS Geotechnical Conference*, Toronto, Canada, 9p.
- Das, B.M. (1990). "Earth Anchors." *Developments in Geotechnical Engineering 47*. Elsevier Science Publishers, Amsterdam, 440p.
- deVries, J. (1981). "An Offshore Seabottom Excavation System." *Proceedings, Symposium on Production and Transportation Systems for the Hibernia Discovery*, St. John's, Newfoundland, pp. 212-222.

- Dinsmore, R.P. (1972). "Ice and Its Drift into the North Atlantic Ocean." *Proceedings, Symposium on environmental Conditions in the Northwest Atlantic, 1960-1969*, ICNAF Special Publication No. 8, pp.89-128.
- Donea, J., A. Huerta, J.-Ph. Ponthot and A. Rodriguez-Ferran (2004). "Arbitrary Lagrangian Eulerian methods." *Encyclopaedia of Computational Mechanics, Erwin Stein, René de Borst and Thomas J.R. Hughes Editors*. Vol. 1: Fundamentals. John Wiley & Sons.
- Dredge, L.A. (1982). "Relict Ice-Scour marks and Late Phases of Lake Agassiz in Northernmost Manitoba." *Canadian Journal of Earth Science*, Vol. 19, pp. 1079-1087.
- Fatemi A., Kenny, S., and Taheri, F. (2007). "Continuum Finite Element Methods to Establish Compressive Strain Limits for Offshore Pipelines in Ice Gouge Environments." *Proceedings of the 26<sup>th</sup> International Conference on Offshore Mechanics and Arctic Engineering*, San Diego, California.
- FENCO – Foundation of Canada Engineering Corporation Limited (1975). "An Analytical Study of the Ice Scour on the Sea Bottom." *Report for the Arctic Petroleum Operators Association, APOA Project No. 69*, 241 p.
- Fernando, N. S. M., and Carter, J. P. (1998). "Elastic analysis of buried pipes under surface patch loadings." *Journal of Geotechnical and Geoenvironmental Engineering*., Vol. 124(8), pp. 720–728.
- Frederking, R. and Barker, A. (2001). "Friction of Sea Ice on Various Construction Materials," PERD/CHC Report 3-49, HYD-TR-067. Ottawa, Canada.
- Frederking, R., Timco, G.W., Kamesaki, K. and Tada, H. (1999). "Review of First-Year Ridge Geometries and Properties in Sakhalin Region," *Proceedings International Workshop on Rational Evaluation of Ice Forces on Structures, REIFS'99, Mombetsu, Japan*, pp 21-33.
- Fredj, A., Comfort, G., and Dinovitzer, A. (2008). "A Case Study of High Pressure/High Temperature Pipeline for Ice Scour Design Using 3D Continuum Modeling." *Proceedings of the 27th International Conference of Offshore Mechanics and Arctic Engineering*, Estoril, Portugal.
- Gibson, C.E. (1981). "Underwater Trench Production Systems." *Proceedings, Symposium on Production and Transportation Systems for the Hibernia Discovery*, St. John's, Newfoundland, pp. 223-237.
- Gilbert, G.R. and Pedersen, K. (1986). "Ice Scour Database for the Beaufort Sea." *Environmental Studies Revolving Funds*, Report No. 055. Ottawa, 99p.

- Green, H.P. (1984). "Geotechnical Modelling of Iceberg-Seabed Interaction." *M. Eng Thesis*, Memorial University of Newfoundland, St. John's, Newfoundland, 165 p.
- Guo, P. and Stolle, D.F. (2005). "Lateral pipe-soil interaction in sand with reference to scale effect." *Journal of Geotechnical and Geoenvironmental Engineering*, ASCE, Vol. 131(3), pp. 338-349.
- Hansen, J.B. (1948). "The stabilizing effect of piles in clay." CN Post No.3, Christiani and Nielson, Copenhagen, Denmark, November, pp. 14-15.
- Hansen, J.B. (1961). "The ultimate resistance of rigid piles against transversal forces." *Bulletin No. 12*, Danish Geotechnical Institute, Copenhagen, Denmark, 5-9.
- Hodder, M. S. and Cassidy, M.J. (2010). "A plasticity model for predicting the vertical and lateral behaviour of pipelines in clay soils." *Geotechnique*, Vol. 60(4), pp. 247-263.
- Hodgson, G.J. Lever, J.H., Woodworth-Lynas, C.M.T. and Lewis, C.F.M. (1989). The Dynamics of iceberg grounding and scouring (DIGS) experiment. E.S.R.F., Rep. 094.
- Honegger, D.G., Hart, J.D., Phillips, R., Popelar, C., and Gailing, R. W. (2010). "Recent PRCI guidelines for pipelines exposed to landslide and ground subsidence hazards." Proceedings of the 8th International Pipeline Conference, Calgary, Canada, ASME, Vol. 2, pp. 71-80.
- Honegger, D.G., and Nyman, J. (2001). "Manual for the Seismic Design and Assessment of Natural Gas Transmission Pipelines." Pipeline Research Council International Project PR-268-9823.
- Honegger, D.G., and Nyman, J. (2004). "Guidelines for the seismic design and assessment of natural gas and liquid hydrocarbon." Pipeline Research Council International, Falls Church, Va. No. L51927.
- Hsu, T.W., Chen, Y.J., and Wu, C.Y. (2001). "Soil friction resistance of oblique pipelines in loose sand." *Journal of Transportation Engineering*, Vol. 127(1), pp. 82-87.
- Hsu, T.W., Chen, Y.J. and Hung, W.Y. (2006). "Soil restraint to oblique movement of buried pipes in dense sand." *Journal of Transportation Engineering*, ASCE, Vol. 32(2), pp.175-181.
- Ishikawa, R., Kioka, S., Kubouchi, A., and Saeki, H. (2005). "Soil deformation within the seabed due to ice-scouring." *Proceedings of the 19th Int. Symposium on Okhotsk Sea and Sea ice*, pp.207-214.

- Jukes, P., Eltahir, A., Abdalla, B., and Duron, B. (2008). "The Design and Simulation of Arctic Subsea Pipelines." Houston, Texas.
- Kennedy, R.P., Chow, A.W. and Williamson, R.A. (1977). "Fault movement effect on buried oil pipeline." *Journal of Transportation Engineering*, Vol. 103(5), pp. 617-633.
- Kenny, S., Phillips, R., and Nobahar, A. (2005). "PRISE Numerical Studies on Subgouge Deformations and Pipeline/Soil Interaction Analysis." *Proceedings of the 18th International Conference on Port and Ocean Engineering under Arctic Conditions*, Potsdam, New York, pp. 43-52.
- Kenny, S., Phillips, R., McKenna, R.F., Clark, J.I. (2000). "Response of Buried Arctic Marine Pipelines to Ice Gouge Events." *Proceedings of the Energy-Sources and Technology Conference and Exposition/International Conference on Offshore Mechanics and Arctic Engineering Joint Conference*, New Orleans, USA, pp. 1-8.
- Kenny, S., Barrett, J., Phillips, R., and Popescu, R. (2007a). "Integrating Geohazard Demand and Structural Capacity Modeling within a Probabilistic Design Framework for Offshore Arctic Pipelines." *Proceedings of the 17th International Offshore and Polar Engineering Conference*, Lisbon, Portugal.
- Kenny, S., Palmer, A.C. and Been, K. (2007b). "Design challenges for offshore pipelines in arctic environments." *Proceedings of Offshore Oil and Gas in Arctic and Cold Waters*, 15p
- Kioka, S., and Ishikawan, R., and Saeki, H, H. (2006). "Medium Scale Model Test on Soil Deformation and Stress within Seabed during Ice Scour event." *Proceedings of the 18th IAHR International Symposium on Ice*, Sapporo, Japan, pp. 317-324.
- Konuk, I., and Gracie, R. (2004). "A 3-Dimensional Eulerian Finite Element Model for Ice Scour." *Proceedings of the International Pipeline Conference*, Calgary, Alberta, Vol. 3, pp. 1911-1918.
- Konuk, I., and Fredj, A. (2004). "FEM Model for Pipeline Analysis of Ice Scour – A Critical Review." *Proceedings of the 23rd International Conference on Offshore Mechanics and Arctic Engineering*, Vancouver, British Columbia.
- Konuk, I., Gracie, R., and Yu, S. (2005). "A 3-Dimensional Continuum ALE Model for Ice Scour – Study of Trench Effects." *Proceedings of the 24th International Conference on Offshore Mechanics and Arctic Engineering*, Halkidiki, Greece.
- Konuk, I., Gracie, R., and Yu, S. (2005). "An ALE FEM Model of Ice Scour." *Proceedings of the 11th International Conference of the International Association of Computer Methods and Advances in Geomechanics*, Turin, Italy, Vol. 3, pp. 63-70.

- Konuk, I., and Yu, S. (2007a). "A Pipeline Case Study for Ice Scour Design." *Proceedings of the 26th International Conference on Offshore Mechanics and Arctic Engineering*, San Diego, California.
- Konuk, I., and Yu, S. (2007b). "Continuum Modeling of Lateral Buckling: Study of Soil Effects." *Proceedings of the 26th International Conference on Offshore Mechanics and Arctic Engineering*, San Diego, California.
- Konuk, I., Liferov, P., and Loset, S. (2007). "Challenges in Modeling Ice Gouge and Pipeline Response," *Proceedings of the 20th International Conference on Port and Ocean Engineering under Arctic Conditions*, Dalian, China.
- Kovacs, A., and Mellor, M. (1974). "Sea Ice Morphology and Ice as a Geological Agent in the Southern Beaufort Sea." *The Coast and Shelf of the Beaufort Sea*, eds. J.C. Reed, and J.E. Sater, Arctic Institute of North America, Arlington, Virginia, Vol. 2, pp. 113-161.
- Kettle, R.J. (1984). "Soil-pipeline interaction: a review of the problem." *Pipelines and Frost Heave*, Proceedings of a Seminar at Caen, France, April, pp. 35-37
- Lach, P.R. (1996). "Centrifuge Modeling of Large Soil Deformation due to Ice Scour." *PhD Thesis*, Memorial University of Newfoundland, St. John's, Canada.
- Lach, R.P., and Clark, J.I. (1996). "Numerical Simulation of Large Soil Deformation Due to Ice Scour." *Proceedings of the 49th Canadian Geotechnical Conference of the Canadian Geotechnical Society*, St. John's, Newfoundland, pp. 189-198.
- Lach, R.P., and Clark, J.I. (1994). "Ice scouring of the seabed," *Proceedings of the International Conference Centrifuge, Centrifuge 94*, Singapore, September, pp. 803 - 808.
- Lach, P.R., Clark, J.I., and Poorooshasb, F. (1993). "Centrifuge modelling of ice scour." *Proceedings of the 4th Canadian Conference on Marine Geotechnical Engineering*, St. John's, Newfoundland, Vol. 1, pp. 357 - 374.
- Liferov, P., Shkhinek, K.N., Vitali, and Serre, N. (2007). "Ice Gouging Study – Actions and Action Effects." *Port and Ocean Engineering Under Arctic Conditions*. Dalian, China.
- Liferov, P., Hoyland, K.V. (2004). "In-situ ice ridge scour tests: experimental setup and basic results." *Journal of Cold Regions Science and Technology*, 40/1-2: 97-110.
- Mackenzie, T.R. (1955). "Strength of deadman anchors in clay." *M.Sc. Thesis*, Princeton University, Princeton, USA.

- Mahdavi, H., Kenny, S., Phillips, R. and Popescu, R. (2008). "Influence of geotechnical loads on local buckling behaviour of buried pipelines." *Proceedings of the 7th International Pipeline Conference*, Calgary, Canada, 7p.
- Mahdavi, H., Kenny, S., Phillips, R. and Popescu, R. (2009). "Effect of embedment ratio on buried pipelines subject to combined loading." *Proceedings of the 62nd Canadian Geotechnical Conference*, Halifax, Canada, 9p.
- Martin, C. M., and Houlsby, G. T. (2001). "Combined loading of spudcan foundations on clay: Numerical modelling." *Geotechnique*, Vol. 51(8), pp. 687-699.
- Matlock, H. (1970). "Correlations for design of laterally loaded piles in soft clay." *Proceedings of the 2nd Offshore Technology Conference*, Houston, USA, OTC 1204, pp. 577-594.
- McKenna, K., King, T., Bruce, J., and Phillips, R. (2003). "Ice Gouge Risk to Offshore Pipelines – Making the Most of Available Data." *Proceedings of the 17th International Conference on Port and Ocean Engineering Under Arctic Conditions*, Trondheim, Norway.
- Merifield, R. S. and Sloan, S. W. (2006). "The ultimate pullout capacity of anchors in frictional soils." *Canadian Geotechnical Journal*, Vol. 43, pp. 852-868.
- Mollard, J.D. (1983). "The origin of reticulate and orbicular patterns on the floor of Lake Agassiz." *Glacial Lake Agassiz, Geological Association of Canada*, Special Paper 26, pp. 355-374.
- Murray, J.E. (1969). "The Drift, Deterioration and Distribution of Icebergs in the North Atlantic Ocean." *Proceedings, Ice Seminar*. Canadian Institute of Mining and Metallurgy, Special Vol. 10, pp. 3-18.
- Myers, R., Blasco, S., Gilbert, G., and Shearer, J. (1996). "1990 Beaufort Sea Ice Scour Repetitive Mapping Program." *Environmental Studies Research Funds Report No. 129*.
- Nadreau, T.P. (1986). "Survey of Physical and Mechanical Properties of Icebergs." *Proceedings, Workshop on Extreme Ice Features*, National Research Council of Canada, Banff, Alberta, pp.155-192.
- Ng, P. C.F. (1994). "Behaviour of buried pipelines subjected to external loading." *PhD Thesis*, University of Sheffield, Sheffield, U.K.
- Nixon, J.F., Palmer, A., and Philips, R. (1996). "Simulations for Buried Pipeline Deformations Beneath Ice Scour." *Proceedings of the 15th Conference of Offshore*

- Mechanics and Arctic Engineers*," Vol. 5, Pipeline Technology, Florence, Italy, pp. 383-392
- Nobahar, A., Kenny, S., Phillips, R. (2007). "Buried Pipelines Subject to Subgouge Deformations." *International Journal of Geomechanics*, ASCE, Vol. 7, No. 3.
- Nobahar, A. (2005). "Coupled Pipe-Soil-Ice Keel Interaction." *Journal of Pipeline Integrity*, Vol. 4, No. 2, 117-137.
- Nyman, K.J. (1982). "Soil response against the horizontal-vertical motion of pipes." Preprint 82-534, Presented at ASCE National Convention, New Orleans.
- Nyman, K.J. (1984). "Soil response against oblique motion of pipes." *Journal of Transportation Engineering*, Vol. 110(2), pp. 190-202.
- Oliveira, J.R.M.S. (2005). "Centrifuge modelling of a case study of soil structure interaction (in Portuguese)." *D.Sc. Thesis*, Federal University of Rio de Janeiro, Brazil.
- Oliveira, J.R.M.S., Almeida, M.S.S., Marques, M.E.S., and Almeida, M.C.F. (2006). "Undrained strength of very soft clay soils used in pipeline studies in the centrifuge." *Internation Conference on Physical Modelling in Geotechnics*, Vol. 1, Taylor and Francis, Hong Kong, 1355-1360.
- Oliveira, J.R.M.S., Almeida, M.S.S., ASCE., M, Almeida, M. C. F. and Borges, R. G. (2010). "Physical modeling of lateral clay-pipe interaction." *Journal of Geotechnical and Geoenvironmental Engineering*, Vol. 136(7), pp. 950-956.
- Ovesen, N. K. (1964). "Anchor slabs, calculation methods and model tests." *Bulletin No. 16*, The Danish Geotechnical Institute, Copenhagen, Denmark.
- Palmer, A. C., Konuk, I., Love, J., Been, K., and Comfort, G. (1989). "Ice Scour Mechanics." A Research Paper prepared for Canada Oil and Gas Lands Administration and Gulf Canada Resources Ltd.
- Palmer, A. C., Konuk, I., Love, J., Been, K., and Comfort, G. (1990). "Ice Gouging and the Safety of Marine Pipelines." *22nd Annual Offshore Technology Conference*, Houston, Texas, pp. 235-244.
- Palmer, A. C., White, D.J., Baumgard, A.J., Bolton, M.D., Barefoot, A.J., Finch, M., Powell, T., Faranski, A.S., Baldry, J.A.S. (2003). "Uplift Resistance of Buried Submarine Pipelines: Comparison Between Centrifuge Modelling and Full-Scale Tests." *Geotechnique*, Vol. 53, Issue 10, pp. 877-883.

- Palmer, A.C., Konuk, I., Niedoroda, A.W., Been, K., and Croasdale, K.R. (2005). "Arctic seabed ice gouging and large sub-gouge deformations." *The International Symposium on Frontiers in Offshore Geotechnics*, Perth, Western Australia.
- Palmer, A.C., White, D.J., Baumgard, A.J., Bolton, M.D., Barefoot, A.J., Finch, M., Powell, T., Faranski, A.S., and Baldry, J.A.S. (2003). "Uplift resistance of buried pipelines: comparison between centrifuge modeling and full-scale tests." *Geotechnique* Vol. 53(10), pp. 877-883.
- Paulin, M.J. (1992). "Physical Model Analysis of Iceberg Scour in Dry and Submerged Sand." *M. Eng Thesis*, Memorial University of Newfoundland, St. John's, Newfoundland, 183 p.
- Paulin, M. J. (1998). "An investigation into pipelines subjected to lateral soil loading." *PhD Thesis*, Memorial Univ. of Newfoundland, St. John's, Canada.
- Paulin, M. J., Phillips, R., Boivin, R. (1995). "Centrifuge modelling of lateral pipeline/soil interaction-Phase II." *Proceeding of the 14<sup>th</sup> International Conference on Offshore Mechanics and Arctic Engineering*, Copenhagen, Denmark, Vol. 5, pp. 107-123.
- Paulin, M. J., Phillips, R., Boivin, R. (1996). "An experimental investigation into lateral pipeline/soil interaction." *Proceedings of the 15th International conference on offshore mechanics and Arctic engineering*, Vol. 5, pp. 313-323.
- Paulin, M. J., Phillips, R., Clark, J.L., Trigg, A., and Konuk, I. (1998). "A full-scale investigation into pipeline/soil interaction." *Proceedings of the International Pipeline Conference*, p779-788, Calgary, AB.
- Phillips, R., and Barrett, J. (2011). "Ice Keel-Seabed Interaction: Numerical Modelling for Sands. *International Conference on Port and Ocean Engineering under Arctic Conditions*, Montreal, Canada, 10p.
- Phillips, R., Barrett, J. and Al-Showaiter, A (2010). "Ice keel-seabed interaction: Numerical modeling validation," *Proceedings of the Ocean Technology Conference*, Houston, Texas, 13p.
- Phillips, R., Kenny, S., and Clark, J.I. (2005). "PRISE studies on gouge forces and subgouge deformations." *International Conference on Port and Ocean Engineering under Arctic Conditions*, pp. 43-52.
- Phillips, R., Nobahar, A., and Zhou, J. (2004a). "Combined axial and lateral pipe-soil interaction relationships." *Proceedings of the 5<sup>th</sup> International Pipeline Conference*, Calgary, Canada., 5p.

- Philips, R; Nobahar, A.; Zhou, J. (2004b). "Trench effects on pipe-soil interaction." *Proceeding of IPC2004*, International Pipeline Conference, Calgary, Alberta, Canada
- Pike, K. and Kenny, S. (2011). "Advancement of CEL procedures to analyze large deformation pipeline/soil interaction events." *Offshore Technology Conference*, Houston, TX, USA. 10p.
- Pike, K., Seo, D. and Kenny, S. (2011). "Continuum Modelling of Ice Gouge Events: Observations and Assessment," *Proceedings of the Arctic Technology Conference*, Houston, Texas, 12p.
- Poorooshasb, F., and Clark, J.I. (1990). "On small scale ice scour modelling." *Workshop on Ice Scouring and the Design of Offshore Pipelines*
- Poorooshasb, F., Clark, J.I., and Woodworth-Lynas, C.M.T. (1989). "Small Scale Modelling of Iceberg Scouring of the Seabed." *Proceedings of the 10th International Conference on Port and Ocean Engineering under Arctic Conditions*, Lulea, Vol. 1, pp. 133-145.
- Poorooshasb, F. R., Paulin, M. J., Rizkalla M., Guo, P., Nobahar, A. (1994). "Centrifuge modelling of laterally loaded pipelines." *Proceedings of the International Conference on Physical Modelling in Geotechnics*.
- Popescu, R. (1999). "Finite element analysis of pipe-soil interaction – phase I- two-dimensional plane strain analyses." *Contract Report for Geological Survey of Canada*, C-CORE Publication 99-C23.
- Popescu, R. and I. Konuk, (2001). "3D finite element analysis of rigid pipe interaction with clay", *Proceedings of the 10<sup>th</sup> International Conference Computer Methods and Advancements in Geomechanics*, Tucson, AZ, Vol. 2, pp. 1203-1208.
- Popescu, R., Konuk I., Guo, P., Nobahar, A. (2002a). "Some aspects in numerical analysis of pipe-soil interaction." *Proceedings of the 2nd Canadian Specialty Conference on Computer Applications in Geotechnique*, Winnipeg, Canada, pp. 290-297.
- Popescu, R., Phillips, R., Konuk, I., and Deacu, D. (1999). "Numerical and physical modeling of pipe-soil interaction." *Proceedings of the 52nd Canadian Geotechnical Conference*, Regina, SK, pp. 437-444.
- Popescu, R., Phillips, R., Konuk, I., Guo, P., and Nobahar, A. (2002b). "Pipe-soil interaction: Large-scale tests and numerical modeling." *Proceedings of the International Conference on Physical Modelling in Geotechnics*, St.John's, Newfoundland, pp. 917-922.

- Poulos, H.G. (1988). "Marine Geotechnics." Unwin Hyman, London.
- Prakash, S. And Sharma, H.D. (1990). "Pile Foundations in Engineering Practice." John Wiley and Sons, New York, 734p.
- Prasad, K.S.R. (1985). "Analytical and Experimental Modelling of Iceberg Scours." *M. Eng. Thesis*, Memorial University of Newfoundland, St. John's, Newfoundland, 170 p.
- Rearic, D.M. and McHendrie, A. G. (1983). "Ice Gouge Data Sets from the Alaskan Beaufort Sea; Magnetic Tape and Documentation for Computer Assisted Analyses and Correlation." United States Geological Survey Open-File Report 83-706.
- Reese, L. C., and Casbarian, A. O. P. (1968). "Pipe soil interaction for a buried offshore pipeline." *Paper SPE 2343, Proceedings of the 43<sup>rd</sup> Annual Fall Meeting of the Society of Petroleum Engineers of AIME*, Houston.
- Rizkalla, M., Poorooshasb, F., and Clark, J. I. (1992). "Centrifuge modelling of lateral pipeline/soil interaction." *Proceedings of the 11<sup>th</sup> International Conference of Offshore Mechanics and Arctic Engineering Symposium*, Calgary, Canada.
- Rowe, R. K., and Davis, E. H. (1982). "The behaviour of anchor plates in clay." *Geotechnique*, 32(1), 9-23.
- Sayed, M., and Timco, G.W. (2008). "A numerical model of iceberg scour." *Cold Regions Science and Technology*, doi:10.1016/j.coldregions.2008.03.007
- Seo, D., Kenny, S., Hawlader, B. (2011). "Yield envelopes for oblique pipeline.soil interaction in cohesive soil using ALE procedure." *Proceedings of the 14<sup>th</sup> Pan-Am CGS Geotechnical Conference*, Toronto, Canada, 7p.
- Schaminee, P.E., Zorn, N.F., and Schotman, G.J.M. (1990). "Soil response for pipeline upheaval buckling analyses: full scale laboratory tests and modeling." *Proceedings of the 22nd Annual Offshore Technology Conference*, Houston, USA, pp. 563-572.
- Shapiro, L.H. and Metzner, R.C. (1987). "Coefficients of friction of sea ice on beach gravel," *Journal of Offshore Mechanics and Arctic Engineering*, Vol. 109, pp. 388-390.
- Shearer, J., Laroche, B. and Fortin, G. (1986). "Canadian Beaufort Sea 1984 Repetitive Mapping of Ice Scour." *Environmental Studies Revolving Funds Report No. 032*, Ottawa.
- Surkov, G.A. and Truskov, P.A. (1995). "Study of ice pressure ridges and stamukhi offshore of Sakhalin." *Proceedings of the 10th Okhotsk Sea and Sea Ice Symposium*, Hokkaido, Japan, pp.53-58.

- Taiebat, H.A., and Carter, G.T. (2000). "Numerical studies of the bearing capacity of shallow foundations on cohesive soil subjected to combined loading." *Geotechnique*, Vol. 50(4), pp. 409–418.
- Timco, G.W. and Burden, R.P. (1997). "An Analysis of the Shapes of Sea Ice Ridge.," *Cold Regions Science and Technology*, Vol. 25, pp. 65-77.
- Trautmann, C.H., and O'Rourke, T.D. (1985). "Behavior of Pipe in Dry Sand Under Lateral and Uplift Loading," Geotechnical Engineering Report 83-6, Cornell University, Ithaca, New York.
- Trautmann, C.H., and O'Rourke, T.D. (1985). "Lateral force-displacement response of buried pipe." *Journal of Geotechnical Engineering*, Vol. 111(9), pp. 1077–1092.
- Trautmann, C.H., O'Rourke, T.D., and Kulhawy, F. H. (1985). "Uplift force-displacement response of buried pipe." *Journal of Geotechnical Engineering*, Vol. 111(9), pp. 1061–1076.
- Tschebotarioff, G.P. (1973) "Foundations, retaining and earth structures." McGraw-Hill Book Company, New York, 642p.
- Utt, M.E. and Clark, R.A. (1980). "Coefficient of friction between submerged ice and soil," *Petroleum Division Journal*, American Society of Mechanical Engineers., No.80-PET-41, United States. pp.1-4.
- Venkatesh, S., and El-Tahan, M. (1988). "Iceberg Life Expectancies in the Grand Banks and Labrador Sea," *Cold Regions Science and Technology*, No. 15, pp. 1-11.
- Vesic, A. S. (1971). "Breakout resistance of objects embedded in ocean bottom." *Journal of the Soil Mechanics and Foundations Division*, Vol. 97(9), pp. 1183–1205.
- Wadhams, P. (1975). "Sea Ice Morphology in the Beaufort Sea." *Beaufort Sea Project*, Technical Report No. 36, Department of the Environment, Victoria, British Columbia, 66 p.
- Wahlgren, R.V. (1979). "Ice-Scour Tracks on the Beaufort Sea Continental Shelf: their form and an interpretation of the processes creating them." Vol. 1, 2, and 3." *M.A. Thesis*, Carlton University, Department of Geography, Ottawa.
- Wantland, G.P., O'Neill, M.B., Reese, L.C., and Coeolgyne, E.H. (1979). "Lateral stability of pipelines in clay," *Proceedings of the 11<sup>th</sup> Offshore Technology Conference*, ASME, Houston, pp. 1025-1034.

- Wantland, G.P., O'Neill, M.B., and Coelogyne, E.H., Reese, L.C. (1982). "Pipeline lateral stability in soft clay." *Journal of Petroleum Technology*, Vol. 34, No.1, pp. 217-220.
- Weber, W.S., Barnes, P.W. and Reimnitz, E. (1989). "Data on the Characteristics of Dated Gouges on the Inner Shelf of the Beaufort Sea, Alaska." 1977-1985. United States Geological Survey Open-File Report 89-151.
- Wijewickreme, D., Karimian, H. and Honegger, D. (2009). "Response of buried steel pipelines subjected to relative axial soil movement." *Canadian Geotechnical Journal*, Vol. (46), pp. 735-752
- Woodworth-Lynas, C.M.T., Bass, D.W., and Bobbitt, J. (1986). "Inventory of Upslope and Downslope Iceberg Scouring." Environmental Studies Revolving Funds Report No. 039, Ottawa, Ontario, 103 p.
- Woodworth-Lynas, C.M.T., and Guigne, J.Y. (1990). "Iceberg Scours in the Geological Record: Examples From Glacial Lake Agassiz." *Glacimarine Environments: Processes and Sediments*, eds. J.A. Dowdeswell, and J.D. Scourse, Geological Society Special Publication No. 53, pp. 217-233.
- Woodworth-Lynas, C.M.T, Nixon, D., Philips, R., and Palmer, A. (1996). "Subgouge deformations and the security of Arctic marine pipelines." *Offshore Technology Conference*, Houston, Texas.
- Yang, Q.S., Lach, P.R., Clark, J.I. and Poorooshasb, H.B. (1994). "Comparison of Physical and Numerical Models of Ice Scour," *Proceedings of the 8<sup>th</sup> International Conference on Computer Methods and Advances in Geomechanics*, Vol. 2, pp. 1795-1801
- Yimsiri, S., Soga, K., Yoshizaki, K., Dasari, G. R. and O'Rourke, T. D. (2004). "Lateral and upward soil-pipeline interactions in sand for deep embedment conditions." *Journal of Geotechnical and Geoenvironmental Engineering*, Vol. 130(8), pp. 830-842.
- Zhang, J., Stewart, D. P. and Randolph, M. F. (2002). "Modeling of shallowly embedded offshore pipelines in calcareous sand." *Journal of Geotechnical and Geoenvironmental Engineering*. ASCE, Vol. 128(5), pp. 363-371.

